UNIVERSITY OF OKLAHOMA
GRADUATE COLLEGE

DEVELOPMENT AND APPLICATION OF SPRAY-CAPILLARY, A NOVEL DEVICE FOR MICROSAMPLING, AND ONLINE CAPILLARY ZONE ELECTROPHORESIS MASS SPECTROMETRY ANALYSIS ON NANOSCALE OMICS STUDY

A DISSERTATION

SUBMITTED TO THE GRADUATE FACULTY

in partial fulfillment of the requirements for the

Degree of

DOCTOR OF PHILOSOPHY

By

LUSHUANG HUANG
Norman, Oklahoma
2021

DEVELOPMENT AND APPLICATION OF SPRAY-CAPILLARY, A NOVEL DEVICE FOR MICROSAMPLING, AND ONLINE CAPILLARY ZONE ELECTROPHORESIS MASS SPECTROMETRY ANALYSIS ON NANOSCALE OMICS STUDY

A DISSERTATION APROVED FOR THE
DEPARTMENT OF CHEMISTRY AND BIOCHEMISTRY

BY THE COMMITTEE CONSISTING OF

Dr. Si Wu, Chair

Dr. Mark Nanny

Dr. Robert White

Dr. Christina Bourne

Acknowledgement

First and foremost, I would like to express my sincere thankfulness to Dr. Wu, who is not only my mentor during the five-year academic and research period, but also a great demonstration on being professional. All the following works would never come to fruition without her invaluable guidance, expertise education and generous support.

Moreover, I would like to thank my committee members, Dr. Mark Nanny, Dr. Robert White, and Dr. Christina Bourne for their insightful advice for my preliminary exam and general exam. Deep appreciation for everything you have provided on helping me to develop.

I would like to thank my lab colleagues: Dr. Zhe Wang for mentoring me during my early days in the lab and helping me on constructing CZE-MS interface, Dr. Kellye A. Cup-Sutton for helping me on paper publications, Dr. Dahang Yu and Mulin Fang for instrument maintenance, Yanting Guo for sample preparation skills, Zhitao Zhao and Jiaxue (Josh) Li for follow up works on spray-capillary, Ji Kang, Trishika Chowdhury, Anju Sunny Teresa, Daniel G. Delafield, Toni Woodard, Drew King for all the helps and consistent backup.

Finally, I would like to thank my family, especially my mom, dad, and Yidi, for their endless love and support, also, my friends who supports me through toughness.

Table of Contents

List of Tables

List of Figures

Appendix

Abstract

The capillary zone electrophoresis-mass spectrometry (CZE-MS) platform, a well-developed analytical methodology, has been widely used for high-throughput nanoscale (*e.g.,* < 5000 cells, single-cell sample) bioanalysis (*e.g.,* proteomics and metabolomics). The sample size for a nanoscale study can be extremely limited in both volume (*e.g*., pL-nL) and amount (*e.g.,* ng). Therefore, it is valuable to construct a high-throughput, user-friendly, and ultrasensitive CZE-MS platform for nanoscale analysis. This dissertation focuses on developing a novel quantitative sample handling device for ultralow-volume samples (*e.g.,* pL-nL) and applying it for the online CZE-MS analysis of single cell samples.

Firstly, a novel sample handling device, spray-capillary, was developed for quantitatively extracting pL-nL level samples (*e.g.,* as low as 15 pL/s). Electrospray ionization (ESI) is an ionization approach that has been routinely applied to couple liquid phase separation with MS detection but not for sample handling. The spray-capillary device is constructed from a commercially available fused silica capillary with one end being treated as the sample inlet and the opposing end being treated as an MS end. The MS end will be fabricated to a sheathless interface for electrospray-assisted sampling handling. Our results show that a low-volume sample (*e.g*., pL range) can be quantitatively introduced into a bare capillary for a pressure-based elution and MS detection. In addition, the spray-capillary can serve as the CZE separation column for on-capillary CEZ-MS analysis, which largely reduced sample loss from the offline sample handling

process. A standard peptides mixture was used for prove-of-concept for the quantitative nanoscale CZE-MS analysis. The sample loading process is reproducible and adjustable.

Secondly, the original spray-capillary setup is manually operated, which makes the workflow low-throughput and prone to human error. Also, the usage of a bare capillary limits the performance of CZE-MS analysis (*e.g.*, sample loss due to the adsorption on the capillary). To address these issues, we incorporated a commercially available CZE autosampler to perform fully automated spray-capillary analysis and utilized polyethylenimine (PEI) as capillary coating material to increase the separation efficiency.

Thirdly, we redesigned the original spray-capillary device to perform the single-cell metabolomics analysis. The sample inlet end was laser pulled to a small tip (*i.e.,* 15 μm o.d.) so it can be directly inserted into single onion cells for ultra-low volume microsampling. The extracted single-cell contents can be directly separated and analyzed in the modified spray-capillary using the online CZE-MS analysis, which significantly decreases sample loss by eliminating off-line sample handling processes. Spray-capillary-based direct infusion single-cell analysis identified 80 cross-verified onion metabolites, while spray-capillary–based CZE-MS single-cell analysis identified 160 cross-verified onion metabolites. Additional experiments include a relative migration time comparison with standard chemicals, and targeted MS/MS analysis were performed to confirm the identification of the metabolites.

Overall, this work has demonstrated that spray-capillary provides a valuable solution for nanoscale microsampling and high-throughput omics analysis using the on-capillary CZE-MS analysis (*e.g.*, single-cell analysis). The spray-capillary approach holds great potential for being incorporated into a variety of CZE-MS-based nanoscale analysis workflows for multi-omics study.

Chapter 1： Introduction

1.1 Background

Metabolome, the complete set of small molecules (with a molecular weight smaller than 1.5 kDa), such as sugars, amino acids, and phosphate compounds in a given biological system, and proteome, the complete set of proteins expressed by the cell system, dictate cell activity when cells interact with the environment. Both metabolome and proteome are highly dynamic and can be affected by environmental stimuli. Metabolomics, which refers to the comprehensive investigation of metabolome, and proteomics, the large-scale study of proteome, provides valuable phenotypic information about cell systems. Studying metabolomics and proteomics on low-number cell population (*e.g.,* cell number <

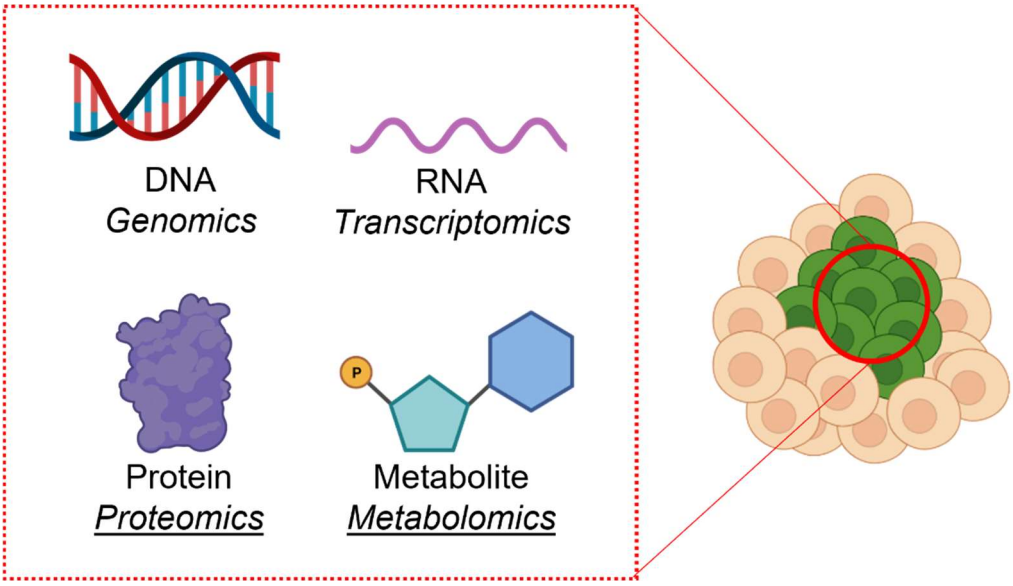

Figure 1-1. Nanoscale omics study (Green cells: minor cell population).

5000) provides biological insights into resolving the heterogeneity of minor cell populations (*e.g.,* circulating tumor cells) from a phenotypic perspective. (**Figure 1-1**) [1]. Unlike genomics and transcriptomics, for which a polymerase chain reaction (PCR)-based amplification method can be applied, nanoscale proteomics and metabolomics require an ultrasensitive analytical platform.

To study proteins from a nanoscale sample, antibody-based immunofluorescence assays have been developed to detect proteins in single cells using microfluidic devices (*e.g.*, antibody microarray [2], microfluidic-based western blot [3]). However, these methods can only analyze a small portion of known proteins due to the availability of antibodies. Mass cytometry, the analytical platform that combines flow cytometry with inductively coupled plasma mass spectrometry, analyzes single cells through the detection of metal isotopes that are conjugated on individual cells through specific antibodies [4, 5]. The use of flow cytometry permits the profiling of single cells at a high speed (*e.g.,* 1,000 cells/s). However, again, the use of an antibody limits the number of proteins that can be measured per cell, and dead volumes, as well as a lack of sample handling methods prevent the application of mass cytometry for minor cell populations [3, 6]. To study metabolites from limited samples, nuclear magnetic resonance (NMR) has been used with laser microdissection for cell type-specific metabolite profiling [7]. However, in general, collecting a signal correspondence matrix requires quality 2D NMR, which is not practical for limited samples [8].

The development of novel MS-based analytical platforms which include small-scale sample handling, high performance liquid phase separation, and high resolution MS instrumentation, has enabled high-throughput analysis of nanoscale complex biological samples [9]. The development of small-scale sample handling methods aims at efficiently handling small-scale samples, which typically possess extremely limited amounts. The general aim for this session is to minimize sample loss. The general strategies include restricting the sample preparation process in a single container and transferring manual steps to an online fashion. The development of microfluidic devices and related techniques also facilitates the growth of the small-scale sample handling field by permitting confident sample handling at low-volume range (*e.g.,* nL). The application of liquid phase front-end separation methods (*e.g.,* liquid chromatography (LC) and capillary electrophoresis (CE)) aims to decrease sample complexity to achieve higher detection coverage (*e.g.,* detecting low abundance species). Moreover, high-throughput analysis is achieved by involving the front-end separation step. Meanwhile, the low sample requirement (*e.g.,* nanogram to microgram level) of certain types of approaches such as nanoLC and CE allows the utilization of these methods on small-scale biological samples. In addition, the resolving power of MS instruments has been continuously improved with the advancement of high-resolution mass analyzers (*e.g.,* time-of-flight (TOF), Orbitrap, ion cyclotron resonance (ICR)) over the past decade. Following the commercialization of the Orbitrap mass analyzer, conducting high-resolution mass spectrometry studies can now be included in the metabolomics and proteomics workflow with significantly

less cost and maintenance. Moreover, the detection limit of the Orbitrap system makes the detection of single protein molecules possible [10]. More recently, the MS instrument has been upgraded to conduct single-cell analysis. Ion mobility units (*e.g.,* field asymmetric ion mobility spectrometry [11], trapped ion mobility spectrometry (TIMS) [12]) has been developed as a commercially available built-in building block for different MS instruments (*e.g.,* Orbitrap Exploris Family, tims TOF) to increase the signal-to-noise ratio [13]. Furthermore, coupling advanced MS instruments with high-resolution liquid phase separation technologies or ambient ionization methods has allowed for high-throughput nanoscale proteomics and metabolomics.

1.2 High-throughput nanoscale omics analysis

In the HeLa cell system, there are about 40,000 metabolites [14] and ~$2x10^9$ proteins [15]. Furthermore, the concentration of these metabolite and protein molecules has a large dynamic range (*e.g.,* several orders of magnitude [16]). Under different conditions (*e.g.,* drug treatment or diseases), the abundance and diversity of metabolites and proteins may vary significantly. The ability to perform ultrasensitive nanoscale metabolomics and proteomics can provide a better understanding of disease-related proteins or metabolites. The highly complex metabolome and proteome requires a high-throughput analytical methodology.

In general, high-throughput nanoscale metabolomics and proteomics normally use untargeted mass spectrometry analysis to analyze all ionizable

analytes in a sample and identify as many metabolites or proteins as possible. The general workflow for high-throughput nanoscale metabolomics and proteomics is also similar (**Figure 1-2**). The molecules of interest (*i.e.,* metabolite, protein) are extracted from the nanoscale sample (*e.g.,* rare cell population, single-cell sample), followed by separation and MS detection. Both accurate mass measurement using full MS data and searching MS/MS fragments against databases can be performed for metabolite and protein identification.

More specifically, for metabolomics, cell contents are obtained from the nanoscale sample through a microsampling process (*e.g.,* single-cell sample). The metabolites are extracted from cell contents using an extraction buffer that contains organic solution (*e.g.,* methanol, acetonitrile (ACN)) and acid (*e.g.,* 0.1% formic acid (FA)), followed by either chromatographic or electrophoretic separation with online MS detection [17, 18]. In addition, single-cell metabolomics can be performed using ambient ionization approaches. Ambient MS is a form of direct MS analysis, which means the sample is directly introduced to MS analysis without front-end separation. Several dedicated designs (*e.g.,* nanospray desorption electrospray ionization (nanoDESI) [19], laser desorption/ionization droplet delivery (LDIDD) [20], single probe [21], laser ablation electrospray ionization (LAESI) [22], liquid extraction surface analysis (LESA) [23], and probe electrospray ionization (PESI) [24]) have been introduced for ambient MS. An advantage of ambient MS is the sample requires minimal or no sample preparation steps before analysis to maintain the native status of the metabolome.

The bottom-up strategy is most frequently used for proteomics. For this method. The extracted proteins are digested to peptides, which are separated by either chromatography or electrophoresis and detected by MS. Bottom-up proteomics is a robust and sensitive method for identifying proteins, but it can lose information about the proteoform, which is defined as "all of the different molecular forms in which the protein product of a single gene can be found." [25] As an emerging technology, top-down proteomics directly performs intact protein level analyses, which preserve the post-translational modification (PTM) information.

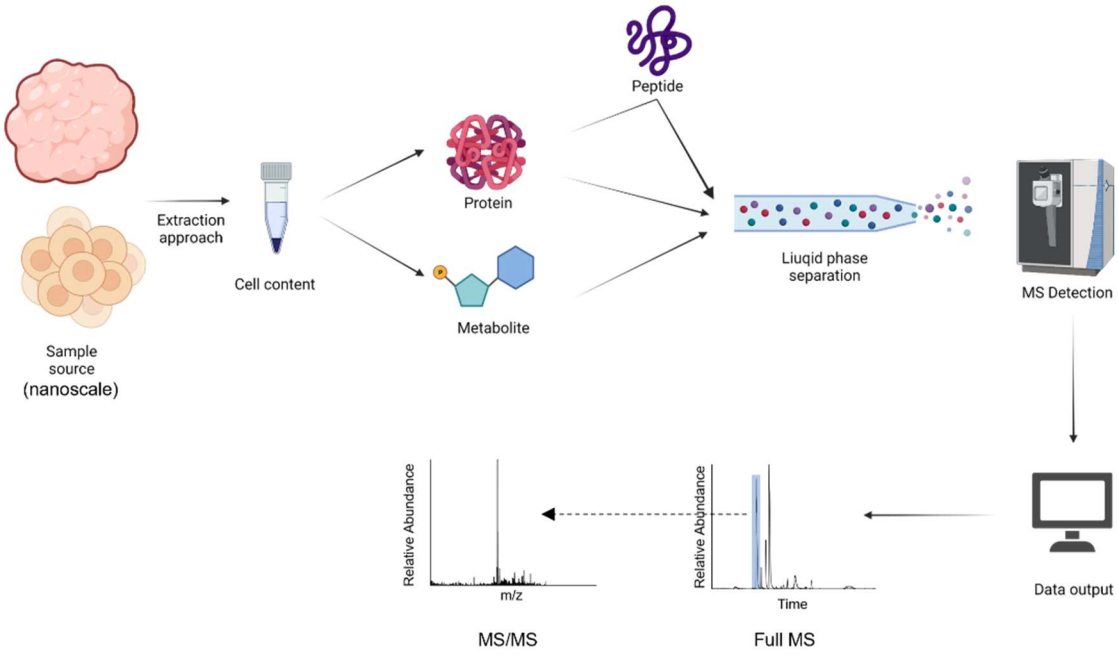

Figure 1-2. High-throughput nanoscale omics workflow.

1.2.1 Separation technologies for nanoscale omics

To detect as many analytes (*i.e.,* protein, metabolite) as possible, high-resolution separation approaches are required. Efficient separation results in concentrating individual analytes in a complex sample into different zones (*i.e.,* peaks), which, therefore, significantly reduces ion suppression and dramatically increase the chances of detecting low abundant analytes. Liquid chromatography (LC) and capillary electrophoresis (CE) are the most commonly used liquid phase separation approaches for nanoscale metabolomics and proteomics.

For LC separation, analytes are separated based on their interactions with the stationary phase. LC has different modes (*e.g.,* size exclusion chromatography (SEC), ion exchange chromatography (IEX), hydrophobic interaction chromatography (HIC), hydrophilic interaction chromatography (HILIC), reverse phase chromatography (RPLC)) when different mobile phases and stationary phases are used, and each mode can separate analytes based on different mechanisms (*e.g.,* size, charge, hydrophobicity, polarity). Among these LC modes, RPLC, which separates analytes based on their different hydrophobicities, is the most widely used technology when coupled with MS for nanoscale proteomics and metabolomics study. Ultrahigh performance liquid chromatography (UHPLC) that uses a reverse phase column has been achieved through different strategies, including using a longer separation column (*e.g.,* 100 cm), packing the column by using smaller-sized particles (*e.g.,* sub-2 μm diameter [26]), using a capillary column with a smaller inner diameter (*e.g.,* 30 μm [27], 15 μm [28]), and using a narrow capillary (*e.g.,* 2 μm I.D. [29]) for a monolithic column. Zmole detection limit for complex samples has also been demonstrated [28]. When coupled with

advanced MS instrumentation, nearly 850 proteins can be identified from a single HeLa cell.

Capillary electrophoresis is a well-developed separation technique family that includes capillary zone electrophoresis (CZE), capillary isoelectric focusing (CIEF), and capillary gel electrophoresis (CGE). Among these techniques, CZE is most often used for nanoscale proteomics and metabolomics. To perform a CZE separation, the capillary inner wall must be "activated" by flushing a NaOH solution, followed by flushing a background electrolyte (BGE) solution. The positive ion is attracted by the negatively charged "activated" wall and forms an electrical double layer; the movement of this layer under electric field forms an electroosmotic flow (EOF). The EOF carries the BGE, and the sample plug moves along the CZE capillary. Since the introduction of modern CZE separation in 1981, the technique has been used as a high-performance nanoscale separation approach. Early efforts have been made to use CZE with an optics detector such as UV-Vis and laser induced fluorescence (LIF). CZE-LIF has demonstrated an extremely low detection limit (zeptomole level) during its application on biological samples [30]. Using MS as detector for CZE was first reported in 1988, and this methodology has been extensively developed since. During the past several decades, the CZE-MS platform has been developed and become a powerful approach for omics analysis. The low sample requirement (*e.g.*, nL) of CZE makes CZE-MS an effective choice for nanoscale omics analysis. Therefore, numerous improvements have developed the CZE-MS platform for nanoscale omics analysis [31].

For most cases, CZE is coupled with MS through electrospray ionization (ESI) or matrix-assisted laser desorption/ionization (MALDI), whereas CZE-ESI-MS is the most widely used CZE-MS platform. Although the sensitivity of modern MS instrumentation has been greatly improved, the overall sensitivity of the CZE-MS platform largely depends on the performance of the interface that couples CZE and MS. The CZE-MS interface is responsible for two tasks: performing the stable electrospray ionization process and completing the electrical path of CZE separation [32]. The CZE interface design can be roughly attributed to two categories: sheath liquid style and sheathless style. The sheath liquid style interface uses a makeup flow to perform ESI and to complete an electric path. The makeup flow and BGE are sprayed and detected by MS. The coaxial sheath-liquid interface represents some early efforts for interfacing CZE with MS [33]. The EOF-driven sheath-liquid CZE-MS interface was uses an electrokinetic pump-based ESI emitter; this interface shows excellent robustness and sensitivity and has now been commercialized by CMP Scientific Inc. [34]. Compared to the sheath-flow design, the sheathless interface discards the makeup flow and has no potential dilution effect. In this way, the CZE column can also be used as an ESI emitter, and the BGE solution is directly sprayed into MS for detection [35]. The sheathless interface design focuses on the emitter shape, establishing electric contact, and the overall assembly process of the components. Because the emitter shape is closely related to ESI performance, strategies such as heat-gravity-based pulling, laser-based pulling, and hydrofluoric acid (HF) etching have been applied to produce a better emitter shape to improve ESI

performance [32]. As with the sheath-liquid design, establishing robust electric contact is a key element for the sheathless interface. Dedicated designs have been implemented to create electric contact, such as depositing a conductive metal coating onto the capillary emitter, inserting a metal wire into the capillary emitter, splitting the BGE solution, and creating porous junctions. One of the most well-developed sheathless interface designs is the porous segment interface. In this design, a porous segment emitter (3 cm in length) was fabricated to perform stable ESI, creating a complete electric path. The capillary wall thickness of the porous segment is reduced to a range of 5-10 micrometers to allow ionic interaction across the porous segment region. A general schematic is shown in **Figure 1-3**.

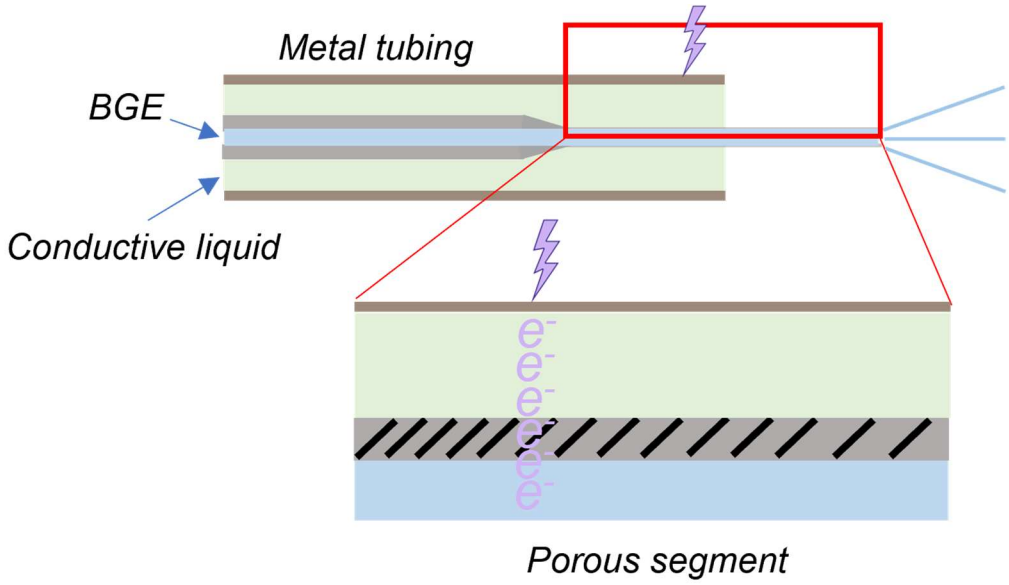

Figure 1-3. A schematic of the porous segment sheathless style interface. (Adapted from Ref. [36])

The separation performance of CZE also depends on several factors such as the capillary inner diameter, field strength (potential difference/capillary length),

capillary inner wall condition, and BGE [37]. Because of practical considerations, current CZE-MS platforms for omics study primarily employ a capillary column with the following parameters: a capillary inner diameter of 20, 30, and 50 μm, and a capillary length of 50–100 cm; 250-300 v/cm is normally used as the field strength. Based on the basic working mechanism of CZE, EOF serves as a vital element for increasing the separation efficiency. On the one hand, the EOF-driven flow possesses a laminar flow profile, which can decrease peak tailing when compared to pressure-based flow profiles, which have a parabolic flow profile. One the other hand, EOF needs to be controlled to perform high-resolution CZE separation. Applying a coating material to the capillary inner wall though a chemical reaction presents an important method of governing the EOF [37]. Depending on the specific coating material, the EOF can either be reduced or reversed. Covalently attaching polymer coating material to the capillary wall is an effective method primarily because covalently coated capillaries can be used for a longer time, and polymer reagents will not be introduced into the MS. Representative polymer materials such as linear polyacrylamide (LPA) [38], a neutral coating that can reduce EOF, and polyethyleneimine (PEI) [39], a cationic coating material that can reverse EOF, have been widely applied in proteomics research. Non-covalent coatings, which use adsorptive secondary interactions, are another solution for controlling EOF, and this approach is more easily implemented because the coating materials are interchangeable; however considerable maintenance is required for stable and reproducible separation. Moreover, because the coating reagent is added to BGE during the separation

process, the signal of the molecule from the sample can be reduced when CZE is coupled with MS.

In addition, sample preconcentration methods have been applied to increase the sample loading capacity and improve separation performance for CZE separation. The aim of preconcentration is to focus more closely on the analyte during separation. A sample stacking strategy can be implemented using BGE, one that has different conductivity with the sample plug, which is achieved by adding an organic solvent to the sample buffer [40]. Furthermore, isotachophoresis can be achieved by introducing the sample to a solution plug in a "sandwich" style. A leading electrolyte plug, which possesses a higher electrophoretic mobility; a sample plug; and a "terminating electrolyte" plug, which possesses lower electrophoretic mobility, are sequentially injected into the separation capillary for a better focusing effect during the CZE separation [41]. Another preconcentration approach that uses the pH difference between the sample plug and BGE solution is also revealed and named the dynamic pH junction [42].

By using a sensitive interface, high-quality capillary coating, online preconcentration methods, and an optimized CZE parameter, Sun's group applied the CZE-MS platform to both bottom-up and top-down proteomics, and they achieved a 140-min separation window for peptide separation with ~380 peak capacity [43]. In another research project, nearly 800 proteoforms and nearly 260 proteins were identified from a 250-ng *Escherichia coli* complex sample [44]. Peter's group identified ~70 metabolites from a single frog embryo cell using an

in-house built CZE-MS platform [45]. These results motivated further development of the CZE-MS platform.

1.2.2 Mass spectrometry for metabolomics and proteomics

An advantage of using a mass spectrometer as a detector is that hundreds and thousands of analytes in a sample can be interrogated during a single run. Mass spectrometers measure the mass-to-charge ratio (m/z) of detected ions, and simultaneously detects all the analytes that have been ionized at the same time through ionization approaches (*e.g.,* ESI, MALDI). The intensity of all the ions detected during an individual scan and the m/z values are used to construct mass spectrums (*i.e.,* Full MS). Modern mass spectrometers use high-resolution mass analyzers (*e.g.,* Orbitrap, ICR, TOF) to perform m/z measurements with high mass accuracy, which means that analytes with similar m/z values (*e.g.,* 10 ppm) can be separated on the same mass spectrum. Moreover, structural information about specific analytes can be obtained using tandem mass spectrometry (*i.e.,* MS/MS), which fragments the detected ions. The MS/MS technique selects ions within a certain m/s range and fragments them through dissociation approaches. The selection can be performed based on the intensity of real-time ion detection, (*i.e.,* data-dependent acquisition) or a preselected m/z value (*i.e.,* targeted MS/MS). Recently, information-rich MS/MS data has been obtained by selecting all ions within a defined m/z window, and this analysis repeats as the window covers the total m/z range (*i.e.,* data-independent acquisition) [46].

For an untargeted metabolomics study, MS-based metabolite identification can be performed through several steps (**Figure 1-4**). Putative identification can be performed through accurate mass measurement with a full MS spectrum, and the m/z values of molecules of interest are searched against databases (*e.g.,* METLIN, HMDB) with mass tolerance. Then, MS/MS analysis, through dissociation methods (*e.g.,* collision induced dissociation (CID)), are performed on both the analyte and the standard reagent of its putative identification result. The MS/MS spectrum is compared to support the putative identification result [47].

For the proteomics study, peptides or proteoforms are identified by MS/MS fragmentation, whereas protein level identification is achieved via a two-step procedure. This procedure includes deconvoluting the spectrum to a list of monoisotopic masses, and each protein can be scored against a deconvoluted spectrum, which results in a Protein-Spectrum-Match (PrSM) [48]. Furthermore, to achieve better sequence coverage (especially for top-down proteomics) and PTM analysis, different dissociation methods can be used to generate different types of fragmentation ions [49]. A collisional- based dissociation method such as CID and higher-energy C-trap dissociation (HCD) can generate b- and y- ions. Electron transfer/capture dissociation (ETD/ECD) and photodissociation (UVPD) generate c- and z- ions, while electron-mediated techniques such as electron detachment dissociation (EDD) and negative electron transfer dissociation (nETD) are used to generate a- and x- ions.

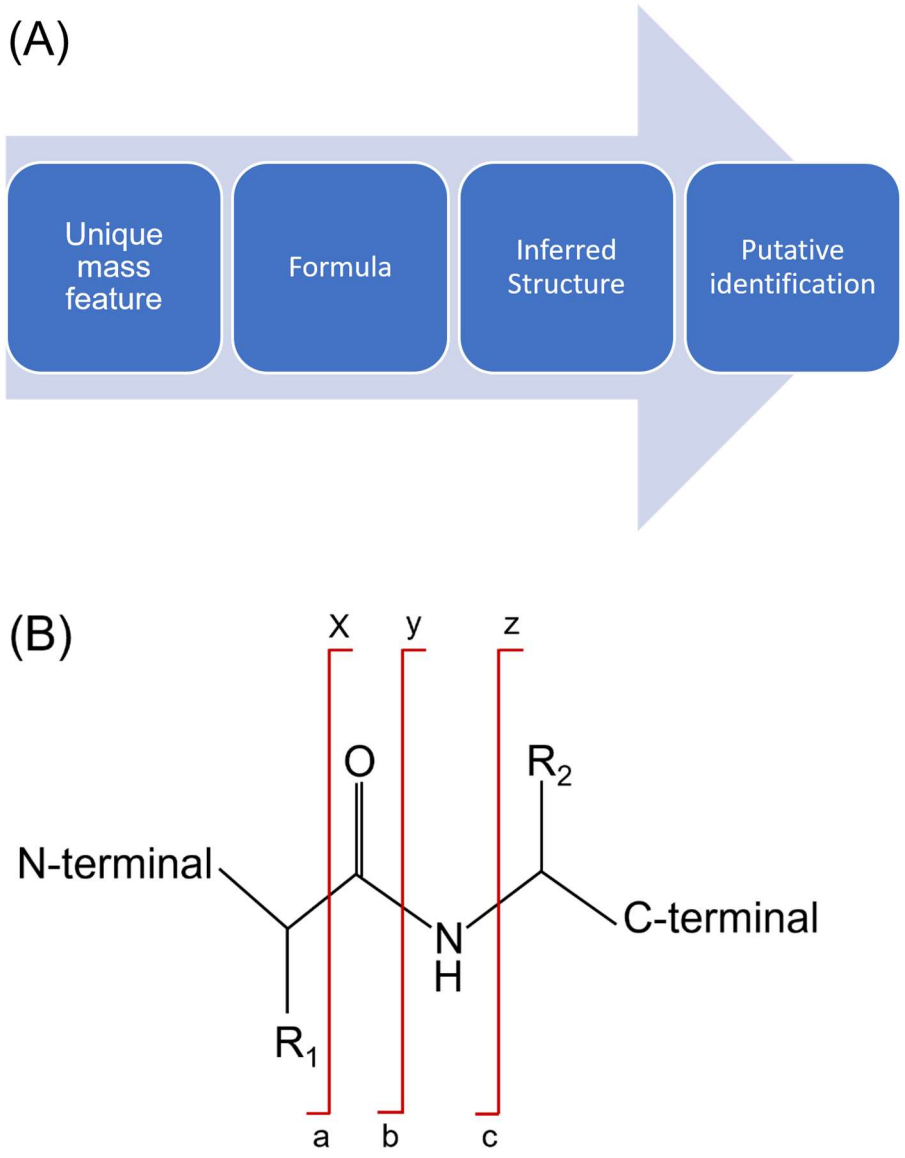

Figure 1-4. (A) Metabolite identification process, and (B) MS/MS fragmentation on peptide (protein) (Adapted from Ref. [50])

1.3 Sample handling/microsampling for nanoscale omics analysis

The sample processing approach is an important component of MS-related analytical workflows [13, 51], especially in nanoscale proteomics and

metabolomics analysis. This step connects the demonstrated sensitivity of the analytical platform with the practical needs for the sample amount and volume. The general goal is to develop a sample process approach for minimizing sample loss and increasing sample processing efficiency (**Figure 1-5**). Practically, the nanoscale sample can be collected through several approaches, such as dissection (*e.g.,* whole-cell dissection [52], laser-capture microdissection (LCM) [53]), and fluorescence-activated cell sorting (FACS) [54], and microsampling [55]. Based on the molecule of interests (*i.e.,* protein, metabolite) and the specific kind of downstream analytical approach (*i.e.,* LC, CZE), numerous efforts have been made to design novel sample preparation workflows for both volume and mass-limited samples.

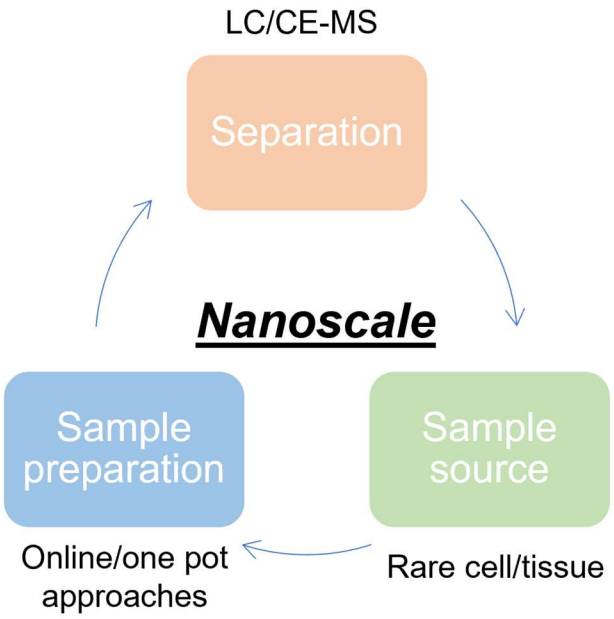

Figure 1-5. Sample preparation and liquid phase separation approaches for nanoscale omics analysis (Adapted from Ref. [1]).

For the CZE-MS platform, because the sample loading volume is limited, dilution should be avoided to minimize sample loss. Therefore, sample handling or microsampling approaches are required to handle and deliver volume-limited samples (*e.g.,* rare cell population, single-cell sample) [56]. Whole-cell dissection has been used to isolate larger single cells (*e.g.,* frog embryos (523 nL) [57]) by using surgical tools such as the fine-sharp forceps, electrolytically sharpened tungsten needles, and microdissection scissors. Micro/nanopipettes have also been widely used to extract cell content directly from single-cell samples. For instance, nanopipettes with a ~20 μm tapered tip were used for microsampling from frog embryos [45], a ~15 μm tip was used for microsampling from an onion cell [58], and a tip with a 10 μm O.D. was used for sampling cell content from a HeLa cell [59]. Furthermore, different driving forces (*e.g.,* vacuum, EOF) have been used for microsampling processes. The extracted cell content is subjected to extraction or reconstruction steps and loaded onto a CZE separation column. Practically, in-house CZE-MS platforms have been constructed with customized sample loading systems [60, 61] to assemble these steps for single-cell CZE-MS analysis. Because the sample size after reconstruction is normally at a low-microliter level, which is well below the requirement for performing a quality sample injection from a commercially available CZE autosampler, in-house CZE-MS platforms are required for single-cell CZE-MS analysis. For the customized sample loading system, two strategies are usually employed: the first strategy is pressure-based injection based on height difference, and the second strategy is EOF-based sample injection. **(Figure 1-6)**. For pressure-based injection by height difference, an

elevatable stage is used to adjust for the height difference, and a dedicated designed control system controls the height. At the same time, the sample and BGE reservoir are fixed to the stage for CZE-MS analysis [55, 60]. A relatively dedicated setup, which consists of removable metal blocks, electrically insulating enclosures, and safety interlock-enabled doors (high voltage consideration), are required for reproducible sample loading. The EOF-based sample injection uses EOF for sample loading, and a liquid junction is created between the sample inlet end and the tissue sample. Sample loading is triggered by applying a high voltage directly to the liquid junction. However, because different molecules have different electrophoretic mobility, the overall sample injection flow rate will differ, which hampers the researcher's ability to estimate the sample injection volume for each analyte. The EOF-sample injection method has been applied for the CZE-MS analysis of mouse tissue samples [62]. Currently, in the nanoscale CE-MS field, it remains challenging to quantitatively analyze volume-limited samples (*e.g.,* pL-nL) with confidence. A simpler method for performing unbiased nanoscale sample loading is desired. Furthermore, the current single-cell CE-MS employs offline microsampling methods, which provides flexibility when determining the sample preparation steps. However, excessive intermediate steps may lead to sample losses. Therefore, strategies that combine online microsampling with CZE separation are desired.

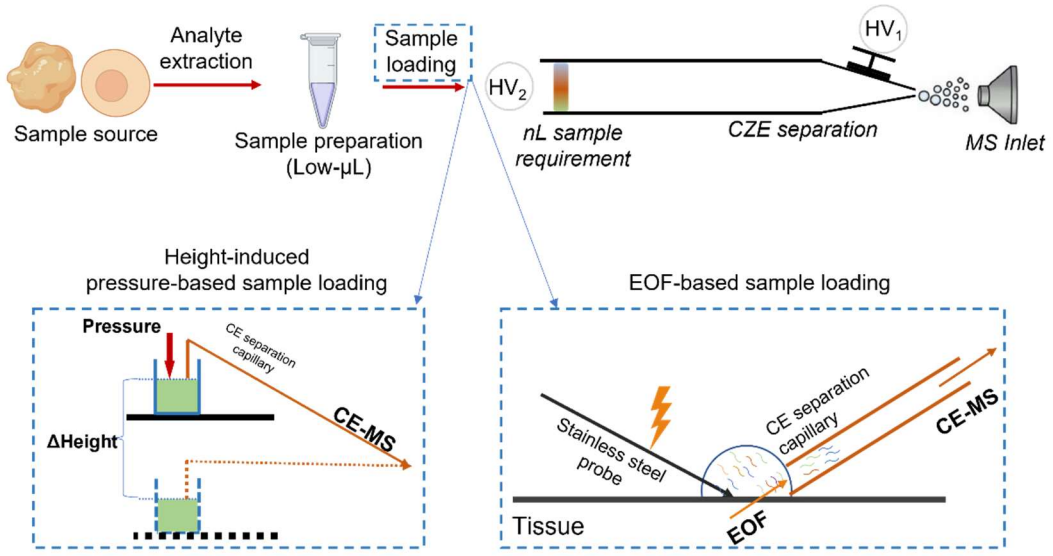

Figure 1-6. Schematic of nanoscale CZE-MS platform and classic sample handling methods.

For the LC-MS platform, significant efforts have been made to use it for nanoscale proteomics. As with bulk scale analysis, a series of sample preparation steps (*e.g.,* cell lysis, reduction, alkylation, and enzymatic digestion) are required. The evolution of sample processing has helped eliminate sample transfers, minimize sample processing volume, and block nonspecific interactions [1]. Significant effort has also been devoted to moving offline sample processing steps to online protocols. In general, samples are trapped in a capillary column to initiate chemical reactions for sample preparation. Strong cation exchange (SCX) has been used to trap protein and reagent solutions for denaturation, alkylation, and enzymatic digestion, which were introduced sequentially [63]. Another approach utilizes an integrated proteome analysis device (iPAD) [64] with an empty fused silica capillary to store both reagents and cell solutions. The reactor is subjected to heat for cell lysis and digestion. The immobilized enzyme reactor

(IMR), which was designed for online digestion, has gained attention from researchers in the nanoscale proteomics field because it can dramatically increase the efficiency of the enzymatic digestion process by increasing the enzyme to substrate ratio. In IMR, enzymes are immobilized into various types of stationary phases (*e.g.,* monolithic, particle-based) through interactions such as affinity binding, adsorption, and covalent linkage. An online IMR device can handle samples as small as a few nanoliters [65, 66].

The use of detergent or chaotropic reagents (*e.g.,* SDS) in a lysis buffer facilitates protein extraction from the cell's content. However, an extra "cleanup" step (*e.g.,* desalting) is required because the detergent will suppress the ESI process [67]. An extra cleanup step can introduce an unexpected sample loss for mass and volume-limited samples. The single-tube strategy is designed to avoid tube transfer for the cleanup step and eliminate sample transfer because the entire sample preparation process can be performed in one tube, which is normally the low binding tube (*e.g.,* Eppendorf Protein LoBind). To follow the single-tube strategy, an MS friendly surfactant, such as RapiGest, ProteaseMAX, or PPS Silent surfactants [68, 69], as well as other reagents, such as organic cosolvent (Trifluoroethanol (TFE)), can be used to replace SDS [1]. Another strategy (SP3) utilizes hydrophilic paramagnetic beads to trap protein samples during sample preparation [70]. Recently, a nanoparticle-aided nanoreactor (Nano3) was invented for nanoscale proteomics, which also uses paramagnetic beads to carry out nanoscale sample processing. The Nano3 can handle a sample volume as low as 30 nL [71]. The advantage of these paramagnetic-based methods is that they

permit the use of strong detergents. Overall, the single-tube strategy has performed impressively when dealing with samples of 100–5,000 cells.

More recently, a promising nanodroplet-based sample processing approach has been introduced. This idea is based on using a microfluidic device to hold the sample in a droplet during the preparation steps. This serves multiple purposes, including increasing digestion efficiency by decreasing total sample volume and deceasing nonspecific adsorptive loss by getting rid of the centrifuge tube for sample preparation. One of the representative droplet-based reports is nanodroplet processing in one pot for trace samples (NanoPOTS) [72], which uses photolithography to fabricate chip-based reactors. NanoPOTS can be effectively used for the sample preparation process with a sample size of 200 nL while reducing the total surface area of the sample to ~0.8 mm^2. Together with an MS-friendly surfactant, more than 1,500 proteins can be identified from 10 HeLa cells using the NanoPOTS device. Moreover, this open configuration of NanoPOTS device allows it to work with pre-fractionation techniques such as FACS and LCM. Moreover, an automated liquid handler, a commercially available autosampler, has been used to upgrade the original NanoPOTS workflow to create a more user friendly setup [73]. Another droplet strategy, an oil-air-droplet (OAD) chip [74], was also developed for droplet-based sample preparation. Here, an in-situ stationary microreactor is used to restrict the possible contact area on the chip surface, an oil layer is used to prevent evaporation, and an air layer is designed to prevent direct contact between the cover oil and the droplet sample. The OAD device can hold a sample at ~550 nL, and the contact area between the sample and

the device is reduced to < 1.3 mm^2. By using the OAD device, more than 50 proteins can be identified from a single HeLa cell.

1.4 Dissertation synopsis

This thesis describes the development and application of a novel microsampling device, "spray-capillary," for quantitatively handling a ultralow-volume sample (*i.e.,* pL-nL) and online capillary electrophoresis mass spectrometry analysis for nanoscale omics analysis. This device, for the first time to our knowledge, uses an ESI process to provide a vacuum-driving force for nanoscale sample handling. The spray-capillary device can be fabricated from a commercially available fused silica capillary with one end fabricated as a sheathless style interface with a porous segment emitter (**Chapter 2**). The sample injection flow rate is at 255 pL/s, using a 50 μm I.D. and a 50 cm-length capillary, and 15 pL/s can be achieved by using a 20 μm I.D. capillary. The potential parameters, including electrospray voltage, capillary length, viscosity of column liquid, and capillary I.D., were investigated to prove the device was adjustable. Its quantitative performance was evaluated by constructing a calibration curve. The electrospray-assisted sample handling method was directly coupled with the CZE-MS platform to demonstrate the quantitative nanoscale CZE-MS analysis. With the assistance of a commercially available CZE autosampler, the original spray-capillary device was upgraded to an automated high-throughput nanoscale analysis platform for picolitre to nanoliter sampling (**Chapter 3**). In addition, PEI

coating material was applied to improve the performance of the CZE separation. A 50-continuous-spray-capillary-based sample injection was carried out with good reproducibility. The quantitative performance of this automated platform was further evaluated by varying the sample injection time. Also, the platform was used to perform automated quantitative nanoscale CZE-MS analyses. Single-cell metabolomics analysis is an intriguing aspect of nanoscale omics. We modified the original spray-capillary device by laser-pulling the regular sample inlet end to a tapered tip, which can be inserted into single onion cell sample (**Chapter 4**). The sampling process was re-evaluated, and spray-capillary microsampling was applied on a single-cell sample. A pressure-based elution step was used to assess the performance of the quantitative microsampling, and for the first time, we online coupled a microsampling process with CZE-MS for single-cell metabolomics analysis.

Chapter 2： Spray-Capillary: An Electrospray-Assisted Device for Quantitative Ultralow-Volume Sample Handling

2.1 Abstract

The analysis of low-volume samples provides valuable insight into complex biological systems. However, the proteomics and metabolomics analysis of low-volume samples remains challenging due to the lack of simple, efficient, and reproducible microsampling techniques. We have developed an electrospray-assisted device for quantitative low-volume sample extraction, referred to here as "Spray-Capillary". Stable electrospray was achieved through a chemically etched tip from a long (*e.g.,* 50 cm) capillary with a conductive sheath flow. This electrospray provided the driving force to quantitatively draw low-volume samples into the capillary. We evaluated the precision and accuracy of sample injection volumes using our spray-capillary as the electrospray voltage, capillary ID, and column length were varied. Our results demonstrate that spray-capillary allows for reproducible and quantitative microsampling with low injection flow rates (as low as 15 pL/s). Furthermore, spray-capillary can be directly coupled with capillary zone electrophoresis (CZE) for separation. Overall, spray-capillary is a simple microsampling device that holds great potential for high-throughput quantitative omics analysis of ultralow-volume samples.

2.2 Introduction

Efforts have been made to improve the sensitivity and throughput of low quantity sample analysis in mass spectrometry (MS)-based omics including the development of specialized sample preparation device [65, 75], high-resolution separation methods [28, 76], efficient spray-MS interfaces (*i.e.,* novel ambient ionization techniques) [34, 35, 77-81], and advancements in MS instrumentation [82]. The sensitivity of low quantity sample analysis has been dramatically improved using these techniques, but many challenges remain in quantitative low-volume sample injection and extraction [72].

Micropipettes has been the most commonly applied tools for the manipulation of low-volume sample [83-91]. Briefly, one end of the capillary tubing is pulled to make a micropipette to aspirate samples into the capillary through a driving force. Two approaches have been applied as the driving force for the operation of micropipettes: pump-based extraction and electroosmotic force. In the pump-based micropipette sample handling method, a syringe is connected to a vacuum or mechanical pump to pull the sample into the capillary. Using this method, low sample injection volume can be accurately controlled [92]. Coupling the pump-based extraction approach with offline capillary zone electrophoresis (CZE)-MS for complex sample analysis has led to promising results [55, 93, 94]. For example, the Nemes group constructed a pump-based micropipette method to study live *Xenopus laevis* and Zebrafish embryos [95]. When an electroosmotic driving force is utilized, and electrode in inserted into a sampling capillary and current is applied to induce electroosmotic flow. Recently,

a micropipetting method based on using electroosmotic flow was develop by the Laskin group and applied to the analysis of single cell [96]. During the collection process, +2 V was maintained to prevent the sample buffer from getting into the laser-pulled tips before the cell was penetrated. Low-volume cellular contents were extracted using -2 V after penetration. This work demonstrated that electroosmotic force could be utilized as the driving force for microsampling low-volume samples such as single onion cells. Another approach utilized an electroosmotic pump for ultralow-volume sample extraction from a Zebrafish embryo [91].

Other microsampling approaches include hydrodynamic methods [45, 60, 97-101], fluidic force microscopy [102], capillary force [103], and electrowetting [86]. A microfluidic chip-based platform, nanoPOTS [72], had been recently developed for low sample volume processing in single-cell proteomics analysis. NanoPOTS reduces total processing volumes from the conventional hundreds of microliters to <200 nL within a single droplet reactor. However, a customized automated droplet-based microfluidic system has to be incorporated for the ultralow-volume manipulation in nanoPOTS.

Dr. Wysocki's group has demonstrated a continuous electrospray using a platinum wire inserted into a laser pulled glass capillary with preinjected samples [104]. Inspired by this research, we developed an electrospray-assisted microsampling method, referred to here as "spray-capillary", The spray-capillary is a simple hydrodynamic device that utilizes electrospray ionization (ESI) as the driving force for the injection of low-volume samples. During the ESI process, a

liquid jet is created when the electrostatic force of the sample overcomes the surface tension, which reduces the pressure around the spray tip and creates a pressure difference between opposing ends of the ESI capillary. The spray-capillary device utilizes this pressure difference to serve as the driving force to move the liquid inside the capillary toward the spray tip. A conductive porous tip, similar to the sheathless interface proposed by Moini [35], was utilized to generate ESI as the driving force to quantitatively draw low-volume samples into

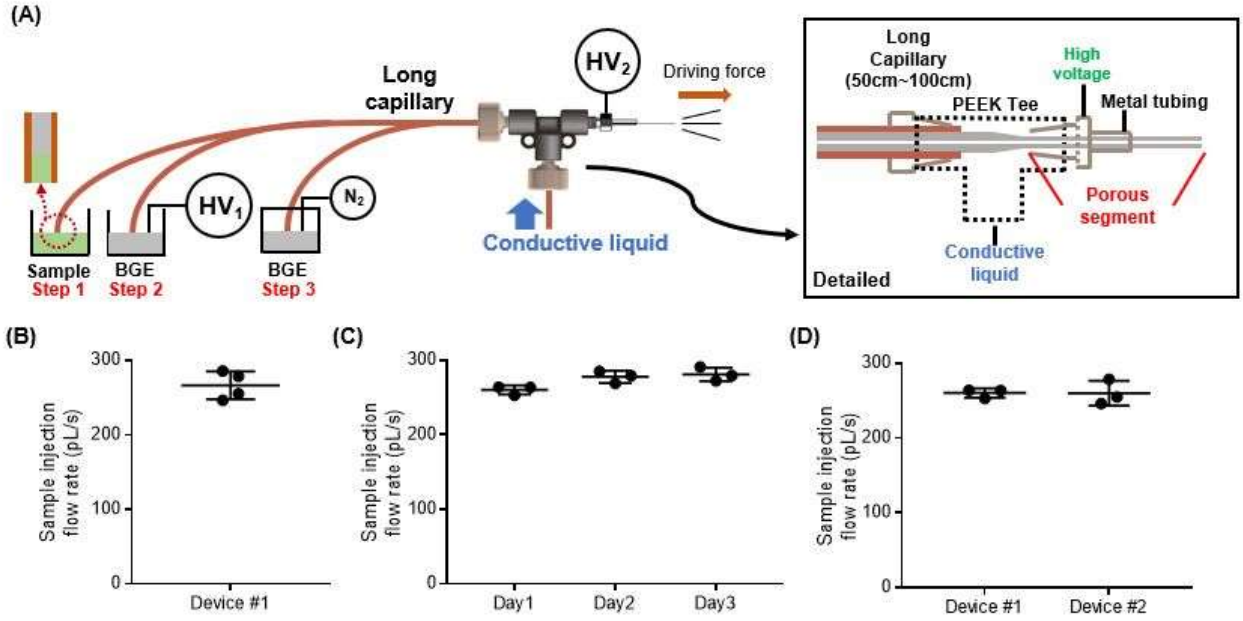

a long (*e.g.,* 50 cm) spray-capillary (**Figure 2-1**).

Figure 2-1. Schematics of the spray-capillary and reproducibility examination

(A) Schematic of the spray-capillary CZE-MS platform and detailed diagram of the sheathless CZE-MS interface. Operation steps are as follows: (1) sample is injected into the separation column; (2) high voltage was initiated for CZE separation; (3) Nitrogen flow was introduced into the BGE vial to perform gas

elution. Reproducibility was demonstrated for (B) Run-to-run, (C) day-to-day, and (D) batch-to-batch sample injection.

The performance of spray-capillary was evaluated to determine the robustness, reproducibility, and flexibility through both offline and online coupling with MS detection, Furthermore, we demonstrated that the spray-capillary can be directly inserted into a background electrolyte (BGE) solution after sample injection for online CZE-MS analysis, which holds great potential for high-throughput omics analysis of ultralow-volume samples.

2.3. Experimental Section

2.3.1 Chemicals and reagents

Angiotensin II (AngII, A9525), Syntide 2 (Syn-2, SCP0250), HPLC water (270733), ACS-reagent acetonitrile (ACN, 360457), formic acid (FA; ≥95%, F0507), and hydrofluoric acid (HF; ≥48%, 30107) were purchased from Sigma-Aldrich (St. Louis, MO). Fused-silica capillaries were purchased from Polymicro Technologies (Phoenix, AZ). AngII and Syn-2 stock solutions were prepared in HPLC water. The standard peptide mixture used here was a solution of 10 μM AngII and 10 μM Syn-2 (0.1% FA in 45% ACN in water).

2.3.2 Spray-capillary device fabrication and operation.

A long capillary (*e.g.,* 360 μm O.D., 50 μm I.D., 50 cm in length) was used to make the spray-capillary. To produce precise, clean and reproducible interfaces, both ends of the capillary (the MS end and the sample inlet end, **Figure 2-1A**) were cut using a Shortix capillary column cutter (purchased from Agilent, San Jose, CA), and were evaluated using an inverted microscope. The MS end of the spray-capillary was fabricated similarity to the previous reported sheathless interface[35]. Briefly, the outside polymer coating of the MS end (~3 cm) was removed by flame. The exposed silica was etched using a 49% HF solution at room temperature to generate a porous segment for electric contact. (Caution: HF is an extremely dangerous chemical and should be handled properly in a ventilated chemical hood.) During the etching process, the capillary was continuously flushed with water at a flow rate of 0.2-0.4 μL/min to prevent etching of the inner wall by the HF solution. After etching, the thickness of the capillary wall was approximately 5 μm. The tip shape and porous condition of the MS end of the spray-capillary was inserted into a PEEK tee connector through a short stainless steel tube (4 cm, 1/16" O.D., 0.04" I.D.) so that ~1.5 cm of the porous segment emerged from the metal tube, A continuous flow of conductive liquid (0.1% FA, 1μL/min) driven by the syringe pump was introduced into the tee to create the electric contact for generating ESI. The ESI voltage was applied to the stainless-steel tube connector through an alligator clip. The sample inlet end of the spray-capillary was either placed directly into a sample vial for sample injection or a BGE vial with a metal wire used to apply high voltage for CE separation.

2.3.3 Pressure-based sample elution setup and fabrication

After spray-capillary sample injection, an in-house sample injector was utilized to apply pressure-based sample elution for the follow-up MS detection, A PEEK tee connector was used in the in-house sample injector (details in **Figure 2-2**).

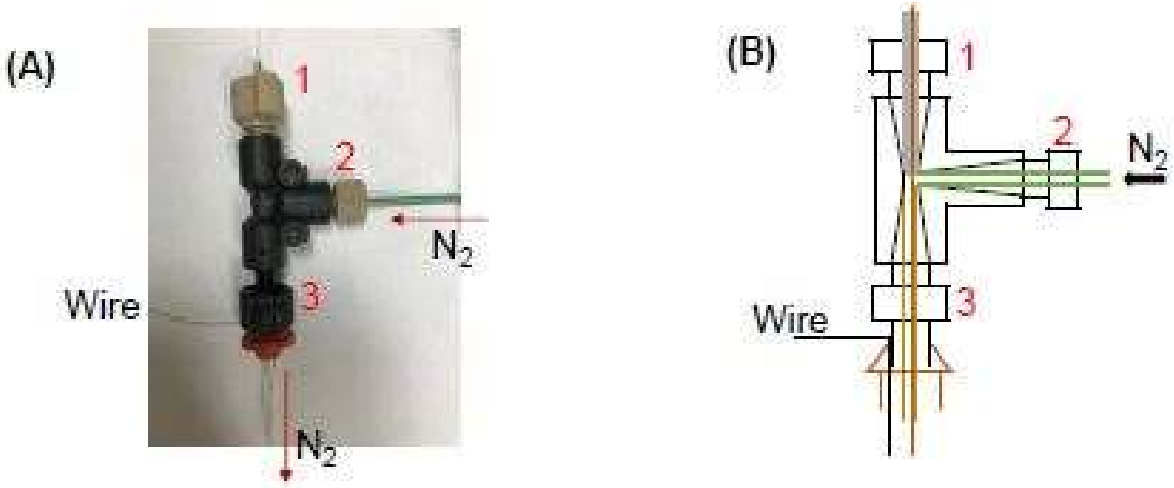

Figure 2-2. Schematic of the in-house built sample injector

The picture (A) and schematic (B) of the in-house pressure-based sample injector. The injector was built using a non-conductive high-pressure PEEK tee unit (P-727, IDEX, CA). The sample inlet end of the spray-capillary was sealed in channel 1 using a PEEK sleeve (1/16" O.D., 360 μm I.D.). Nitrogen was introduced into the TEE through channel 2 using PEEK tubing (1/16" O.D., 0.0245" I.D.). The PEEK tubing (1/16" O.D., 0.04" I.D.) in channel 3 was used to introduce nitrogen into

the sample vial. A stainless wire, used for applying the high voltage for CE experiments, was inserted from the rubber cap into the solution in the sample vial. The sample inlet end of the spray-capillary was inserted into a glass sample vial with a rubber cap to seal the inlet when pressure was applied through channel 1 and channel 3. Nitrogen was introduced into the electrospray buffer vial (i.e., 0.1% FA) through the gas inlet (channel 2) on the PEEK too to move the injected sample toward the MS end of the spray-capillary. A gas gauge (0-3 psi) was used to control nitrogen pressure for sample elution.

2.3.4 CZE separation of standard peptide mixture.

A spray-capillary (360 μm O.D., 50 μm I.D., 50 cm in length) was used for the CE separation of standard peptide mixtures. The MS end of the spray-capillary, with a 3 cm porous section, was inserted into the sheathless interface, as described above for spray-capillary-based sample injection. Then the sample inlet end was inserted into the sample vial. After sample injection, the sample inlet end of the spray-capillary was inserted into the BGE solution (0.1% FA). The CE separation was then conducted by applying 15 kV (300 V/cm) at the sample inlet end. High voltage (HV) was applied to the sample injector via a stainless-steel wire. The sample injector was assembled in-house according to **Figure 2-2**. (Attention is needed when performing experiments with high voltage. Only manual operation of HV power supply is allowed here, and all the other conductive parts in the system are grounded as needed. Proper warning signs were provided and displayed.) after a 15 min CZE separation, nitrogen was introduced

at low pressure to elute peptides. A total of 2.6 kV was used for the electrospray ionization at the sheathless interface.

2.3.5 Mass spectrometry analysis.

An LTQ Orbitrap Elite mass spectrometer was utilized for related spray-capillary experiments. The temperature of the inlet capillary was 275 °C. For pressure elution experiments, both 2+ and 3+ AngII ions were targeted with two scan ranges: 523-527 m/z for 2+ ions and 348-352 m/z for 3+ ions. Both scans were acquired at the resolving power of 120000 at m/z = 400. For the CZE-MS experiments, full MS scans were acquired at the resolving power of 120000 at m/z =400, and the auto gain control (AGC) target was set as 1E6 with maximum ion injection of 1000 ms. The scan range is 150-2000 m/z. All data files were collected in profile mode. Peak extraction was done in XCalibur using RAW files. Results were processed and plotted using GraphPad Prism. In addition, chromatograms extracted from raw data were processed using boxcar smoothing algorithms.

2.4. Results and discussion

2.4.1 Development and characterization of the spray-capillary device.

Before sample injection, the sample inlet end of the spray-capillary was placed in the sample vial with the electrospray buffer (0.1% FA). Low-pressure

nitrogen was introduced into the sample vial to fill the capillary until a droplet was observed at the MS end. Then the sample inlet end of the spray-capillary was immersed in the sample vial with standard peptide samples; the sample injection process was initiated by application of high voltage on the metal tee of the sheathless interface to generate continuous ESI (**Figure 2-1**). The sample-injection flow rate was monitored and recorded using a digital camera. A segment of the polymer coating on the sample inlet end of the capillary was removed by flame so that the capillary was transparent, and the contents could be visually observed. For the proof-of-principle experiments, H_2O was used as the column liquid and an organic solution (90% n-butanol) was used as sample so a clear boundary could be observed, as suggested in a previous study. The sample injection flow rate was calculated by measuring the injection rate of sample/column liquid interface movement in the spray-capillary (**Figure 2-3**).

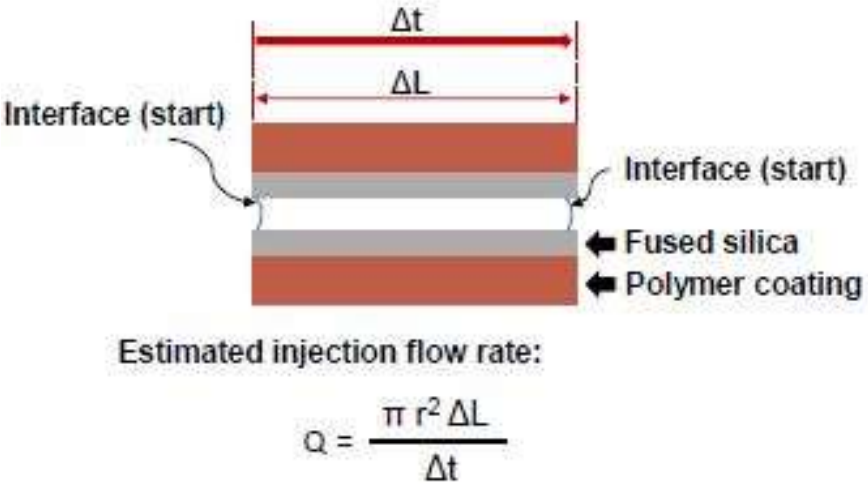

Figure 2-3. Geometry of the capillary and formula for sample injection flow rate calculation.

Sample injection flow rate estimation based on the video of the micro-sampling process using spray-capillary (https://pubs.acs.org/doi/suppl/10.1021/acs.analchem.9b04131/suppl_file/ac9b04131_si_002.mp4): Q is the sample injection flow rate; r is the capillary inner radius; ΔL us the length of the observed capillary segment; Δt is the time for liquid to flow through the capillary segment.

A 50 cm spray-capillary (360 μm O.D., 50 μm I.D.) was used for proof-of-concept experiments. Initially, to determine the primary driving force for sample injection into the spray-capillary device, a grounded copper plate was used as the spray target instead of the MS inlet to eliminate the vacuum force from the MS inlet capillary. The sample injection flow rate was estimated using the aforementioned monitoring method (H_2O as the column liquid). The results shown in **Figure 2-4**, indicate that ESI can be used along as the driving force for sample injection, with an injection flow rate of 160,7 pL/s. The vacuum of the ESI inlet can increase the sample injection flow rate to about 263.8 pL/s. However, the vacuum from the MS inlet alone does not initiate the injection procedure as there was no obvious movement of the sample boundary observed under the camera.

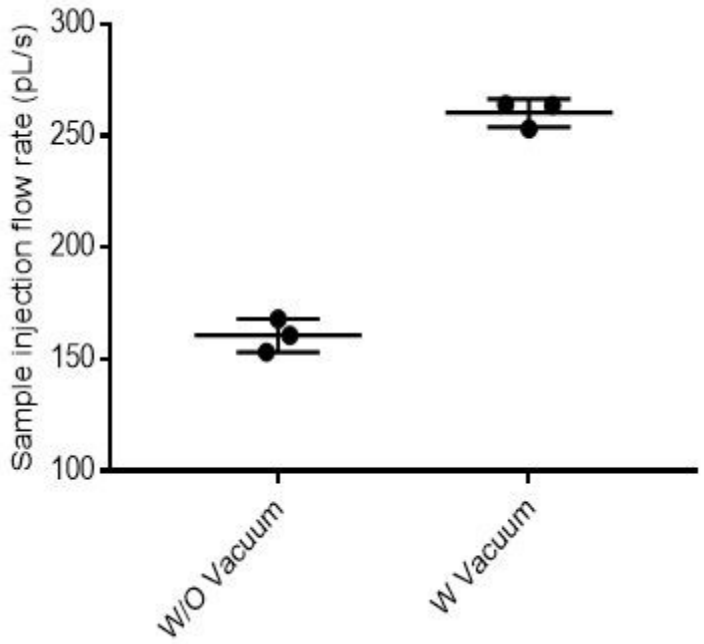

Figure 2-4. The effect of vacuum force on the spray-capillary performance.

We further evaluated the reproducibility of sample injection using the same spray-capillary and using duplicate measurements, The 50 cm spray-capillary (360 μm O.D., 50 μm I.D.) was used here with the injection voltage of 4 kV. Four individual sample injections were evaluated using the same capillary and conditions. The average sample injection flow rate in this capillary was estimated to be 255.2 pL/s and an RSD value of 4.9% was obtained demonstrating reasonable reproducibility among runs (**Figure 2-1B**). Similarly, we evaluated the day-to-day reproducibility and calculated an RSD value of 3.29% (**Figure 2-1C**). Triplicate experiments were also performed using two different spray-capillaries to determine batch-to-batch reproducibility, which yielded an RSD value of 5.8% (**Figure 2-1D**).

The effect of the viscosity of the column liquid on injection flow rate was also tested to evaluate the influence of friction on liquid motion in the capillary. For evaluation, three types of column liquids with different viscosities (H_2O, 50% ACN, 90% n-butanol, theoretical viscosities [105] are listed in **Figure 2-5**) were evaluated using the spray-capillary device; injection flow rates were calculated. Samples were chosen so that a clear boundary could be observed between the column liquid and the sample (**Figure 2-5A**). Our results (**Figure 2-5B**) suggested an inverse proportionality between flow rate and viscosity such that higher sample injection flow rates were observed for low viscosity column liquids. The increase in friction of the higher viscosity liquid may result in slower liquid motion, as suggested by Poiseuille's law [91, 106].

(A)

Sample	Column liquid	
	Solution	Viscosity
Cyclohexane	50% ACN in H_2O	0.563
90% n-butanol in H_2O	H_2O	0.891
H_2O	90% n-butanol in H_2O	2.246

(B)

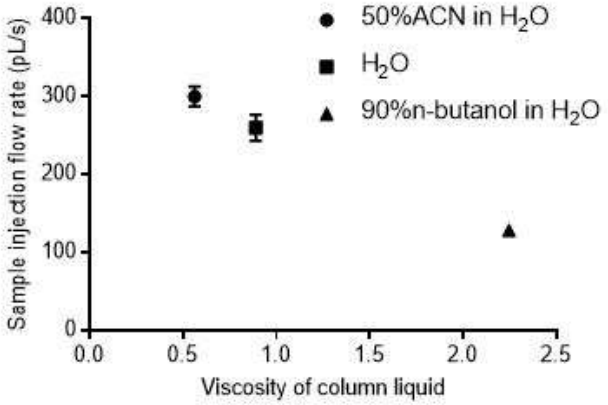

Figure 2-5. Influence from viscosity (mPa s) of column liquid.

(A) The effect of the viscosity of column liquid on the spray-capillary performance. Three types of column liquid were selected based on their viscosity. (B) The calculated sample injection flow rates were plotted against the viscosity.

2.4.2 Characterization of the spray-capillary device coupled with MS detection.

Next, we investigated the feasibility of the spray-capillary to be directly coupled with MS for quantitative sample injection and analysis. After the spray-capillary sample injection, a pressure-based sample elution step was incorporated to flush the sample through the capillary for MS detection. Briefly, nitrogen (~2.5 psi) was introduced into a glass sample vial filled with electrospray buffer (0.1% FA in 45% ACN), as described in the Experimental Section. For MS detection, 2.3-2.6 kV was used for the electrospray ionization on the metal tee of the sheathless interface.

A 100 μM solution of AngII (0.1% FA in 45% ACN) was used to characterize the efficiency of the spray-capillary (360 μm O.D., 50 μm I.D., 50 cm in length) coupled with MS detection. Sample was injected into the spray-capillary using an ESI voltage of 4 kV for 2, 15, 30, 60, and 90 s (**Figure 2-6A**). An injection time correlation plot (**Figure 2-6B**) was constructed based on the integrated peak areas of extracted ion chromatogram (EICs) of AngII 2+ ions. Good linearity (R^2 = 0.98) indicates the proposed method is quantifiable for a wide range of injection times. This result demonstrated the proposed electrospray

assisted microsampling method on a wide range of sample volume. The total injection volume ranges from 520 pL to 23.7 nL, which was estimated based on our precalculated capillary flow rates (~260 pL/s) from camera monitoring. We also evaluated the reproducibility of the spray-capillary coupled with MS detection. Triplicate experiments with 60 s injection time were demonstrated in **Figure 2-6C** with an average RSD value of 5.79%, which is comparable to previous camera-based evaluation.

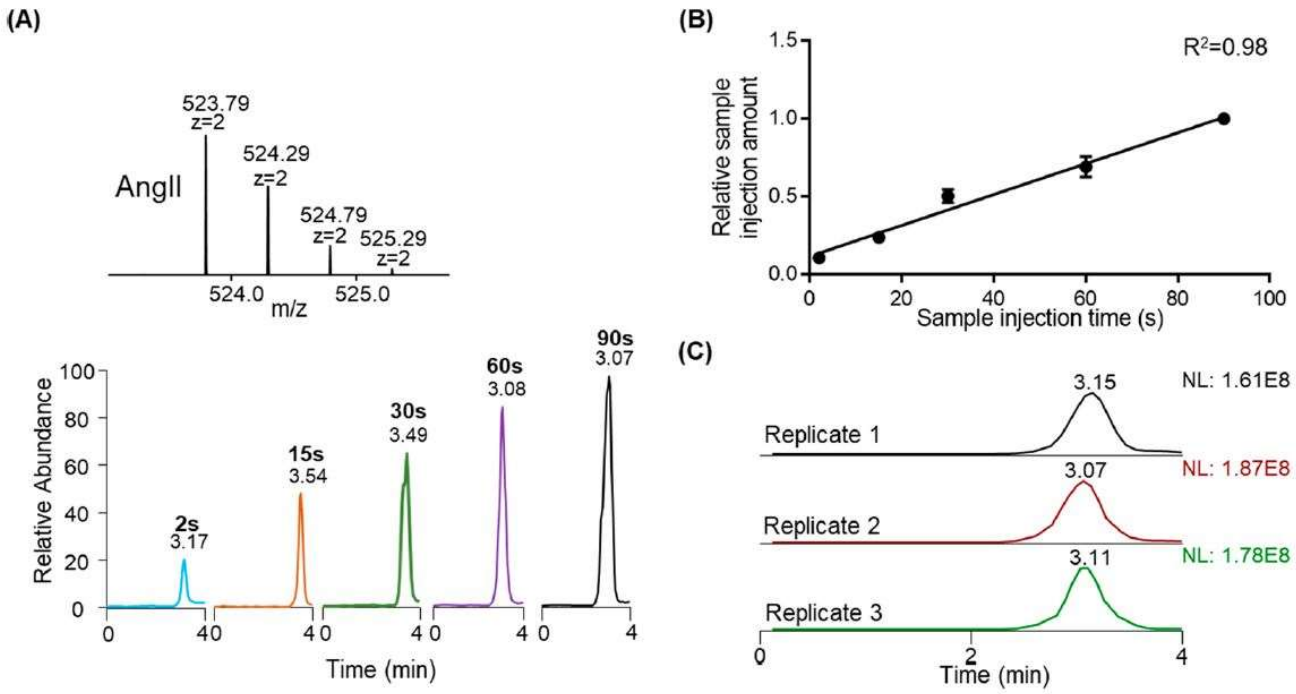

Figure 2-6. Quantitative microsampling using spray-capillary device.

Spray-capillary coupled with MS for quantitative sample injection. (A) EICs of AngII (m/z = 523.77 – 523.80) were evaluated with different injection times; (B) Calibration curve was constructed as a function of injection time (N=3 for each

experiment condition); (C) The injection reproducibility was demonstrated here using three replicated injections with 60 s injection times using the EICs of AngII (m/z = 523.77 – 523.80).

Several other parameters can be tuned to vary the rate of sample injection, such as capillary inner diameter, capillary length, and ESI voltage. (1) Capillary inner diameter: 20 μm, 50 μm, and 75 μm I.D. (other parameters of the spray-capillary device stay the same). The sample injection time was 60 s for all spray-capillaries. Our results suggested that the sample injection volume increase as the spray-capillary inner diameter increased (**Figure 2-7A**). **Figure 2-7B** shows a relatively high reproducibility (RSD = 11.3%) of detected MS signals for spray-capillary injections with 20 μm I.D. We also calculated the sample injection rate using the spray-capillary with 20 μm I.D. using camera monitoring. The estimated injection rate is 15.0 pL/s without vacuum and 48.2 pL/s when the spray-capillary was placed in front of the MS inlet. Some discontinuity in the peak shape and deviations from linearity was observed as the spray-capillary parameters were varied, which may be caused by the fluctuations of the nitrogen source. The flow resistance at the interface between the sample and running buffer under pressure may also contribute to some of the observed variation. (2) Spray-capillary length: 30 cm, 40 cm, and 50 cm (other parameters of the spray-capillary device stay the same). To minimize potential errors, we used the same spray-capillary for all the experiments by trimming the capillary from the sample inlet end to produce the desired capillary lengths while the same MS inlet end was used. The strength of the MS signal decreased as the length of the spray-capillary increased, **Figure 2-**

7C. This inverse trend may be the result of the longer plug of the column liquid present in longer capillaries, which leads to a stronger friction force and lower injection flow rate. (3) ESI voltage: 2.6 kV, 3 kV, 3.5 kV, 4 kV, and 4.5 kV (other parameters of the spray-capillary device stay the same) (**Figure 2-8D**). The voltage of 2.6 kV was the lowest ESI voltage with the 50 μm I.D. spray-capillary. The voltage of 4.5 kV was the highest ESI voltage selected because arcing started to affect the ESI process when the voltage was raised beyond this limit. A linear relationship was found between injection volume and electrospray voltage. The formation of the cone-jet depends on the balance between the surface tension of the spraying liquid and the electric field force. Therefore, a linear relationship between sample injection volume and ESI voltage is expected because, when electrospray voltage increases, the electric field force increases as well, resulting in a higher sample injection rate.

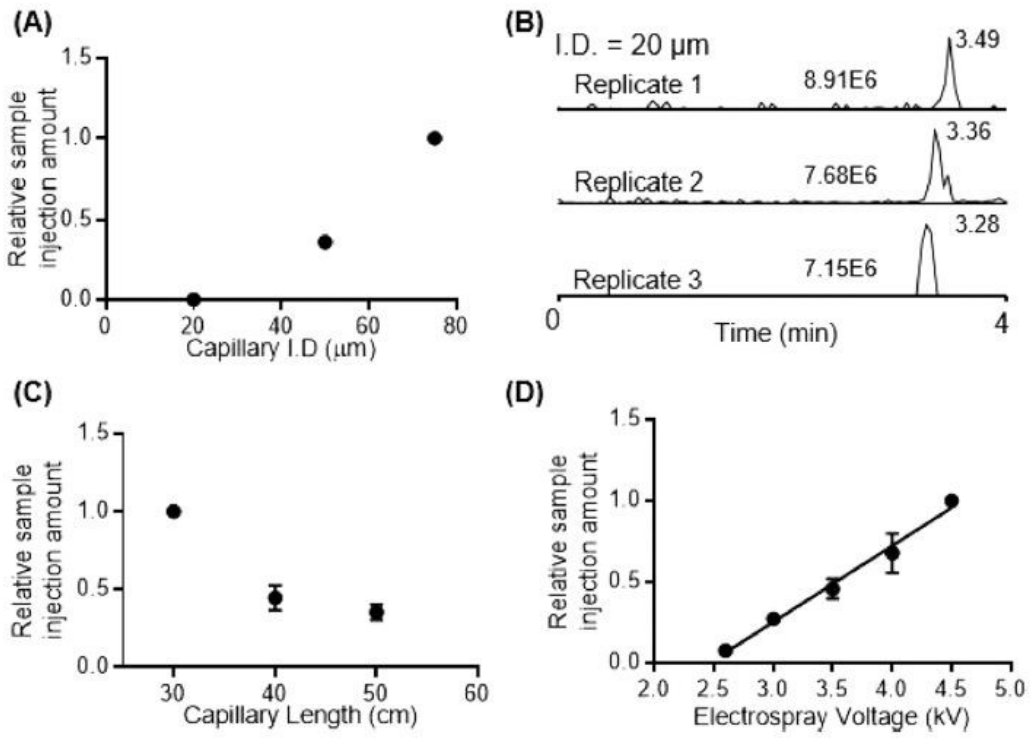

Figure 2-7. Evaluation of potential parameters on spray-capillary sample handling.

Evaluation of spray-capillary performance as (A, B) capillary inner diameter, (C) capillary length, and (D) electrospray voltage was varied. Three spray-capillary injections using 20 μm I.D. spray-capillary were plotted in (B). N = 3 and the sample injection time of 60 s was used for each experiment condition.

Other factors that may affect the spray-capillary injection process such as EOF, capillary action, and sample adherence to the surface were evaluated based on the following set of experiments (**Figure 2-8**). (1) Background experiments (evaluation of random sample injection such as capillary action or sample adherence to the surface): the sample inlet end of spray-capillary was inserted into sample vials (10, 30, and 60 s N = 3) with the application of 100 and 500 V. There voltages values were chosen because no electrospray is formed under these

conditions. This experiment can provide us with a quantitative measurement of EOF during the injection, if any EOF exists. We found that the capillary action or sample adherence to the surface does contribute a relatively small amount of the sample that is injected into the capillary during the spray-capillary process (less than 10%). The EOF effect on the tip contributes minimally to the sample injection process. Overall, our results suggest that ESI is the main driving force for our spray-capillary experiments and EOF by itself does not significantly affect the sample aspiration.

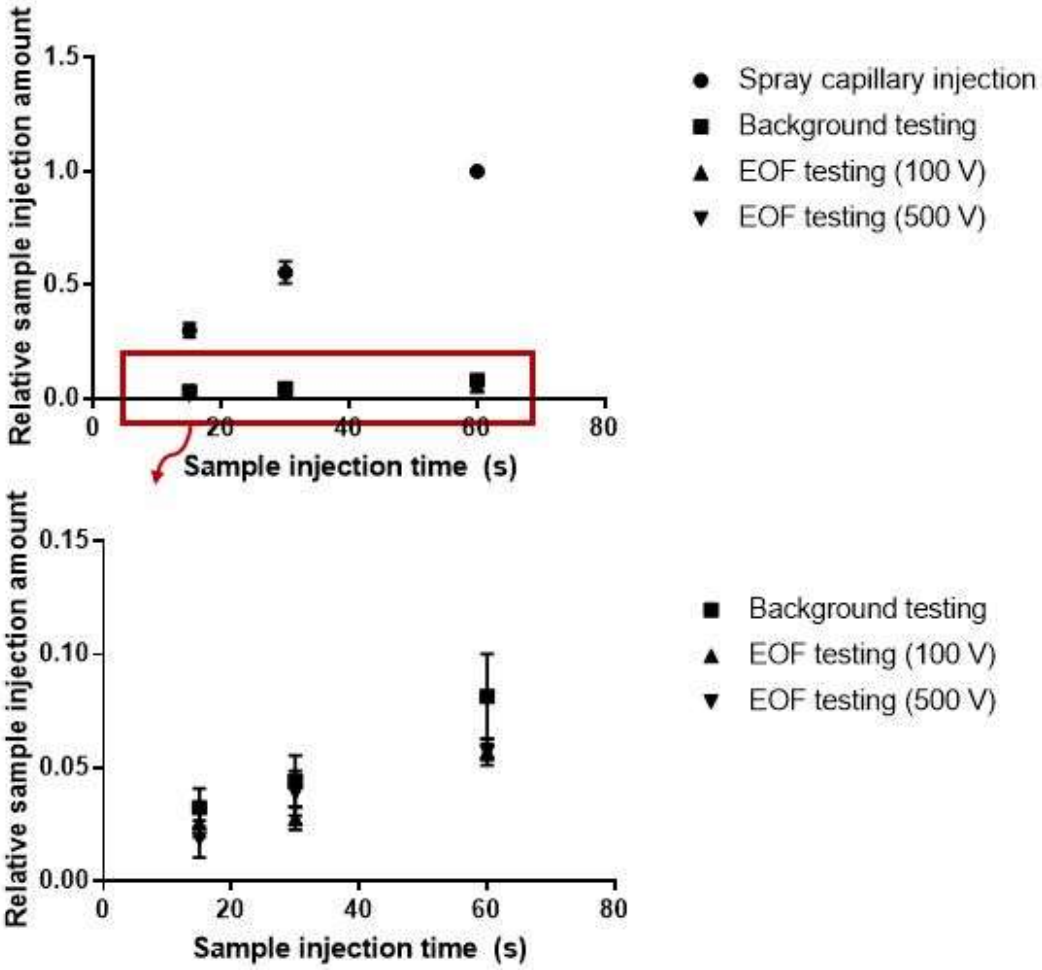

Figure 2-8. Evaluation of the influence of random injection force (*e.g.,* capillary action or sample adherence to the surface) and the EOF effect on the spray-capillary injection.

2.4.3 Direct coupling of the spray-capillary with a CZE-MS platform

One advantage of the spray-capillary device is its ability to directly serve as the CZE separation column after sample injection. The device can be directly coupled to the MS to produce an online spray-capillary CZE-MS platform. We tested the performance of the spray-capillary CZE-MS using a standard peptide mixture (10 μM AngII and 10 μM Syn-2). A bare spray-capillary (50 cm in length, 360 μm O.D., 50 μm I.D.) was used for these experiments. For sample injection, the ESI voltage was set as 3 kV, and the sample injection time was varied from 5 to 60 s (N = 3 for each condition). Baseline separation was achieved for these two peptides under these conditions. We also observed reasonably good reproducibility for both CZE-MS elution time (RSD = 9.3%) and extract ion intensities of individual peptides (RSD = 6.64% for Syn-2 and RSD = 9.71% for AngII; **Figure 2-9**). In addition, a good linear relationship between detected signals and sample injection time were detected for both AngII (R^2 = 0.93) and Syn-2 (R^2 = 0.97), indicating that spray-capillary is capable of quantitative sample injection when coupled with the CZE-MS platform (**Figure 2-9A**).

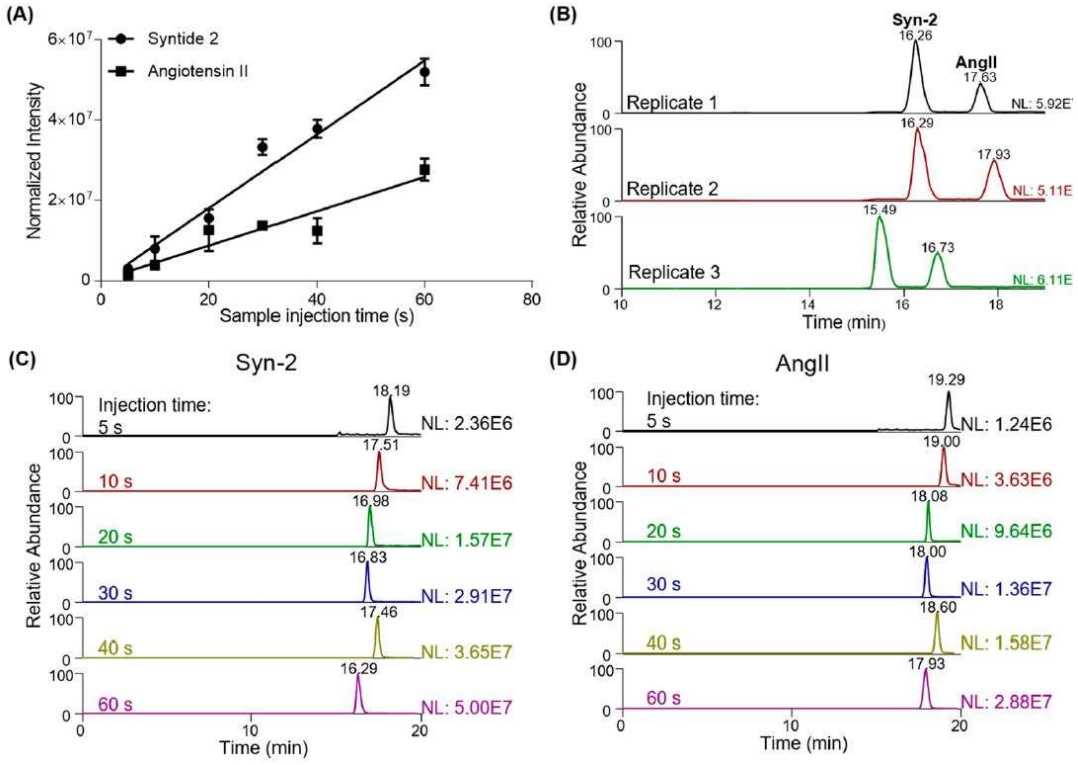

Figure 2-9. Application of spray-capillary for low-volume sample injection and CE-MS analysis. (A) Calibration of curve of standard peptides separation using the spray-capillary CZE-MS platform (N = 3 for each experiment condition). (B) Reproducibility of peptide separation using the spray-capillary CZE-MS platform. Sample injection time is 60 s for all replicates, (C) EICs for Syn-2 (m/z = 503.30-503.37) with different sample injection times. (D) EICs of AngII (m/z = 523.77-523.80) with different sample injection times.

In our proof-of-principle experiments, the calculated theoretical plate number of Angiotensin II was approximately 30, 000, which is lower than recent CZE studies using the same peptide (~300,000) [80]. To improve the separation resolution for complex sample analysis, several improvements to the CZE separation can be made. For example, experiments that utilize a longer capillary

with a smaller inner diameter combined with higher applied voltages have resulted in higher sensitivity and resolution separations of peptides and metabolites. These experiments have also demonstrated utility when the sample is limited, such as in the analysis of single cells [45]. In addition, high-quality capillary coatings such as linear polyacrylamide (LPA), have been used to improve separation power by eliminating EOF [31, 38]. We note that the performance of the spray-capillary may be evaluated and improved using the modifications described above to achieve better quantitative results.

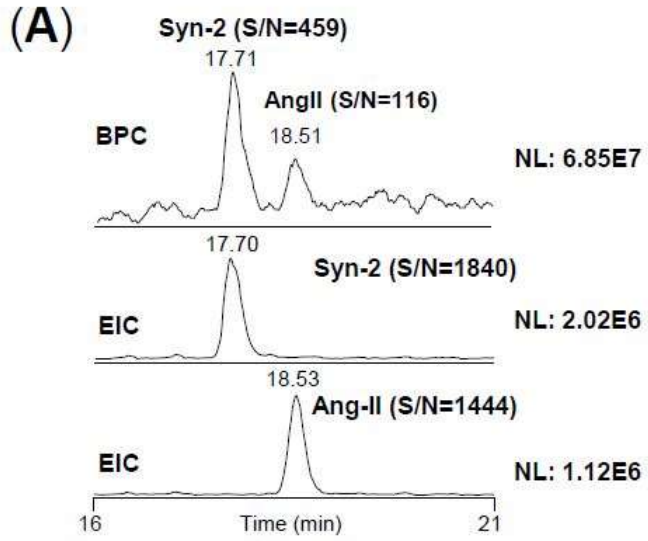

(**B**)

$$\text{Detection limit} = \frac{3\,X\ \ analyte\ injection\ amount}{S/N}$$

Trials	S/N from BPC		Detection limit (amol)	
	Syn-2	AngII	Syn-2	AngII
Replicate 1	459	116	19	75
Replicate 2	465	106	19	82
Replicate 3	703	236	12	37
Average	**542.3**	**152.7**	**16.7**	**64.7**

Figure 2-10. Evaluation of the detection limit of the spray-capillary sample injection (50 cm in length, 360 µm O.D., 50 µm I.D.) for CZE-MS. (A) An example of online peptide separation of Syn-2 and AngII (3 kV ESI voltage and 5 s sample injection time). (B) Calculated detection limits of Syn-2 and AngII based on the EICs as reported by Faserl et al[107]. (Equation above). The sample injection amount was calculated to be 2.9 fmol for both peptides. The S/N values from the BPCs were reported by XCalibur and were used for the extrapolation.

The detection limit for reproducible sample injection volume was estimated based on data collected using 3 kV ESI voltage and 5 s sample injection. The sample injection flow rate (57.8 pL/s) was estimated using the previously described video-monitoring approach. For the 3 kV and 5 s sample injection, the total injected sample volume was 290 pL, and the injection amount of each peptide was about 2.9 fmol. Based on the approach described by Faserl et al., [107] the estimated average detection limits were calculated through extrapolation and was found to be 17 and 65 amole for Syn-2 and AngII, respectively (**Figure 2-10**).

The highly reproducible separation performance of the standard peptide mixture indicates the spray-capillary holds the potential to analyze complex biological samples with optimized CE conditions such as longer columns or coated capillaries.

2.5. Conclusion

The spray-capillary is a simple quantitative microsampling approach that is capable of handling low-volume samples. In this study, we estimated the sample injection flow rate of the spray-capillary using a camera-monitoring approach. The performance of the spray-capillary was further evaluated using MS detection after sample injection. Different parameters such as viscosities of the column liquid, vacuum force, capillary inner diameter, capillary length, and electrospray voltage were evaluated. We demonstrated that the spray-capillary can directly serve as a CZE capillary after sample injection for online separation and MS detection with no additional devices. However, there is room for improvement and optimization of the CZE separation and spray-capillary device. The separation power of the system is relatively low compared to other reported CZE-MS works [43, 45] and requires further optimization (*e.g.,* background electrolyte, separation voltage, capillary coating). Additionally, a fine ESI emitter tip is required for a stable electrospray and quantitative sample injection. This spray-capillary tip is extremely fragile and requires careful handling. Despite the shortcomings the current spray-capillary CZE-MS platform, we believe that the

performance can be elevated with the usage of high-quality, coated CZE capillary (LPA-coating, PEI-coating) and the automation of the operation workflow, which would open some new avenues for analyzing biological samples. For example, a microscale fractionation method can be applied to fractionate the elution from a nanoflow RPLC separation of complex biological samples, and the low-volume fractions can be injected into the spray-capillary for the online CZE-MS analysis. Moreover, spray-capillary holds great potential for the high-throughput omics analysis of ultralow-volume samples such as single-cell mass spectrometry.

*The materials in Chapter 2 are adapted from

Huang, L., Wang, Z., Cupp-Sutton, K. A., Smith, K., & Wu, S. (2019). Spray-Capillary: An Electrospray-Assisted Device for Quantitative Ultralow-Volume Sample Handling. *Analytical chemistry*, *92*(1), 640-646.

Chapter 3: Optimization of a high-performance and automatic spray-capillary platform for microsampling and online CZE-MS

3.1 Abstract

Capillary zone electrophoresis mass spectrometry (CZE-MS) is a well-developed analytical platform for the analysis of nanoscale complex biological samples. Recently, we developed a device, the spray-capillary, for quantitative handling of ultralow-volume samples (*e.g.,* pL-nL) and online CZE-MS analysis. We demonstrated that the device is capable of quantitative picolitre level microsampling directly from a single-cell sample (*e.g.,* onion cells). Furthermore, the device can be directly used for online CZE-MS single-cell metabolomics analysis. The original spray-capillary platform is manually operated, which is relatively low throughout and requires high proficiency for consistent results. Moreover, the CZE separation resolution using the spray-capillary is relatively low for complex sample analysis. To address these challenges, we endeavored to improve the throughput and separation power of the spray capillary device. In addition, we utilized a commercially available CZE autosampler to automatically operate the spray-capillary system, and applied polymer-coated capillary to boost the separation performance. The results demonstrated that automation of the spray-capillary microsampling process allowed reproducible analysis to be performed without supervision or interruption (*e.g.,* 50 runs). Furthermore, implementation of the coated capillary allowed for automated and high throughput spray-capillary-based CZE-MS analyses.

3.2 Introduction

Many previous studies have focused on the construction of MS-based high-performance analytical platforms for nanoscale omics analysis [1, 108]. These omics analyses, however, are challenging because of the high degree of sample complexity and high dynamic range of biological samples. Therefore, a number of technological improvements had to be made to typical MS analysis platforms to facilitate the analysis of these samples. Previous improvements to the overall performance of these analytical platforms include: the application of ion mobility techniques to reduced experimental noise [54, 109]; ultrahigh-resolution separation to reduce sample complexity [95, 110]; improved sample processing strategies to minimize sample loss [74, 111]; and efficient sample handling appropriate for low-volume samples (*e.g.,* pL-nL). Further research regarding the implementation of high-throughput sample handling methods is currently being conducted to enhance the performance of MS-based nanoscale analysis.

Robotic liquid handlers have been extensively used for high throughput sample handling [112]. Because nanoscale biological samples are processed in their liquid phases, involving a liquid handler to facilitate sample preparation is a popular choice in nanoscale proteomics study [72, 113]. Advanced liquid handler instruments have been developed utilized various sampling mechanisms such as acoustics [114], flow sensors [115], and pin tools [115] to construct advanced instruments for accurately handling nanoliter volume samples; however, the cost of these liquid handlers is high (*e.g.,* > $100,000) [116].

Approaches have been reported for adapting higher volume liquid handlers for nanoscale liquid handling. A specially designed tip ,PocketTip, has been used to enable nanoscale liquid handling for assay development [112]. Additionally, a low-cost, automated pipetting system ,OT-1, that is capable of handling microliter-level samples has been modified for nanoliter sample handling (*e.g.,* as low as 15 nL) [116]. The modified OT-1 system coupled with a microfluidic chip-based trace-level sample preparation platform (*i.e.,* nanoPOTS) for proteomic profiling on low-input samples (*e.g.,* 70 *HeLa* cells). The nanoPOTS platform enables droplet sample preparation on a hydrophobic well chip for LC-MS proteomics of small volume samples (*e.g.,* ~ 200 nL) [72]. The throughput of the nanoPOTS workflow was further elevated by incorporating a modified autosampler [117]. More recently, a fully automated sample processing platform, autoPOTS (automated processing in one pot for trace samples), utilized an OT-2 liquid handler, modified autosampler, and a 10-port valve [73]. The autoPOTS sample processing was conducted in a 384-well plate. Also, other techniques such as online immobilized enzyme reactors [65]and tip-based nanoreactors [118]have been applied for high-throughput nanoscale sample processing of LC-MS nanoscale proteomics.

Elevating the throughput of microsampling process has been a trend for increasing the performance of nanoscale CZE-MS analysis have been reported [18]. Sweedler's group utilizes a dissection-based sampling protocol for single-cell metabolomics analysis [90]. However, because low-microliter volume samples are too small to be analyzed using commercial CZE autosamplers, a

custom hydrodynamic-based sample handling platform was constructed for sample loading to consistently deliver approximately 10 nL for CZE separation [60]. The throughput of this sample processing workflow was improved by implementing a pump-based microprobe platform for sampling [45]. The speed of sampling from a single frog embryo was accelerated to 5 s/cell using the microprobe approach compared to 5 min/cell using the dissection approach.

Our lab recently developed a microsampling device, spray-capillary [119], for ultralow-volume sample handling (*e.g.,* 15 pL/s) and online CZE-MS analysis. The spray-capillary utilizes electrospray ionization (ESI) to provide a vacuum-based driving force for nanoscale sample handling. Using the spray-capillary, we performed single onion cell microsampling [58] and online CZE-MS for single-cell metabolomics analysis. All spray-capillary steps in our original setup were executed manually, which requires expertise in controlling the spray-capillary platform. Although the manual protocol is robust and replicable, it significantly inhibits the throughput of the platform. Here, we present a fully automated spray-capillary CZE-MS platform to analyze low-volume samples. Our results demonstrate that continuous spray-capillary analysis can be performed without interruption or supervision (*e.g.,* 50 runs).

Moreover, the original spray-capillary device utilized bare capillary for CZE separation. It has been shown that adding polymer coating material to capillary inner wall can boosts separation efficiency by have better regulation of EOF [120, 121]. Polyethyleneimine (PEI) is a cationic polymer coating, which attracts negative changed ions in BGE solution[39]. Linear polyacrylamide (LPA) is a

neutral polymer coating, which blocks the inner capillary to decrease EOF[38]. Here, to improve the separation performance of the spray-capillary device, PEI coating is adopted due to a relatively simpler fabrication process[39].

3.3 Experimental section

3.3.1 Chemicals and reagents

Angiotensin II (AngII, A9525), Syntide 2 (Syn-2, SCP0250), HPLC grade water, HPLC grade acetonitrile (ACN, 360547), formic acid (FA, ≥ 95%, F0507), Methanol (MeOH, 34860), and hydrofluoric acid (HF, ≥ 48%, 30107) were purchased from Sigma-Aldrich (St. Louis, MO). Fused-silica capillaries (360 μm O.D., 50 μm I.D.) were purchased from Polymicro Technologies (Phoenix, AZ). Standard peptides mixture containing 10 μM AngII and 10 μM Syn-2 (0.1% FA in 45% ACN water solution) and trimethoxysilylpropyl modified polyethyleneimine (50% in isopropanol) (SSP-060, Gelest, Morrisville, PA) were used as coating material for the spray-capillary.

3.3.2 Automated spray-capillary platform

A 100 cm spray-capillary device (360 μm O.D., 50 μm I.D.) was fabricated based on our previously reported protocols [119]. The MS end of the spray-capillary was trimmed, and about 3 cm of the polymer outer layer was removed using an open flame. The exposed capillary segment was etched using 48% HF for 86 min to produce a porous segment for the sheathless style interface. Water was flushed through the capillary at 0.2 μL/min during the etching process to prevent etching of the inner wall of the capillary. A PEEK tee union was used to assemble all parts. 0.1% FA was flowed through the tee as an electric carrier to maintain stable ESI.

A CZE autosampler (ECE-001-840) by CMP Scientific Inc. (Brooklyn, NY) was used to automate the spray-capillary platform. The connection between the autosampler and spray-capillary device was described step-by-step in the discussion section. The autosampler automatically applies gas pressure and high voltage independently or simultaneously, which allows the system to be used for pressure-based elution or CZE separation.

3.3.3 Automated spray-capillary-based CZE-MS analysis of a standard peptide mixture

The spray-capillary used for CZE separation was PEI coated to boost the separation performance. The coating process was performed in-house according to a protocol available online [39]. The spray-capillary device was briefly flushed with 0.1 M NaOH, 0.1 M HCl, and D.I. water sequentially at a flow rate of 2 μL/min. During the flushing process, the porous segment was immersed in the D.I. water. Next, the device was flushed using MeOH at a flow rate of 2 μL/min while the porous segment was immersed in MeOH solution. The coating solution was freshly prepared 15 min before the coating process. Trimethoxysiylpropyl modified polyethylenimine (50% in isopropanol) (300 μL) was combined with 1.5 mL MeOH and vortexed thoroughly to make the coating solution. The device was flushed with the coating solution at a flow rate of 2 μL/min for 30 min and incubated overnight. During the coating process (*i.e.,* flushing and incubation), the porous segment remained immersed in MeOH. The device was flushed using MeOH at a flow rate of 2 μL/min for 15 min after the incubation.

A 100 cm PEI-coated spray-capillary device (360 μm O.D., 50 μm I.D.) was used for CZE separation of a standard peptide mixture. The spray-capillary-based sample handling, CZE separation, and MS detection were triggered by a customized sequence,

which will be described in the discussion section. The background electrolyte (BGE) for CZE separation was 0.1% FA ~300 V/cm electric strength (-30 kV – 2.6 kV) was used during CZE separation. The conductive liquid was 0.1% FA.

3.3.4 Mass spectrometry

An Orbitrap elite mass spectrometer (Thermo Fisher Scientific) was utilized for all CZE-MS and direct infusion analysis. The inlet capillary temperature was 275°C. MS data were collected through MS scans with a resolution of 120,000 and m/z range of 350-1350. The AGC target was 1×10^6, and 1000 ms was the max ion injection time with 2 micro scans.

3.4 Results and discussion

3.4.1 Design of the Automated high-performance spray-capillary platform

We previously designed the spray-capillary device for quantitative and reproducible small volume sampling for direct CZE-MS analysis [119]. This device, however, required manual manipulation including transferring the sample inlet end between the sample, column liquid (CL), and BGE vials, triggering electrospray ionization for nanoscale sample handling, and triggering high voltage for CZE separation. The manual manipulation required for use of the spray-capillary device limited the limited the throughput and made the system prone to human error. Moreover, the in-house platform (*e.g.,* flow generator) is complicated to operate. To address these challenges, we coupled the spray-capillary device with a commercially available, unmodified CZE autosampler (CMP Scientific Inc., Brooklyn, NY). The use of a CZE autosampler permits automated, high-throughput spray-capillary analyses (*e.g.,* direct infusion, online CZE-MS).

Additionally, it has been reported that the utilization of a polymer capillary coating (*e.g.,* LPA, PEI) can increase CZE separation performance [43, 120]. Therefore, we implemented a PEI-coating on the automated spray-capillary platform for high-performance spray-capillary CZE-MS. A schematic of the high-performance spray-capillary platform is depicted in **Figure 3-1**.

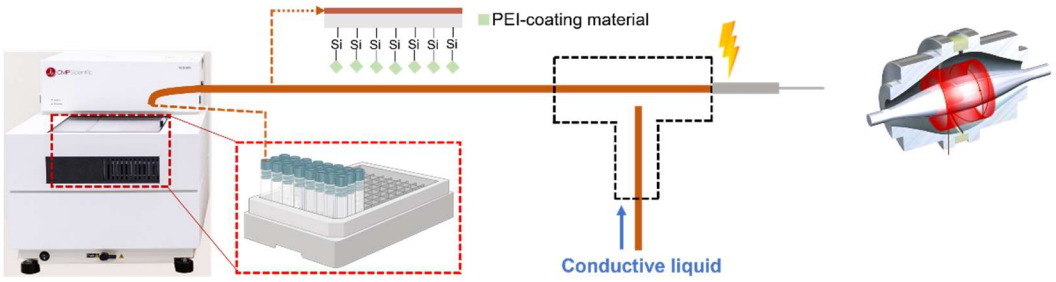

Figure 3-1. The schematic of the high-performance spray-capillary platform. The original spray-capillary device is connected to a commercially available CZE autosampler and PEI-coating material was applied.

An elevatable table was used to hold the CZE autosampler and its control computer. The height of the table was then carefully adjusted to be level with the inlet capillary so there was no height difference between the sample inlet end and the MS end of the spray-capillary. A modified nanospray ion source was used to host the sheathless interface. The sample inlet end of the spray-capillary was coupled with the CZE autosampler through a capillary inlet channel and hand-turned to tighten (over tightening should be avoided). In this way, the CZE autosampler controls the sample inlet end, while the MS end is controlled by MS instrument.

3.4.2 Fully automated spray-capillary analysis

One of the challenges for constructing an automated analysis platform is the coordination of different instruments. For this automated spray-capillary platform, the

CZE autosampler and MS instrument are coordinated through a customized sequence. A 100 cm spray-capillary (360 μm O.D. and 50 μm I.D.) device was used for all analyses. The sample injection flow rate of the spray-capillary is estimated to be approximately 270 pL/s as measured using a camera-based monitoring method described in our previous report [119].

The CZE and MS sequences are paired and contain six events including column setting (**Figure 3-2**), arm transfer (two times), spray-capillary injection, pressure elution, and column washing. The sequence starts with column setting (30 seconds); during this time the sample inlet end was placed in the column liquid and 690 mbar was applied to flush column liquid into the spray-capillary without ESI voltage application. The aim for column setting was to obtain a consistent droplet before spray-capillary injection. The second event was arm transfer (7 s); the sample inlet end was transferred from the column liquid vial to the sample vial. There was no pressure or ESI voltage during arm transfer. The third event was spray-capillary injection (6 s); the sample inlet end was in the sample vial and the ESI voltage was set at 3 kV for the electrospray assisted sampling process. The fourth event was arm transfer (7 s); The sample inlet end was transferred to column liquid vial from sample vial with the ESI voltage at 2.6 kV. The fifth event was pressure elution (378 s); the sample inlet end remained in the column liquid vial and 690 mbar was applied for elution. The ESI voltage was set to 2.6 kV during elution. The sixth event was column washing (300 s); The sample inlet end remained in the column liquid vial and 1380 mbar was applied to wash the spray-capillary device. The electrospray voltage was 0 kV. The aim for this event was to flush out potential trapped air bubbles and potential carry over. In this sequence, the time for spray-capillary injection can be adjusted based on experimental requirement. Also, several parameters (*e.g.,* elution pressure, column washing time) may be further optimized to reach better overall performance of the system.

This method was used to perform a semi-automated test to estimate the feasibility of performing spray-capillary injections using the CZE autosampler. During the semi-automated test, the timed-event segments listed in **Figure 3-2** were carried out through manual operation of the CZE computer. The result (**Figure 3-3A**) demonstrated that the CZE autosampler was capable of reproducible spray-capillary injection. Subsequently, a sequence of 50-continuous analyses was performed using a standard peptide solution (100 μM Angiotensin II). **Figure 3-3B** displays the overlap of 5 randomly selected spray-capillary injections from 50-runs demonstrating a highly similar elution profile.

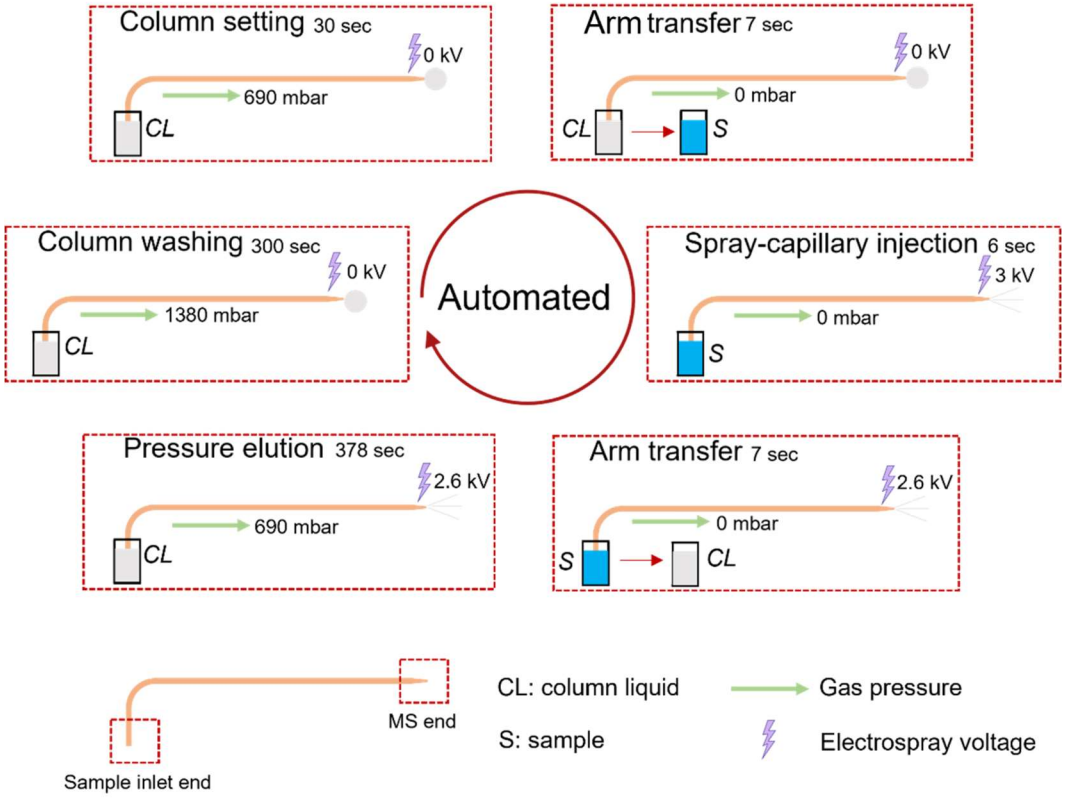

Figure 3-2. Sequence design of the automated spray-capillary platform.

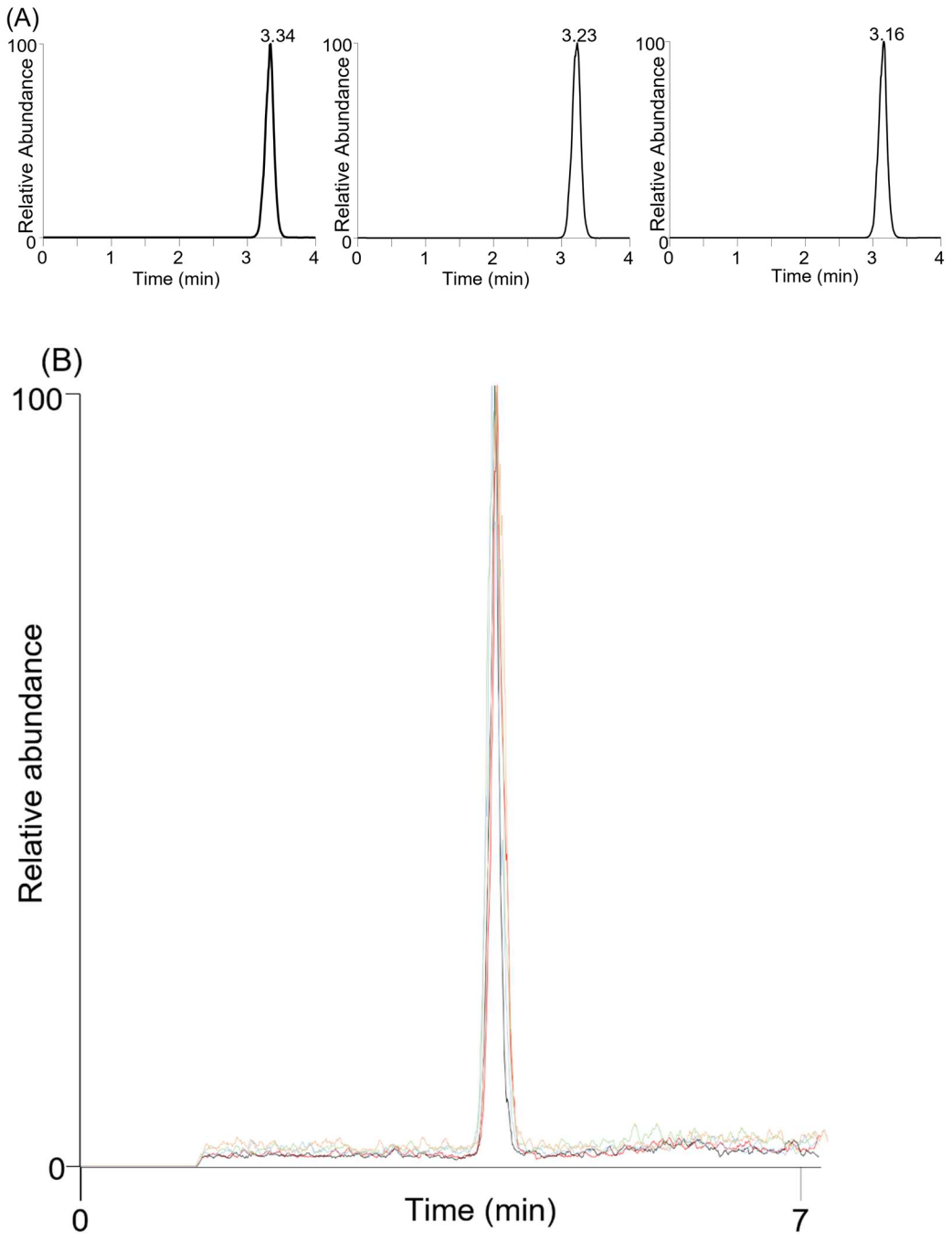

Figure 3-3. Evaluation of spray-capillary injection using CZE autosampler. (A) Triplicate trials of semi-automated injections. (B) Five randomly selected, fully automated spray-capillary injections from 50 continuous runs.

3.4.3 Performance evaluation of automated spray-capillary CZE-MS platform

Because one of the advantages of the spray-capillary is the online coupling of the microsampling process with CZE-MS analysis, we evaluated a spray-capillary-based automated CZE-MS platform for an ultralow-volume standard sample. The sequence for pressure-based elution analysis was modified for CZE-MS analysis. The pressure elution step was replaced with a period of high voltage application. -30 kV was applied to sample inlet end for CZE separation, and 2.6 kV was used to generate stable ESI. A calibration curve was constructed using this automated spray-capillary CZE-MS platform by varying the sample injection time from 6 to 90 s (N=3 for each time point). The estimated sample injection volume is from 1.6 nL to 24.3 nL. 3 kV was applied for spray-capillary-based sample loading. **Figure 3-4A** displays electropherograms of the triplicate trials using 6 s injection times. Experiments for all conditions were performed continuously without interruption. R^2 values of 0.96 and 0.99 were achieved for Angiotensin II and Syntide 2, respectively (**Figure 3-4B** and **Figure 3-4C**).

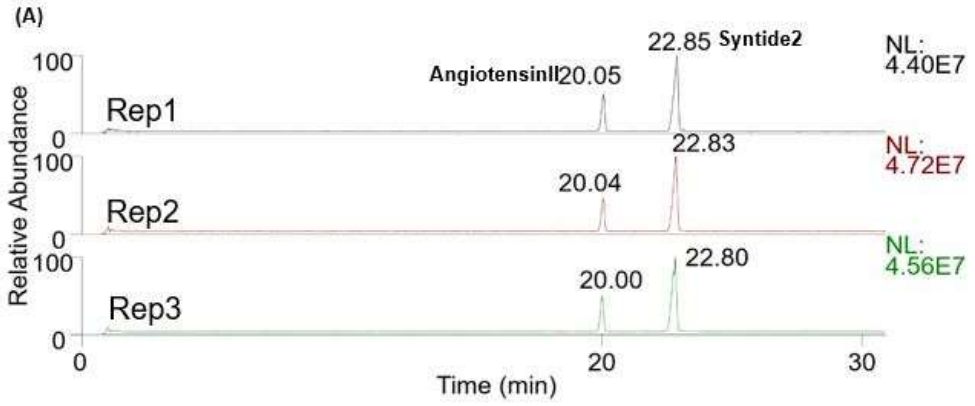

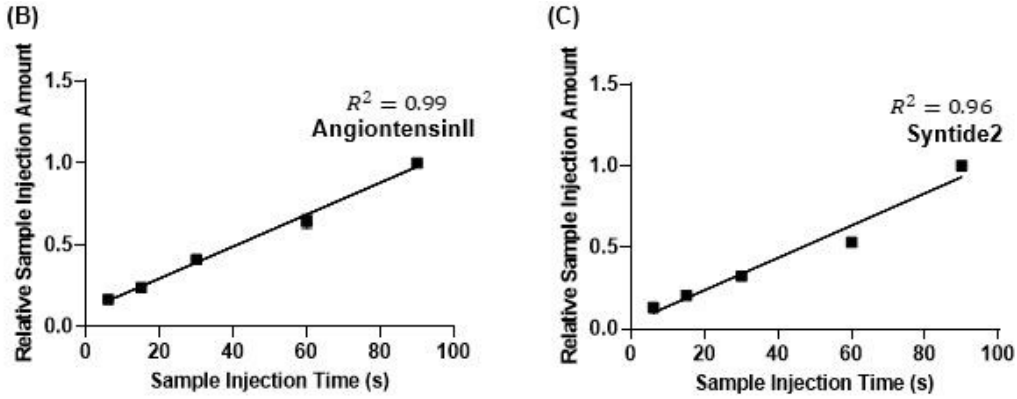

Figure 3-4. Separation of a standard peptide mixture using the automated spray-capillary CZE-MS platform. (A) Electropherograms of triplicate trials using 6 s as injection time. Calibration curve of AngII (B) and Syn2 (C) as a function of injection time.

To increase the separation power and provide a more stable electroosmotic flow (EOF) for CZE separation, polyethylenimine (PEI) was utilized as a capillary coating for CZE-MS analysis. The coating process was performed according to protocol from Sciex Inc. [39]. A standard peptide mixture (Angiotensin II, Syntide 2) was used for the proof-of-concept experiments. The comparison of spray-capillary-based CZE-MS analyses between the bared capillary device and PEI-coated device on standard peptides demonstrated that the separation performance got significantly elevated (Bare device: 19 K vs PEI-coated device 105 K for Angiotensin II), which meets our expectation (**Figure 3-5**).

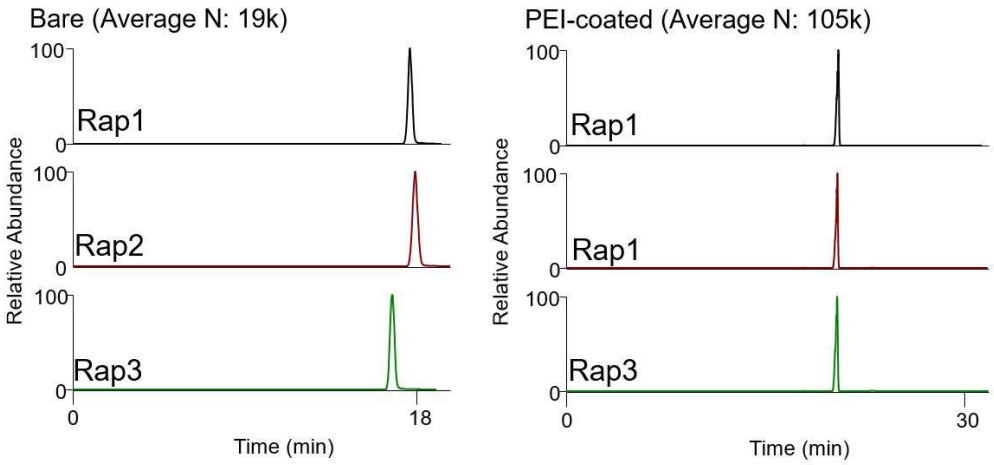

Figure 3-5. Comparison on theoretical plate number between spray-capillary-based CZE-MS analyses on Angiotensin II between bare device and PEI-coated device (N: Theoretical plate number).

3.5 Conclusion

We improved upon the original spray-capillary workflow from two perspectives: (1) throughput and (2) CZE separation performance. A commercially available CZE autosampler was utilized to automatically perform spray-capillary-based microsampling and direct MS detection. We performed 50 continuous analyses overnight without interruption or supervision. The robustness of the system was evaluated by comparing the elution profile of 5 randomly selected analysis results. Quantitative microsampling processes were automatically performed by altering sample injection times. CZE separation performance was elevated by the application of PEI coating and optimization of CZE parameter and evaluated through separating the standard peptide mixture.

We demonstrated that automated, quantitative CZE-MS on low-volume samples can be reliably performed using this automated spray-capillary platform. However, there is still room for improvement. The fabrication of the ESI tip is a primarily manual process that may limit the application of this platform. In addition, optimization of this system, such as capillary inner diameter and capillary coating condition, can be performed to further boost the performance. Current results demonstrated that the system is capable of handling and analyze low nanoliter level sample (*e.g.,* 1.6 nL), and we believe that the analysis of pL level sample is feasible through further optimization (*e.g.,* capillary inner diameter) based on previous study [119]. Overall, we believe this automated spray-capillary platform has the potential to benefit the nanoscale omics analysis and provide a high-throughput solution for the field.

Authors: Jiaxue Li, Lushuang Huang, Kellye A. Cupp-Sutton, and Si Wu

JL and LH contributed equally.

Sequence design, feasibility of the semi-automated spray-capillary, feasibility of fully automated spray-capillary, and feasibility of using PEI-coated spray-capillary device for peptide separation are performed by Lushuang Huang.

Sample injection flow rate estimation, reproducibility of the spray-capillary analyses (Semi-automated, fully automated), and quantitative peptide analysis were performed by Jiaxue Li.

Chapter 4： Spray-Capillary-Based Capillary Zone Electrophoresis Mass Spectrometry for Metabolite analysis in Single Cells

4.1 Abstract

Single-cell capillary zone electrophoresis mass spectrometry (CZE-MS) is a promising platform to analyze cellular contents and probe cell heterogeneity. However, current single-cell CZE-MS methods often rely on offline microsampling processes and may demonstrate low sampling precision and accuracy. We have recently developed an electrospray-assisted device, spray-capillary, for low-volume sample extraction. With the spray-capillary, low-volume samples (pL-nL) are drawn into the sampling end of the device, which can be used directly for CZE separation and online MS detection. Here, we redesigned the spray-capillary by utilizing a capillary with a <15 μm tapered tip so that it can be directly inserted into single cells for sample collection and on-capillary CZE-MS analysis. We evaluated the performance of the modified spray-capillary by performing single-cell microsampling on single onion cells with varying sample injection times and direct MS analysis or online CZE-MS analysis. We have demonstrated, for the first time, online sample collection and CZE-MS for the analysis of single cells. This application of the modified spray-capillary device facilitates the characterization and relative quantification of hundreds of metabolites in single cells.

4.2. Introduction

Capillary zone electrophoresis mass spectrometry (CZE-MS) has been one of the most promising techniques for single-cell analysis during the past decade [18, 55, 122-125] due to inherent advantages such as low sample loading amount (nL to μL level)[43, 121], high separation power [31, 126], and high sensitivity with online MS detection [127, 128]. Many studies have successfully applied single-cell CE-MS approaches to address biological questions such as cell heterogeneity, cell signaling, and intrinsic cellular variation [124]. However, there is still room for improvement of the overall performance of the single-cell CZE-MS, especially from the perspective of developing efficient microsampling methods for CZE-MS platforms [75].

Microdissection-based microsampling methods have been routinely used for isolating single-cell samples followed by offline manual manipulation [129]. This sampling method involves the isolation of the cell of interest from the tissue using surgical tools followed by further sample preparation steps. The Sweedler group has extensively applied microdissection methods for CZE-MS analysis of single cells including the metabolites analysis of *A. Califonica* neuron cells, which demonstrated one of the best limits of detection (LODs) of neurotransmitter metabolites among their peers at the time [52]. The same group later shared a detailed protocol of their single-cell CZE-MS platform using microdissection-based microsampling and a sheath-liquid style interface for CZE-MS [60]. They further improved the performance of the platform by incorporating

preconcentration approaches together with CZE separation [90, 130]. Sun et al. performed single-cell proteomics using microdissection followed by CZE with an electrokinetically pumped sheath-liquid interface on isolated blastomeres from different stages of *Xenopus laevis* embryos [61], and a similar strategy was used for metabolic profiling on kidney tissue [131]. Although the microdissection-based microsampling methods are mature and straightforward, relatively lengthy offline sample preparation impedes the throughput of these methods.

Nanopipettes have been heavily used during ambient ionization MS microsampling for single-cell analysis [94, 96, 132-139]. In these studies, nanopipettes (*e.g.,* μm-scale diameter) were directly inserted into single cells and the cellular contents were analyzed by MS without further separation. Nanopipettes can also be coupled offline with CZE-MS analysis of single cells. Nanopipettes (*e.g.,* μm-scale diameter) can be directly inserted into single cells for microsampling of offline single-cell CZE-MS analysis [55, 60, 84]. The Nemes group has constructed a microprobe CZE-MS platform for single-cell metabolomics, which consists of a pump-based nanopipette microsampling platform (microprobe) and a CZE-MS platform with a sheath-liquid interface [45, 140]. They successfully used this platform to probe the cell heterogeneity of the left and right blastomeres in *Xenopus laevis* embryos (8-cell stage) [141]. In addition, they reported that microsampling using this platform permits in situ analysis of individual blastomeres, which allows for the monitoring of metabolites in the same blastomere at different stage of *Xenopus laevis* embryonic development [45]. Kawai et al. utilized a similar platform for ultrasensitive single

HeLa cell metabolomics, in which the vacuum driving force was manually provided by a syringe and a thin-walled sheathless interface was utilized for the CZE-MS platform [142]. Using Kawai's platform, a total of 40 metabolites were identified and 20 amino acids were quantified. Further modifications to the nanopipette methods including electrophysiological method such as the patch clamp have also been incorporated to improve the microsampling process [143]. Meanwhile, other microsampling strategies (*e.g.,* electroosmotic flow (EOF) [62], microfluid chip [122, 144, 145], micro-junction extraction [146]) that have been coupled with CZE-MS may potentially be applied to single-cell analyses in the future.

The microsampling approaches used in the aforementioned platforms were generally coupled in an off-line fashion with the CZE-MS platform in the single-cell analysis; however, a microsampling technique capable of online coupling with CZE-MS analysis may provide more sensitive and quantitative sampling for single cells. Therefore, our group has modified our spray-capillary device for direct microsampling of single cells followed by online CZE-MS separation and analysis. The spray-capillary utilizes electrospray ionization (ESI) as the driving force for ultralow-volume sample handling (pL-nL) through a long capillary (*e.g.,* 50 cm) [119]. The spray-capillary is capable of performing quantitative, low-volume sample injection (*e.g.,* ~15 pL/s injection flow rate) by utilizing the pressure difference produced when electrospray is formed at the ESI end of the spray-capillary. The spray-capillary can directly serve as a CZE capillary for online separation and MS detection and eliminates sample loss that my occur

during offline sample handling steps of previously reported microsampling methods. Here, we redesigned the sample inlet end of the spray-capillary so it can be directly inserted into a single cell (*e.g.,* onion cell) for microvolume sample injection and CZE-MS analysis. Onion cell is a normal single-cell sample for proof-of-concept experiment since it is easy to obtain. The size of an onion cell is about 400 nL, which is also easier to handle compared to HeLa cell (volume smaller than 1 nL) [142]. We investigated the sample injection flow rate and the performance of sample extraction from single onion cells using different sample injection times to control the amount of cellular material injected, we also performed online single-cell CZE-MS analysis using the modified spray-capillary device. Overall, we demonstrated that the modified spray-capillary device can perform microsampling from single cells with on-capillary CZE-MS analysis. To our knowledge, this represents the first online single-cell CZE-MS platform.

4.3 Experimental section

4.3.1 Chemical and reagents

Red onion (Allium cepa) was purchased from a local supermarket. All chemicals such as formic acid, HPLC grade water, n-butanol, acetonitrile, hydrofluoric acid (HF), and standard metabolites (malic acid, phenylalanine, and glucose) were purchased from Sigma-Aldrich (St. Louis, MO) unless noted otherwise. The fused silica capillary with the tapered tip (SilicaTip, 50 cm length,

360 μm O.D., 50 μm I.D., and 15 μm tip size) was purchased from New Objective (littleton, MA).

4.3.2. Fabrication and operation of the modified spray-capillary device

A long pre-tapered-tip capillary purchased from New Objective was used to fabricate the modified spray-capillary. We used the tapered-tip end as the sample inlet, and the opposite end was fabricated for the MS inlet similarly to previously described [119]. First the MS end of the capillary was slightly trimmed using a Shortix capillary column cutter (Agilent, San Jose, CA). Next, the polymer coating of the MS end (~3 cm) was removed using flame. The porous segment of the MS end was produced through chemical etching using HF while water was flowed through the column to prevent etching of the inner wall of the capillary [35, 119]. To introduce the water flow into the capillary through the small sample end (*e.g.,* 15 μm tip) without damage, we inserted the tapered tip into a flow generator [119] that used nitrogen gas to produce the flow through the modified spray-capillary. The water flow was adjusted to approximately 0.2 μL/min, and the exposed segment of the MS end was submerged in 48% HF for approximately 90 min to reduce the thick ness of the capillary wall to 5 – 10 μm so that efficient electric contact through the through the porous wall to produce ESI was achieved. (*Caution: HF should be handled properly in a ventilated chemical hood.*) After etching, the capillary was thoroughly washed with water to remove residual HF. An inverted microscope was used throughput etching to monitor the thickness of the capillary. The sheathless interface for MS coupling was assembled by

inserting the capillary through a PEEK tee union, which was then pushed through a short stainless-steel tube (4 cm, 1/16 in. O.D., 0.04 in. I.D.) until about 1.5 cm of etched fused silica emerged from the metal tube, as detailed previously [119]. The performance of the etched tip on the spray-capillary was evaluated primarily by its ability to produce stable electrospray. Briefly, a microscope was used to observe the formation of the electrospray, and, for each etched tip, the injection flow rate was measured in triplicate to ensure reproducible microsampling.

4.3.3 Microsampling from single cells

Onion cells were chosen as the model system because onion is relatively easy to handle and has been extensively used in previous studies [22, 147-149]. An inverted microscope (AmScope, FMA050, CA) was used to monitor the microsampling process. The epidermal tissue was freshly peeled from the red onion and placed on a piece of parafilm. Two glass slides were used to fix the parafilm on the platform of the inverted microscope. Several drops of 0.1% FA were used to cover the target area to facilitate the sample extraction. The modified spray-capillary was prefilled with column liquid (0.1% FA) until a droplet was observed at the tip. Then, the sample inlet end was moved to the targeted cell using an in-house assembled micromanipulator consisting of two lifting platforms, one probe holder, and one tube rack for the column liquid vials placed under the inverted microscope. The microsampling process was triggered by initiating the ESI voltage on the MS end (2-4 kV). Sample injection volume was controlled by varying the sample injection time. After the microsampling process was finished,

the electrospray voltage was turned off and the sample inlet end was moved back to the column liquid. Between the analysis of individual samples, the spray-capillary device was flushed using 0.1% FA for 10 min. In addition, a blank run (column liquid) was included between sample analyses to ensure no significant contaminants were detectable from the previous sampling. New cells were probed for each sample injection. If the sample inlet becomes clogged with cell debris, the capillary can be flushed with organic solution (0.1% FA in ACN) at 40 psi, or the sample inlet end can be sonicated in organic solution (50% MeOH in HPLC grade water).

4.3.4 Pressure-based sample elution and MS detection

After single-cell sample injection using the modified spray-capillary, the same flow generator used in the etching step was utilized to apply pressure-based sample elution [119] for the follow-up MS detection. Generally, for direct infusion analysis, the extracted cellular content was eluted at 3 psi (from an in-house nitrogen source). However, fine adjustments were made (2.5-5 psi) to maintain a stable electrospray as determined by monitoring the MS signal. 0.1% FA was used as the elution buffer. The MS end of the spray-capillary was used directly to produce the ESI to introduce the sample to an Orbitrap Elite mass spectrometer (Thermo Scientific, San Jose, CA) for MS analysis, The temperature of the inlet capillary was 275°C. MS scans were acquired at a resolving power of 120 000 at m/z = 400. The AGC target was 1×10^6 with a maximum ion injection of 1000 ms. The m/z scan rage is 150-2000. All data files were collected in profile

mode. Online MS/MS sans were acquired using ITMS with collisional induced dissociation (CID) at a normalized collision energy setting of 35%. The AGC for MS/MS was 3 x 10^4, and the max ion injection time was 50 ms with 3 microscans.

4.3.5 Single-cell CZE-MS analysis

The spray-capillary device was subjected to a preconditioning procedure before single-cell CE-MS analysis. The device was flushed using 1 M NaOH, HPLC grade water, and 0.1% FA in water (Background electrolyte, BGE), consecutively. The device was flushed with each solvent for 20 min. Before single-cell microsampling, the spray-capillary was filled with BGE, the sample inlet was inserted into an intact onion cell, and the microsampling process was triggered by applying the ESI voltage (2-4 kV) on the MS end of the spray-capillary. After microsampling, the sample inlet end was moved to the sample vial containing BGE solution for online CE separation. A metal wire was inserted into the vial containing the sample inlet end of the 50 cm spray-capillary [119], and high voltage (15 kV) was applied on metal wire to facilitate CZE separation; 2.8 or 2.9 kV was used to produce electrospray at the MS end. (Note: to prevent electrical hazards, all the other conductive parts in the system were grounded as needed and proper warning signs were displayed.) The MS end of the spray-capillary was directly coupled in front of the Orbitrap Elite mass spectrometer inlet for MS analysis. The temperature of the inlet capillary was 275°C. MS scans were acquired at the resolving power of 120 000 at m/z = 400. The AGC target was 1 x 10^6 with a maximum ion injection time of 1000 ms. The m/z scan rage

was 150-2000. All data files were collected in profile mode. Online MS/MS scans were acquired using ITMS with collisional induced dissociation (CID) at a normalized collision energy setting of 35%. The AGC for MS/MS was 3 x 10^4, and the max ion injection time was 50 ms with 3 microscans. After sample analysis, the spray-capillary device was flushed using the BGE buffer (0.1% FA). A blank run (BGE buffer) was included between sample analyses to ensure no significant contaminants were detectable from previous sampling as needed.

4.3.6 Data analysis

All raw MS data sets were converted to mzML files using MSConvert [150] and processed using an in-house developed python software, For each spray-capillary MS analysis using pressure-based sample elution, all mass spectra collected during the elution window were summed, and peaks were extracted to produce a table of m/z values and intensities for each data set. To reduce random noise, all m/z values with an intensity lower than 500 were removed. For single-cell CZE-MS analysis, similar mass feature lists were generated including elution time information. The generated mass feature lists from different injection conditions (*e.g.,* various injection times) were further compared using GraphPad Prism (San Diego, CA). A mass measurement accuracy of 10 ppm was used to determine shared m/z values from different injection conditions or different runs under the same injection conditions. Significantly changed features were characterized using volcano plots.

For putative metabolite identification, mass features were searched using METLIN[151], and online metabolite-searching (https://metlin.scripps.edu/landing_page.php?pgcontent=mainPage). The mass measurement accuracy was set to 10 ppm. An onion metabolite database (a total of 280 reported onion metabolites) was created by compiling previously reported onion metabolites [152] and the human metabolome databased (filtered with "onion metabolites") [153, 154] for manual cross-checking of the metabolites putatively identified in this work to previous literature (List 4-1).

4.4 Results and discussion

4.4.1 Performance evaluation of the modified spray-capillary device

We first evaluated the sample injection flow rate of the modified spray-capillary device (**Figure 4-1A**) using a digital camera as previously described [119]. The sample injection flow rate was likely to be altered from the original spray-capillary device due to the tapered tip at the sample inlet end (*i.e.,* the inner diameter of the sample inlet tip decreased from 50 μm to less than 15 μm). In this study, H_2O was used as the column liquid while an organic solution (90% n-butanol in water) was used to mimic the sample so that a clear boundary could be monitored and recorded using the camera. The microsampling process was filmed and used to calculate the sample injection flow rate(https://pubs.acs.org/doi/suppl/10.1021/acs.analchem.0c04624/suppl_file/ac0c04624_si_002.mp4). The average sample collection flow rate was 17.72 pL/s with

an RSD value of 6.24%. This value is approximately 15-fold smaller than the original spray-capillary without the tapered tip [119] (**Figure 4-1B**). Furthermore, we evaluated the durability of the device 86 days after fabrication and found that the performance of the modified spray-capillary device was relatively unchanged after ~3 months (15.30 pL/s with an RSD value of 11.35%; **Figure 4-1C**). Likewise, the day-to-day reproducibility of the same spray-capillary was evaluated, and the average sample injection flow rate was similar on Day 1, Day 86, and Day 87.

It has been reported that different batches of nanopipette tips (sample inlet end) may result in inconsistent results for single-cell sampling, which can make reproducible sample handling challenging [96]. To determine how batch-to-batch variation might affect the performance of the modified spray-capillary, we compared the microsampling reproducibility of three separate spray-capillaries. The average sample injection flow rates for these three devices are 17.72 pL/s (RSD = 6.27%), 15.07 pL/s (RSD = 3.43%), and 16.80 pL/s (RSD = 7.21%) (**Figure 4-1D**). The high reproducibility of our single-cell spray-capillary devices is likely due to the consistency of the commercial laser-pulled sampling ends (SilicaTip Emitter) purchased from New Objective.

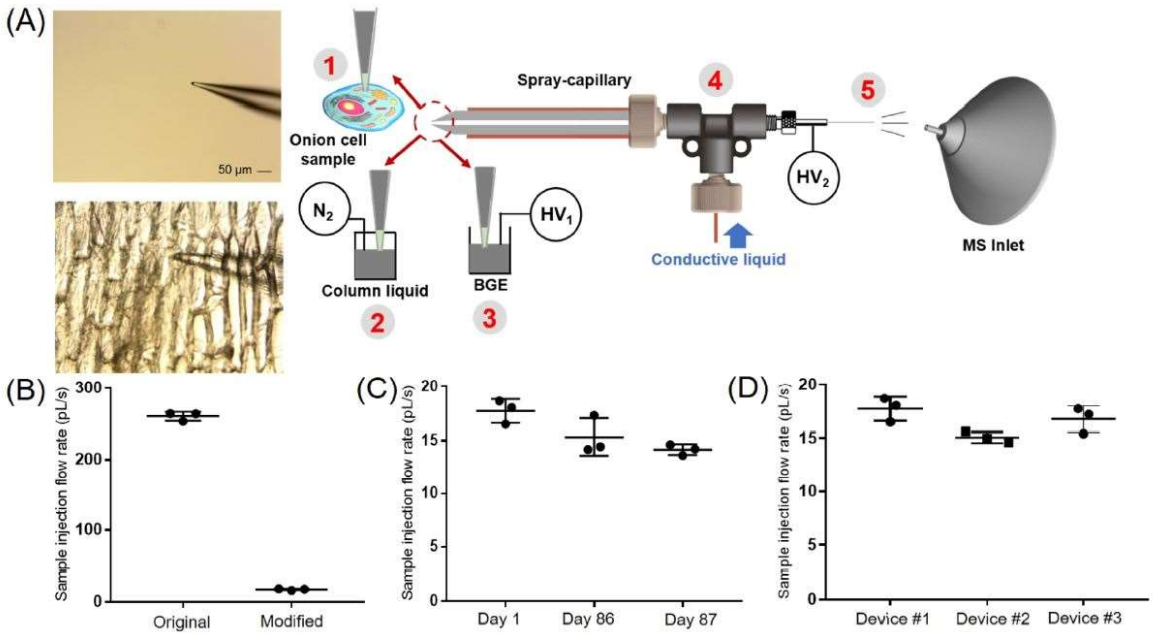

Figure 4-1. Single-cell MS analysis using the modified spray-capillary. (A) Schematic of the modified spray-capillary device for single-cell microsampling (*A. cepa*): The laser pulled sample inlet end (1) for penetrating single cells. The extracted cell content was either (2) directly analyzed by MS using an in-house built pressure generator or (3) used to perform online CE-MS analysis in the spray-capillary. The sheathless interface (4) with a porous capillary and the modified spray-capillary. The day-to-day performance (C) and batch-to-batch reproducibility (D) were also evaluated. Error bars represent relative standard deviation.

4.4.2 Single-cell microsampling coupled with MS detection

As detailed in the Experimental Section, we utilized an inverted microscope to monitor the single-cell sampling process. To avoid damaging the tip during the

sampling process, we used a piece of parafilm to hold the freshly peeled onion epidermal tissue on top of a glass slide. A proof-of-principle injection was performed in triplicate with three different onion cells. The single-cell microsampling process was triggered by initiating a 3 kV ESI voltage for 5 s on the MS end of the spray-capillary. After sample injection, the sample inlet end of the spray-capillary was inserted into the ESI buffer and extracted cellular content was pressure eluted through the spray-capillary for online MS detection (**Figure 4-2A**). The average intensity of the total ion chromatograms (TICs) in the elution window was determined as the area under the curve (AUC), which was 1.45 x 10^8 with an RSD value of 10.69%. With the same elution pressure, the elution time of the single-cell components was highly reproducible (3.01 ± 0.13 min). The summed mass spectra for these three replicates are displayed in **Figure 4-2B**. In total, 1895 mass features were detection in these three replicate injections and 822 of these mass features were detected in all three runs.

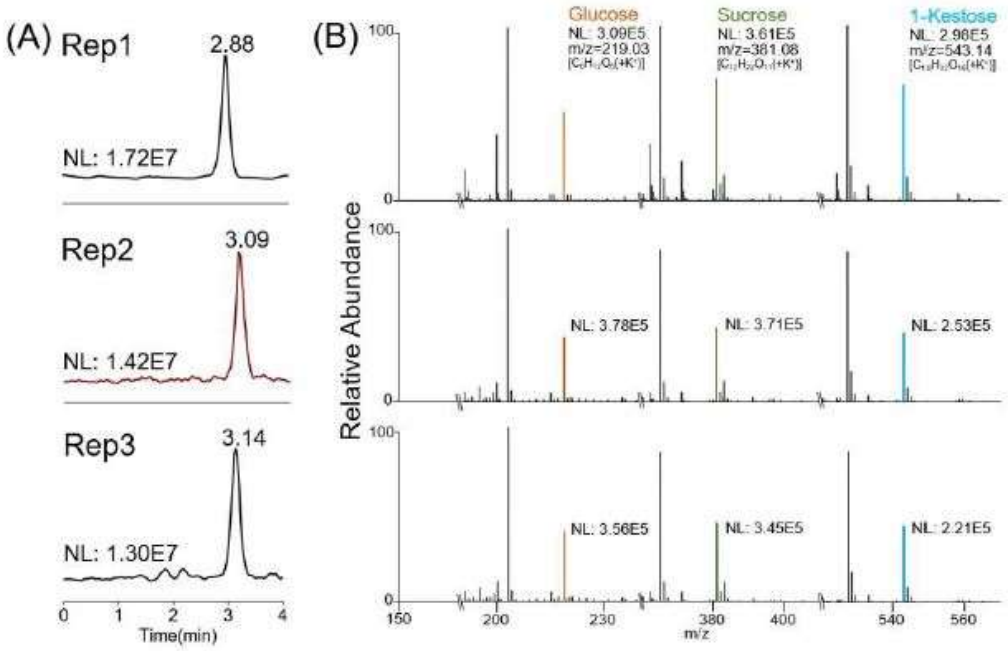

Figure 4-2. Triplicate sample extraction from A. cepa single cells using the modified spray-capillary device. (A) Total ion chromatograms from three replicate single cell injections; (B) the summed spectrum of the eluted peak from each analysis. The spray-capillary used is a 360 μm O.D X 50 μm I.D. long capillary (50 cm in length) with a tapered tip at the sample inlet end. For sample injection, the electrospray voltage was 3 kV, and the sample injection time was 5 s (NL: normalization level).

We evaluated the performance of the modified spray-capillary utilizing different sample injection times (2, 5, and 10 s) to determine if the device can be applied to relative quantification of single-cell metabolites (**Figure 4-3**). A 3 kV electrospray voltage was used to collect the sample for all runs, and experiments were performed in triplicate for each sample injection time. According to the previously measured sample injection flow rate, the estimated sample extraction volume is about 32-160 pL at 3 kV ESI voltage (average volume of onion epidermal cells is ~30 nL [155, 156]). We evaluated the reproducibility for each sample injection time using triplicate analysis. Using a 2 s sample collection duration, a total of 1939 mass features were detected; 837 mass features were detected in all three runs and 1354 mass features were detected in at least two runs. At 5 s, a total of 1895 mass features were detected; 822 mass features were detected in all three runs, and 1330 mass features were detected in at least two runs. At 10 s, a total of 2248 mass features were detected; 1276 mass features were detected in all three runs, and 1706 mass features were detected in at least two runs (**Figure 4-3A**). Some runs appeared to be more similar than others

performed under the same conditions demonstrating more similar mass feature identifications. This variation in reproducibility may be due to natural variation in onion cell contents and probing different regions of the cell. Still, we are encouraged by the relative metabolite quantification for single cells using our modified spray-capillary.

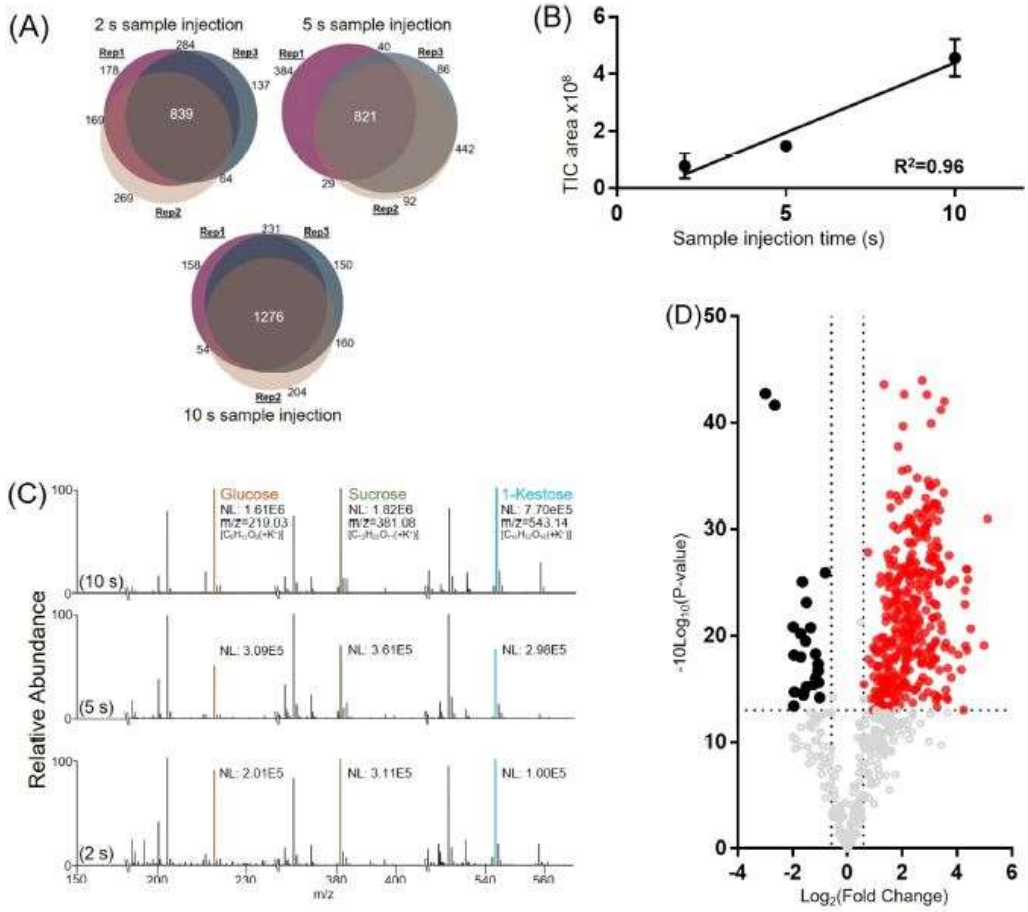

Figure 4-3. Sample extraction from *A. cepa* single-cell samples using the modifies spray-capillary device. (A) Venn diagrams comparing mass features (intensity > 500) in the elution window among triplicate trials for each sample injection time (2, 5, and 10 s). (B) Calibration curve demonstrating intensity as a function of sample injection time (n = 3 for each sample injection time). The error bars

represent the relative standard deviation. (C) Representative mass spectra from different sample injection times (2, 5, and 10 s) labeled with putatively identified metabolites (NL: normalized intensity). (D) Volcano plot for comparing detected shared mass features between the 2 and 10 s sample injection times (red and black: fold change > 1.5, p value < 0.05, red dot indicates increased fold change, black dot indicates decrease fold change (10 s vs 2 s)).

We then studied the effect of sample injection time on the total amount of cellular material injected from a single cell. A good linear relationship ($R^2 = 0.96$) was observed when correlating the area under the curves (AUCs) of the total ion chromatograms (TICs) to the sample injection time (**Figure 4-3B**), indicating that the amount of cellular material injected has linear proportionality with the sample injection time. We averaged the MS scans over the entire elution range for each injection time (**Figure 4-3C**) and found that the detected mass feature patterns were similar, but the intensity increased linearly with injection time. For example, simple sugar (*e.g.,* monosaccharides or oligosaccharides) are commonly observed with high abundance in onion cells [152]. Three high-intensity peaks that were observed in all MS spectra were confirmed to be monosaccharides or oligosaccharides that are known carbohydrates in onions. The detected m/z of 219.0281 is the potassium adduct ion of the monosaccharide (glucose or fructose). Its sodium adduct ion was also detected with high intensity. Similarity, the potassium adducts ions of a disaccharide (m/z = 381.0825, possibly sucrose) and a trisaccharide (m/z = 543.1560, possibly 1-ketose) were detected together with

their sodium adduct ions. The intensities of these detected ions increased with increased injection time.

We further compared the intensities of all the shared mass features in the 2 and 10 s injection time runs using a volcano plot (**Figure 4-3D**) and found that a majority of the detected mass features (357 in 620) have significantly higher abundance (p value < 0.05 and fold change > 1.5) in the 10 s injection time run. This further suggests that a higher quantity of cellular material was injected into the spray-capillary with longer injection times. We note that some detected mass features have similar abundance or decreased abundance with longer injection time. To further evaluate the source of these mass features, the buffer was analyzed (N = 3) to detect any impurities that may be mistaken for onion metabolites (**Figure 4-4**). Unique mass features detected in the buffer were selected and compared with mass features detected in the onion sample. The volcano plot (**Figure 4-3D**) revealed 163 mass features that were not upregulated with increased injection volume. These 163 mass features were compared with the buffer control, and 122 (~75%) mass features were detected in both the onion sample and the buffer control. This result confirmed that these mass features may originate from impurities in the buffer and instrumental noise.

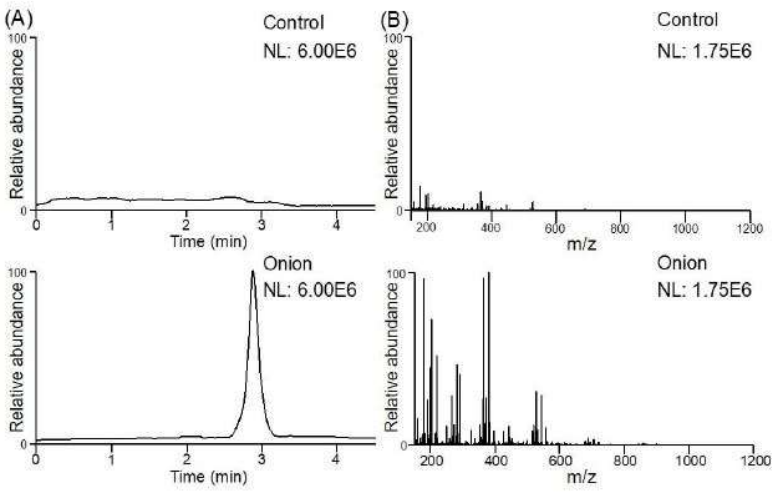

Figure 4-4. Comparison between control (buffer) and normal (onion) trial. (A) Normalized base peak chromatogram of control and onion trial. (B) Normalized averaged spectrum of control trial and onion trial. NL: normalized level.

4.4.3 Putative metabolite identification in single onion cell analysis

A total of 3247 mass features were detected from nine pressure elution runs (2, 5, and 10 s injection time, triplicate runs for each injection time). Among these mass features, 510 were detected in all nine runs. We searched these 510 shared mass features using the METLIN [151] databased for putative metabolite identifications and found possible hits for 441 mass features. Among them, 80 putative METLIN identifications with low m/z values were confirmed by manual cross-checking with previously reported onion metabolites (**List 4-2**). Also, among the 367 upregulated mass features between the 10 and 2 s injection time runs, 62 were confirmed to be onion metabolites by cross-checking with previous literature (**List 4-3**). We selected 6 putative identified metabolites that have been

reported previously in onion samples (*A. cepa*) and plotted their detected intensities across different injection times (**Figure 4-5**). The amount of metabolite injected is proportional to the injection time as demonstrated by the linearity between peak intensity and injection time. The relatively large standard deviations may result from variation attributed to cell-to-cell heterogeneity. Our results suggested that the modified spray-capillary is capable of performing relative metabolite quantitation analysis at the single-cell level, which may provide better insights into biomarker characterization and cell-to-cell variation. Because some low-abundance metabolites may not be detected in shorter sample injection times (2 and 5 s), we also searched the 1276 mass features detected in the 10 s injection time trials using METLIN and putatively assigned 978 potential metabolites, 148 of these metabolites were also previously reported onion metabolites.

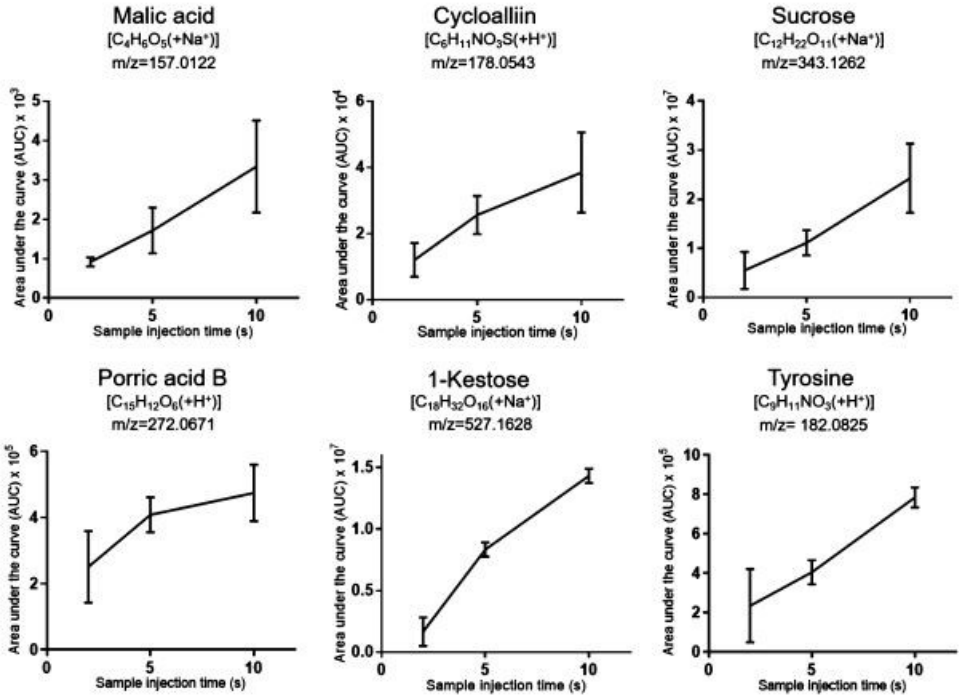

Figure 4-5. Single-cell MS analysis (onion cells) with different sample injection times using the modified spray-capillary. Triplicate injections were performed for each injection time, and the error bars represent the relative standard deviation between the measurements.

4.4.4 Spray-capillary-based single-cell CZE-MS analysis

We have previously demonstrated that the spray-capillary can directly serve as a CZE separation capillary after microsampling for online separation and quantitative MS detection without additional devices. Here, we performed single-cell CZE-MS analysis using the modified spray-capillary. An example CZE-MS analysis of a single onion cell using the modified spray-capillary is shown in **Figure 4-6** (3 kV injection ESI voltage and 10 s sample injection time, ~160 pL of injected volume). Most of the detected metabolites were eluted between 3- and 16-min. Representative metabolites with their extracted ion electropherograms (EIEs) were selected to evaluate the CZE separation performance. Many detected metabolites were efficiently separated with an intensity range from 1.89×10^3 to 7.81×10^5, demonstrating a good dynamic range of detection by the single-cell CE-MS analysis using the modified spray-capillary. A single-cell CE-MS experiment using our modified spray-capillary takes approximately 15-20 min.

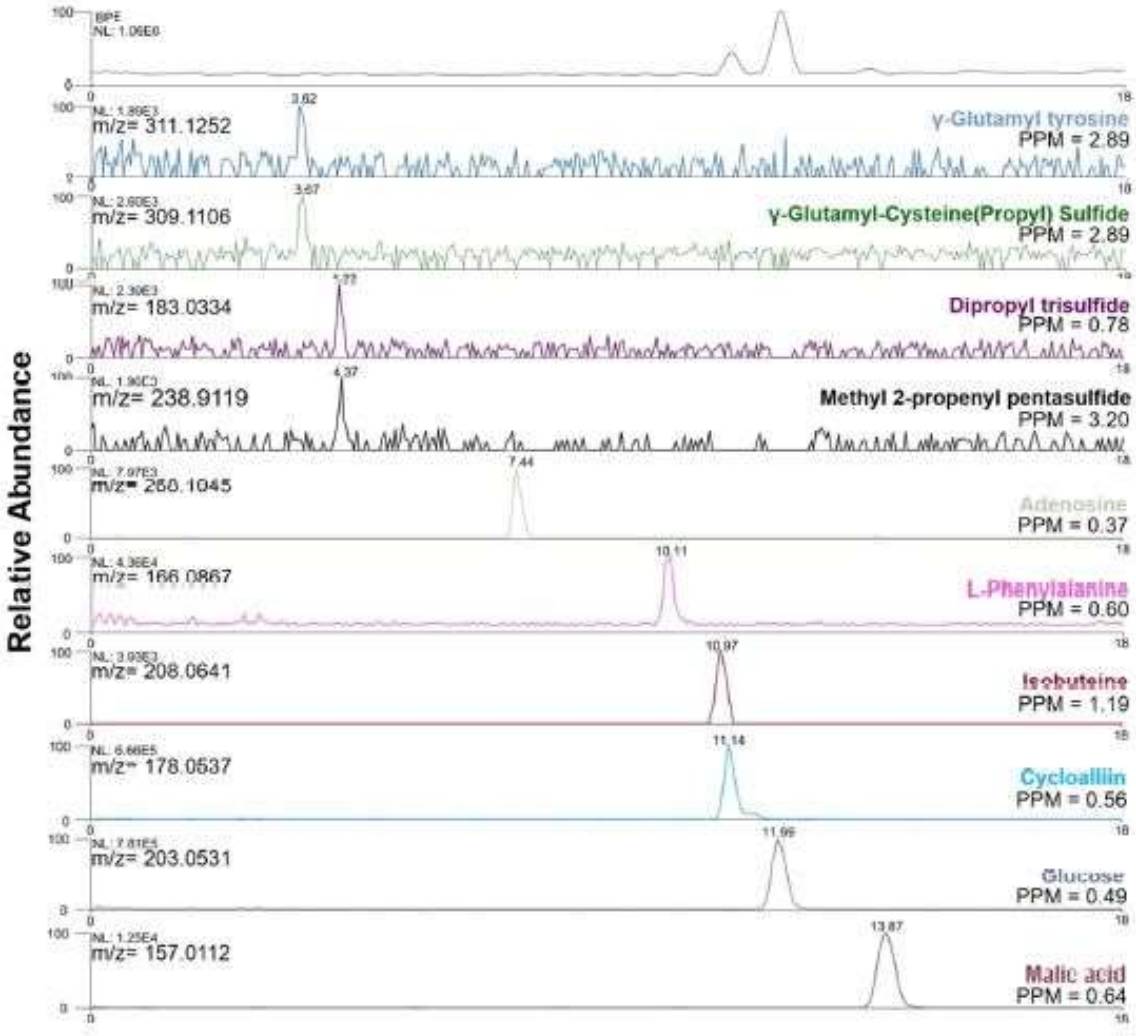

Figure 4-6. Example extracted ion electropherograms (EIEs) of putatively identified metabolites using spray-capillary-based single-cell (onion cells) CZE-MS analysis (NL: normalized intensity).

Figure 4-7 shows extracted EIEs from replicate trials using 3 kV as the electrospray voltage and 10 s as the single-cell sample injection time. Six putative identified metabolites were evaluated in three individual single-cell CZE-MS analyses on the basis of their relative migration times and measured intensities (**Table 4-1**). The migration times of all metabolites were normalized according to

the migration time of malic acid in the corresponding run. The RSD of the relative migration times was less than 10% for each putatively identified metabolite. The measured peak areas of the same metabolites in different cells were also compared. RSDs of the peak areas for 5 of the 6 metabolites were less than 20%, which demonstrates the cell-to-cell reproducibility using the modified spray-capillary with online CZE-MS analysis. However, a lightly higher variation of the peak area RSD of phenylalanine was observed (RSD = 35.3%), which may be attributed to cell-to-cell metabolite variation. Interestingly, a shoulder peak was repeatedly observed on the extracted in electropherogram for cycloalliin (Putatively assigned). It has been reported that the cycloalliin possesses a structural isomer [157] (*e.g.,* alliin, isoalliin) in onion, and the shoulder peak may be a result of the separation of the isomers. In total, 2407 mass features were detected from replicate single-cell CZE-MS experiments. Among them, 1620 were putatively assigned by searching METLIN and 163 were previously reported onion metabolites (**List 4-1** and **List 4-4**). the mass features detected here that were not identified as onion metabolites may be the product of instrument or ambient chemical noise or impurities from the buffer solutions used to facilitate the microsampling and separation processes. We further compared the identification result between CZE-MS analysis and direct infusion and observed 349 overlapped mass features. Among these 349 mass features, 324 were putatively assigned using METLIN. To confirm that the spray-capillary CZE-MS device can be used to confidently identify metabolites, a selection of standard metabolites (phenylalanine, glucose, and malic acid) was analyzed, and the results

were compared with the putative identification result from the onion cells. Relative migration times (normalized by the migration time of malic acid) are list in Table 4-2. The relative migration time for the phenylalanine ion [$C_9H_{11}NO_2(+H^+)$] in the single onion cell CZE-MS/MS analysis was 0.703 (RSD = 4.97%), which is comparable with the measured migration time for the standard phenylalanine sample. 0.754 (RSD = 0.80%). Similarly, the relative migration time for the measured glucose ion [$C_6H_{12}O_6(+Na^+)$] in the single onion cell CZE-MS/mS analysis is 0.849 (RSD = 2.41%), and the measured migration time for the standard glucose sample is 0.872 (RSD = 1.18%). Additionally, the online CZE-MS/MS fragmentation was used to confirm the identity of the metabolites in both the standard mixture and the onion cell (**Figure 4-8**). Additional MS/MS examples from the single-cell CZE-MS/MS analysis are listed in **Figure 4-9**. The proof-of-principle experiments suggested that the CE migration time and online CZE-MS/MS results can improve the identification confidence in single-cell spray-capillary-based CZE-MS analysis.

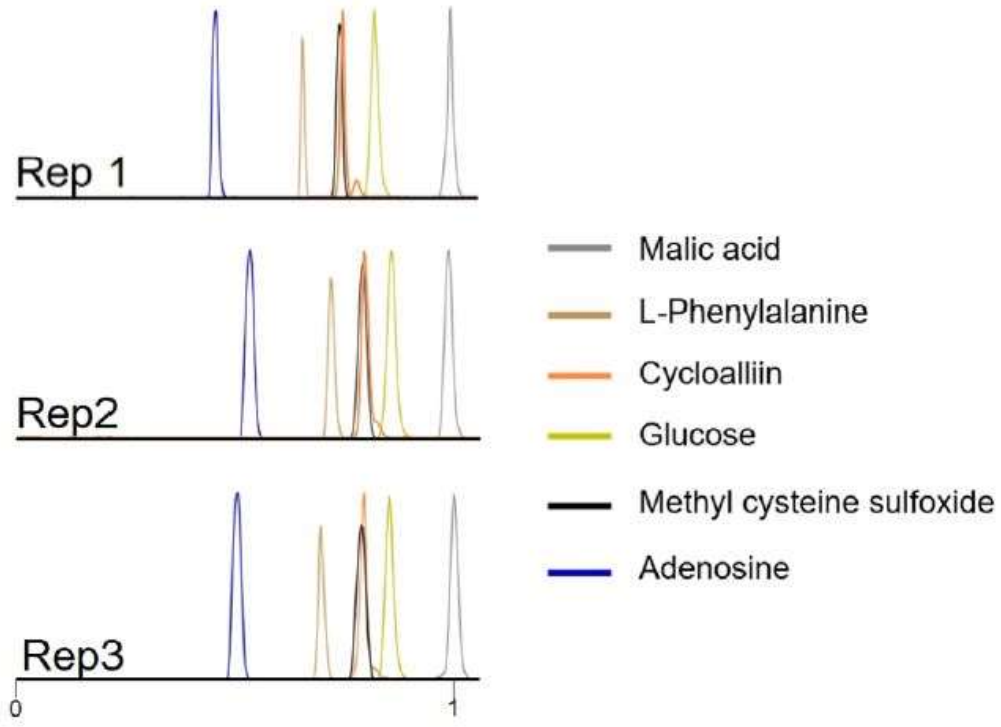

Figure 4-7. Representative extracted ion electropherograms (EIEs) of putatively identified metabolites in replicates single-cell CZE-MS runs (malic acid [$C_4H_6O_5$ + Na^+], L-phenyalanine [$C_9H_{11}NO_2$ + H^+], cycloalliin [$C_6H_{11}NO_3S$ + H^+], glucose [$C_6H_{12}O_6$ + Na^+], methyl-cysteine sulfoxide [$C_4H_9NO_3S$ + H^+], and adenosine [$C_{10}H_{13}N_5O_4$ + H^+]). The migration time of each metabolite was normalized with the migration time of malic acid.

Metabolite	Replicate #	Peak area	RSD (Peak area)	Relative migration time	RSD
Malic acid [$C_4H_6O_5(+Na^+)$]	R1	2.98E5	17.0%	1	N/A
	R2	2.62E5		1	
	R3	3.66E5		1	
Phenylalanine [$C_9H_{11}NO_2(+H^+)$]	R1	2.62E5	35.3%	0.664	4.89%
	R2	5.20E5		0.728	
	R3	5.49E5		0.717	
Cycloalliin [$C_6H_{11}NO_3S(+H^+)$]	R1	1.08E7	16.3%	0.752	3.85%
	R2	9.72E6		0.806	
	R3	1.33E7		0.802	
Glucose [$C_6H_{12}O_6(Na^+)$]	R1	1.64E7	16.8%	0.824	2.63%
	R2	1.40E7		0.867	
	R3	1.96E7		0.858	
Methyl cysteine sulfoxide [$C_4H_9NO_3S(+H^+)$]	R1	1.58E5	3.78%	0.748	3.79%
	R2	1.49E5		0.801	
	R3	1.48E5		0.798	
Adenosine [$C_{10}H_{13}N_5O_4(+H^+)$]	R1	7.67E4	10.7%	0.459	8.61%
	R2	7.82E4		0.540	
	R3	6.39E4		0.529	

Table 4-1. Characterization of metabolites using spray-capillary CZE-MS system.

Trials	Replicate #	Relative migration time	
		Phenylalanine	Glucose
Standard metabolites mixture	Rep1	0.755	0.884
	Rep2	0.760	0.870
	Rep3	0.748	0.864
Average (Standards)	N/A	0.754	0.872
RSD (Standards)	N/A	0.80%	1.18%
Onion extracts	Rep1	0.717	0.858
	Rep2	0.664	0.826
	Rep3	0.730	0.864
Average (Onion extracts)	N/A	0.703	0.849
RSD (Onion extracts)	N/A	4.97%	2.41%

Table 4-2. Relative migration time comparison between standard metabolites and corresponding onion metabolites.

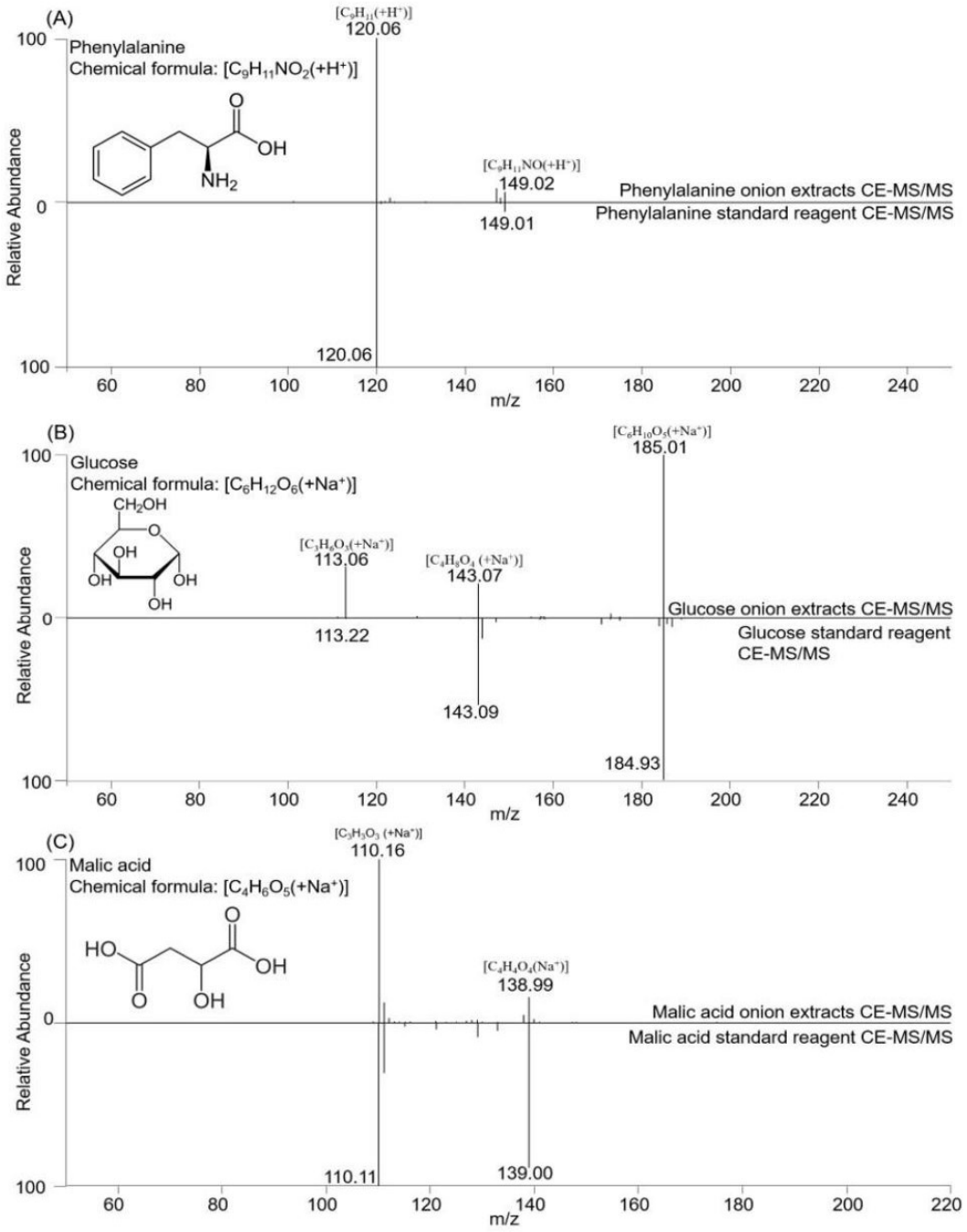

Figure 4-8. MS/MS comparison between onion extracts and standard reagent. (A) phenyalanine, (B) glucose with sodium adduct, and (C) malic acid with sodium adduct.

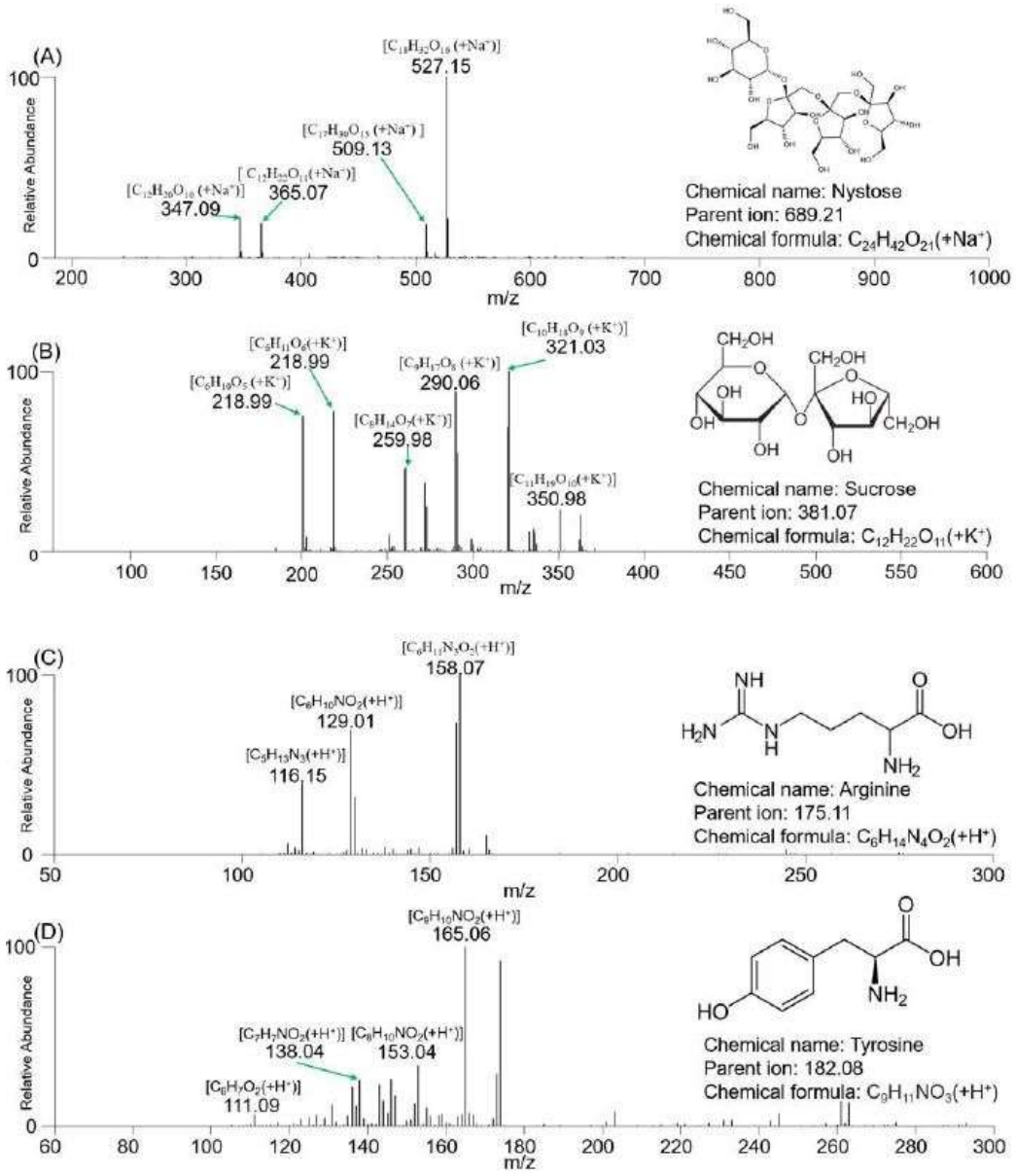

Figure 4-9. MS/MS spectra of putative identification result. (A) nystose (DP4) with sodium adduct, (B) sucrose with potassium adduct, (C) arginine, and (D) tyrosine.

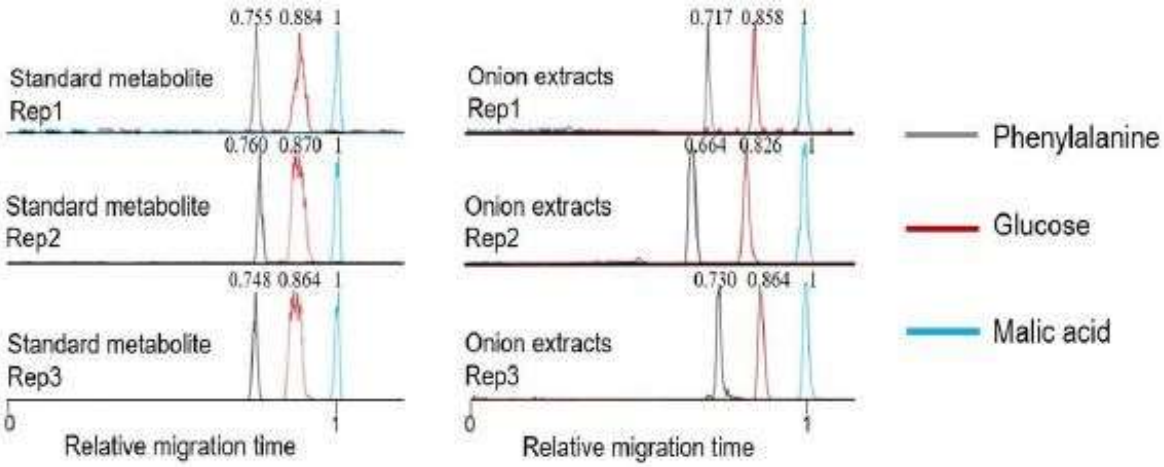

Figure 4-10. CZE separation of standard metabolites and comparison with same metabolites from onion extracts.

Overall, our results demonstrate that metabolites can be reproducibly separated using the on-capillary CZE-MS separation, and the single-cell metabolite profiling is similar between different single onion cells. Also, with the elimination of any intermediate steps between microsampling and sample injection for CZE separation, the while workflow has been largely simplified with minimized sample loss. The CZE-MS provides separation of metabolites prior to MS detection and allows additional mass features to be detected with increased signal-to-noise ratios when compared with direct infusion experiments. However, some mass features were only detected in the direct infusion experiments. These compounds may bind more strongly to the column and may not elute within the detection window. In addition, a bare capillary was used in our proof-of-principle

experiments, and some metabolites may adsorb to the negatively charged capillary wall, which may result in loss of signal.

4.5 Conclusion

Here, for the first time, we demonstrated a platform for online single-cell CZE-MS analysis using the modified spray-capillary device. The simple and straightforward transition from microsampling using the modified spray-capillary device to CZE separation largely eliminates potential contamination and/or sample loss introduced by intermediate or offline sample handling steps. The robustness of the proposed device was investigated by measuring sample injection flow rate directly after the device was fabricated and after ~3 months. Batch-to-batch reproducibility was also studied by comparing the injection flow rate of three independently fabricated devices. Microsampling on single onion cells with MS detection was evaluated using various sample injection times, and single onion cell CZE-MS analysis was successfully demonstrated. The modified spray-capillary device separated and putatively identified hundreds of metabolites; however, the system currently relies on manual operation, which requires caution throughout the process since the laser pulled tip (sample inlet end) as well as the MS end (porous interface) are both damage-prone. Future improvements to spray-capillary-based single-cell CZE-MS analysis may be made to improve CZE separation performance, for example, the application of coating material (*e.g.,* linear polyacrylamide, polyethylenimine)[38, 158] and the increase in capillary

length or electric filed strength[45]. High quality coating processes can also help avoid the formation of unwanted adduct ions in the CZE-MS analysis. Despite these weaknesses, the modified spray-capillary electrospray-assisted microsampling and CZE-MS analysis platform was capable of metabolite analysis at the single-cell level. The throughput of this system can be elevated by automation and motorization. More importantly, with smaller laser pulled tips (8 μm or smaller), the simple design of the spray-capillary device may allow it to be applied to different types of single-cell samples (*e.g.,* human cell lines), and the device holds great potential for the field of single-cell metabolomics.

*The materials in Chapter 4 are adapted from

Huang, L., Fang, M., Cupp-Sutton, K. A., Wang, Z., Smith, K., & Wu, S. (2021). Spray-capillary-based capillary electrophoresis mass spectrometry for metabolite analysis in single cells. *Analytical Chemistry*, *93*(10), 4479-4487.

Chapter 5 Overall summary and future directions

5.1 Overall summary

This dissertation describes the process of developing and applying a novel microsampling device for online CZE-MS analysis for omics study. There is a desire to perform an MS-based nanoscale omics study is growing stronger each day because of the potential to reveal heterogeneity that was masked by bulk measurement. Being able to quantitatively handle a sample at an ultralow-volume range (*e.g.,* pL-nL) can significantly benefit the nanoscale omics field.

Chapter 2 showed the characterization process of the spray-capillary device. The idea was to use an ESI process to provide a vacuum-based driving force to handle an ultralow-volume sample (*e.g.,* pL-nL). The device was fabricated based on a sheathless interface design. When the electrospray is triggered, a pressure difference will be created across the long capillary, which can be used to perform the quantitative ultralow-level sample injection. This electrospray-assisted sample handling process is reproducible and tunable. Moreover, the same device can be directly used for CZE-MS analysis, which offers a new solution for performing nanoscale quantitative CZE-MS analysis.

In Chapter 3, the original spray capillary device was upgraded in two ways: its throughput and separation performance were improved. The throughput of the spray-capillary workflow was improved by incorporating a CZE autosampler, while the separation performance of CZE was boosted by applying a capillary

coating (*i.e.*, PEI). Combing these two steps, we constructed a high-performance automated spray-capillary platform for the analysis of a picolitre to nanoliter sample.

We further applied this electrospray-assisted sample handling concept to the microsampling field for single-cell metabolomics analysis in Chapter 4. The sample inlet end of the original spray-capillary was laser-pulled to reach a size of 15 μm to perform microsampling directly from a single onion cell sample. This microsampling process was first coupled with direct MS detection through a pressure-based elution step to improve the reproducibility and quantitative performance of the microsample process. Eighty detected mass features were cross verified as onion metabolites. This modified device enabled us, for the first time, to combine an online microsampling process with CZE-MS analysis for single-cell metabolomics analysis. More than 160 detected mass features were cross verified as onion metabolites. The confidence of putative identification results was elevated by a relative migration time comparison and targeted MS/MS comparison between the selected metabolite from onion extracts and its standard reagent.

5.2 Future directions

Sample handling and microsampling processes play vital roles for the application of CZE-MS for a nanoscale omics study. The current high performance of the CZE-MS platform suggests this is a promising tool for performing nanoscale proteomics and identifying thousands of peptides from nanograms of a sample. Additionally, the development of sample processing

approaches allows for efficiently preparing samples with a low number of cell populations, particularly with a nanoliter-level total volume. The spray-capillary device can connect a sensitive CZE-MS platform with nanoscale sample processing approaches to increase the overall sensitivity of the CZE-MS methodology for nanoscale proteomics. In addition, the automated, high-performance spray-capillary platform demonstrated the electrospray-assisted sample handling method can be applied to high-throughput analysis with the help of a commercially available CZE autosampler.

Single-cell analysis can resolve the cell-heterogeneity that bulk-style analysis could not achieve. Single-cell analysis is challenging because the complexity of the cell content and extremely low sample volume (*e.g.,* pL-nL). This CZE-MS platform has been a powerful method to conduct single-cell metabolomics. The development of a novel microsampling approach facilitates the overall workflow and promotes CZE-MS–based single-cell metabolomics. The modified spray-capillary device greatly simplified the workload of sample delivery by an online couples microsampling process with CZE separation, which, at the same time, reduced the risk of sample loss. With a smaller I.D. of the laser-pulled tip, the platform can be used for different kinds of cells. Moreover, with an improved sample handling platform such as a motorized capillary manipulator, high-throughput CZE-MS single-cell analysis is achievable.

Appendix

Chemical name	Chemical formula	Monoisotopic mass
Allyl alcohol *	C_3H_6O	58.0419
1-Propene-1-thiol *	C_3H_6S	74.0190
1-Propanethiol *	C_3H_8S	76.0347
Methanedithiol *	CH_4S_2	79.9754
Tiglic aldehyde *	C_5H_8O	84.0575
Divinyl sulfide *	C_4H_6S	86.0190
3-(Methylthio)-1-propene *	C_4H_8S	88.0347
Ala **	$C_3H_7NO_2$	89.0477
Thial-1-Propene-1-thiol S-oxide *	C_3H_6OS	90.0139
Cibulins *	C_3H_8OS	92.0296
2,4-Dimethylfuran *	C_6H_8O	96.0575
(Z)-4-Hexenal *	$C_6H_{10}O$	98.0732
2-Methyl-1-propenethiol *	$C_5H_{10}S$	102.0503
g-Aminobutyric acid **	$C_4H_9NO_2$	103.0633
Choline **	$C_5H_{14}NO$	104.1075
Ser **	$C_3H_7NO_3$	105.0426
Dimethyl selenide *	C_2H_6Se	109.9635
S-Methyl methanesulfinothioate *	$C_2H_6OS_2$	109.9860
2,5-Dimethylthiophene *	C_6H_8S	112.0347
Di-1-propenyl sulfide *	$C_6H_{10}S$	114.0503
Pro **	$C_5H_9NO_2$	115.0633
1-Propenyl propyl sulfide *	$C_6H_{12}S$	116.0660
Val **	$C_5H_{11}NO_2$	117.0790
xi-2-Methyl-1,3-oxathiane *	$C_5H_{10}OS$	118.0452
Dipropyl sulfide *	$C_6H_{14}S$	118.0816
1,1-Diethoxyethane *	$C_6H_{14}O_2$	118.0994
Thr **	$C_4H_9NO_3$	119.0582
1,3-Dithiane *	$C_4H_8S_2$	120.0067
Methyl propyl disulfide *	$C_4H_{10}S_2$	122.0224
1-(2-Furanyl)-2-propanone *	$C_7H_8O_2$	124.0524
Dimethyl trisulfide *	$C_2H_6S_3$	125.9632
5-Hydroxymethyl-2-furancarboxaldehyde *	$C_6H_6O_3$	126.0317

pyro-Glu **	$C_5H_7NO_3$	129.0426
Pipecolic acid **	$C_6H_{11}NO_2$	129.0790
Leu **	$C_6H_{13}NO_2$	131.0946
Asn **	$C_4H_8N_2O_3$	132.0535
3-Mercapto-2-methylpentanal *	$C_6H_{12}OS$	132.0609
Orn **	$C_5H_{12}N_2O_2$	132.0899
Asp **	$C_4H_7NO_4$	133.0375
Malic acid **	$C_4H_6O_5$	134.0215
3-Mercapto-2-methylpentanol *	$C_6H_{14}OS$	134.0765
Cys (Me) (Deoxymethiin) **	$C_4H_9NO_2S$	135.0354
Methyl 2-propenyl selenide *	C_4H_8Se	135.9791
(Z)-S-1-Propenyl methanesulfinothioate *	$C_4H_8OS_2$	136.0017
Ethyl isopropyl disulfide *	$C_5H_{12}S_2$	136.0380
Tyramine **	$C_8H_{11}NO$	137.0841
1,2,3-Trithiane *	$C_3H_6S_3$	137.9632
Trigonelline **	$C_7H_8NO_2$	138.0555
Furfuryl acetate *	$C_7H_8O_3$	140.0473
Methyl methylthio selenide *	C_2H_6SSe	141.9355
Methyl 2-thiofuroate *	$C_6H_6O_2S$	142.0089
2-Vinyl-4H-1,3-dithiine *	$C_6H_8S_2$	144.0067
Pro Betaine (N,N-Dimethyl-Pro) **	$C_7H_{14}NO_2$	144.1025
(E,E)-Di-1-propenyl disulfide *	$C_6H_{10}S_2$	146.0224
Gln **	$C_5H_{10}N_2O_3$	146.0691
2,3-Dimethylbenzofuran *	$C_{10}H_{10}O$	146.0732
Lys **	$C_6H_{14}N_2O_2$	146.1055
Glu **	$C_5H_9NO_4$	147.0532
1-Propenyl propyl disulfide *	$C_6H_{12}S_2$	148.0380
2,4,6-Trimethyl-1,3,5-dioxathiane *	$C_6H_{12}O_2S$	148.0558
xi-1-(Propylthio)-1-propanethiol *	$C_6H_{14}S_2$	150.0537
(S)C(S)S-S-Methylcysteine sulfoxide (Methiin) *	$C_4H_9NO_3S$	151.0303
a-Phenylglycine **	$C_8H_9NO_2$	151.0633
Methyl 2-propenyl trisulfide *	$C_4H_8S_3$	151.9788
2-Isopropyl-6-methoxypyrazine *	$C_8H_{12}N_2O$	152.0950
(E)-S-1-Propenyl thiosulfate *	$C_3H_6O_3S_2$	153.9758
Methyl propyl trisulfide *	$C_4H_{10}S_3$	153.9945
His **	$C_6H_9N_3O_2$	155.0695

S-Propyl thiosulfate *	$C_3H_8O_3S_2$	155.9915
Dimethyl tetrasulfide *	$C_2H_6S_4$	157.9352
Tryptamine *	$C_{10}H_{12}N_2$	160.1000
Cys(Prop-1-enyl) (Deoxyisoalliin) **	$C_6H_{11}NO_2S$	161.0510
Zwiebelane B *	$C_6H_{10}OS_2$	162.0173
Carnitine **	$C_7H_{16}NO_3$	162.1130
Cys(Propyl) (Deoxypropiin) **	$C_6H_{13}NO_2S$	163.0667
R-Propyl 1-propenesulfinothioate *	$C_6H_{12}OS_2$	164.0330
Butyl isopropyl disulfide *	$C_7H_{16}S_2$	164.0693
S-Methyl Met **	$C_6H_{14}NO_2S$	164.0745
Ethiin *	$C_5H_{11}NO_3S$	165.0460
Phe **	$C_9H_{11}NO_2$	165.0790
S-Propyl 1-propanesulfinothioate *	$C_6H_{14}OS_2$	166.0486
3-Methoxytyramine **	$C_9H_{13}NO_2$	167.0946
Methyl (2-propenylthio) selenide *	C_4H_8SSe	167.9512
Methyl 1-(methylthio) propyl disulfide *	$C_5H_{12}S_3$	168.3440
Pyridoxin **	$C_8H_{11}NO_3$	169.0739
2,4,6-Trihydroxybenzoic acid *	$C_7H_6O_5$	170.0215
Allyl thiohexanoate *	$C_9H_{16}OS$	172.0922
Bis(methylthio) selenide *	$C_2H_6S_2Se$	173.9076
2-Isopropyl-3-oxosuccinate *	$C_7H_{10}O_5$	174.0528
Hexanethioic acid S-propyl ester *	$C_9H_{18}OS$	174.1078
Arg **	$C_6H_{14}N_4O_2$	174.1117
2,4,6-Triethyl-1,3,5-trioxane *	$C_9H_{18}O_3$	174.1256
Citrullin *	$C_6H_{13}N_3O_3$	175.0957
Cycloalliin *	$C_6H_{11}NO_3S$	177.0460
Allitridin *	$C_6H_{10}S_3$	177.9945
Bissulfine *	$C_6H_{10}O_2S_2$	178.0122
(R)C(R)S-S-Propylcysteine sulfoxide (propiin) *	$C_6H_{13}NO_3S$	179.0616
1-(Methylthio) ethyl 2-propenyl disulfide *	$C_6H_{12}S_3$	180.0101
Glucose (DP1) **	$C_6H_{12}O_6$	180.0634
Tyr **	$C_9H_{11}NO_3$	181.0739
(Z)-Methyl 3-(methylsulfinyl)-1-propenyl disulfide *	$C_5H_{10}OS_3$	181.9894
Dipropyl trisulfide *	$C_6H_{14}S_3$	182.0258
Tsibulin 2 *	$C_{11}H_{18}O_2$	182.1307
Methyl 2-propenyl tetrasulfide *	$C_4H_8S_4$	183.9509

Methyl 1-(methylsulfinyl) propyl disulfide *	$C_5H_{12}OS_3$	184.0050
Methyl 2,4,6-trihydroxybenzoate *	$C_8H_8O_5$	184.0372
Phosphorylcholine **	$C_5H_{15}NO_4P$	184.0739
N^w-Methyl-Arg **	$C_7H_{16}N_4O_2$	188.1273
Dimethyl diselenide *	$C_2H_6Se_2$	189.8800
Alline *	$C_{11}H_{14}N_2O$	190.1106
Citric acid **	$C_6H_8O_7$	192.0270
S-(Allylthio)-L-cysteine *	$C_6H_{11}NO_2S_2$	193.0231
Methyl 1-(1-propenylthio) propyl disulfide *	$C_7H_{14}S_3$	194.0258
Cys(SPropyl) **	$C_6H_{13}NO_2S_2$	195.0388
1-(Methylthio) propyl propyl disulfide *	$C_7H_{16}S_3$	196.0414
2-Tridecanone *	$C_{13}H_{26}O$	198.1984
Trp **	$C_{11}H_{12}N_2O_2$	204.0899
2,4,6-Triethyl-1,3,5-oxadithiane *	$C_9H_{18}OS_2$	206.0799
(2R,2'S)-Isobuteine *	$C_7H_{13}NO_4S$	207.0565
(Z)-[3-(Methylsulfinyl)-1-propenyl] 2-propenyl disulfide *	$C_7H_{12}OS_3$	208.0050
Di-2-propenyl tetrasulfide *	$C_6H_{10}S_4$	209.9665
1-(Methylsulfinyl) propyl 1-propenyl disulfide *	$C_7H_{14}OS_3$	210.0207
Butyl 1-(methylthio) propyl disulfide *	$C_8H_{18}S_3$	210.0571
Tsibulin 1 *	$C_{13}H_{22}O_2$	210.1620
1-(Methylsulfinyl) propyl propyl disulfide *	$C_7H_{16}OS_3$	212.0363
Methyl 2-propenyl pentasulfide *	$C_4H_8S_5$	215.9230
g-Glu-Ala **	$C_8H_{14}N_2O_5$	218.0903
Pantothenic acid **	$C_9H_{17}NO_5$	219.1107
1-Propenyl 1-(1-propenylthio)propyl disulfide *	$C_9H_{16}S_3$	220.0414
1-(1-Propenylthio)propyl propyl disulfide *	$C_9H_{18}S_3$	222.0571
Propyl 1-(propylthio)propyl disulfide *	$C_9H_{20}S_3$	224.0727
Allixin *	$C_{12}H_{18}O_4$	226.1205
Ajoene *	$C_9H_{14}OS_3$	234.0207
1-Propenyl 1-(1-propenylsulfinyl) propyl disulfide *	$C_9H_{16}OS_3$	236.0363
1-(1-Propenylsulfinyl) propyl propyl disulfide *	$C_9H_{18}OS_3$	238.0520
Propyl 1-(propylsulfinyl) propyl disulfide *	$C_9H_{20}OS_3$	240.0676
Di-2-propenyl pentasulfide *	$C_6H_{10}S_5$	241.9386
g-Glu-Val **	$C_{10}H_{18}N_2O_5$	246.1216
2-Propenyl 3-(2-propenylsulfonyl)-1-propenyl disulfide *	$C_9H_{14}O_2S_3$	250.0156
(E)-2-Propenyl [3-(2-propenylthio)-2-propenyl] sulfate*	$C_9H_{14}O_4S_2$	250.0334

Porric acid C *	$C_{14}H_{10}O_5$	258.0528
Lunularic acid **	$C_{15}H_{14}O_4$	258.0892
Glycerophosphorylcholine **	$C_8H_{21}NO_6P$	258.1106
g-Glu-Leu **	$C_{11}H_{20}N_2O_5$	260.1372
gamma-Glutamyl-S-methylcysteine *	$C_9H_{16}N_2O_5S$	264.0780
Adenosine **	$C_{10}H_{13}N_5O_4$	267.0968
Arbutin **	$C_{12}H_{16}O_7$	272.0896
Di-2-propenyl hexasulfide *	$C_6H_{10}S_6$	273.9107
g-Glu-Gln **	$C_{10}H_{17}N_3O_6$	275.1117
g-Glu-Met **	$C_{10}H_{18}N_2O_5S$	278.0936
gamma-Glutamyl-S-methylcysteine sulfoxide *	$C_9H_{16}N_2O_6S$	280.0729
Ajocysteine *	$C_9H_{15}NO_3S_3$	281.0214
Deoxyadenosine **	$C_{10}H_{13}N_5O_5$	283.0917
N-(p-Coumaroyl)-tyramine **	$C_{17}H_{17}NO_3$	283.1208
Biochanin A **	$C_{16}H_{12}O_5$	284.0685
g-Glu-His **	$C_{11}H_{16}N_4O_5$	284.1121
Kaempferol (K) **	$C_{15}H_{10}O_6$	286.0477
Porric acid B *	$C_{15}H_{12}O_6$	288.0634
3´-Methoxylunularic acid **	$C_{16}H_{16}O_5$	288.0998
N-gamma-Glutamyl-S-(1-propenyl) cysteine *	$C_{11}H_{18}N_2O_5S$	290.0936
N^a-(Hydroxysuccinyl)arginine^c **	$C_{10}H_{18}N_4O_6$	290.1226
g-Glu-Cys(Propyl) **	$C_{11}H_{20}N_2O_5S$	292.1093
g-Glu-Met S-Oxide **	$C_{10}H_{18}N_2O_6S$	294.0886
gamma-Glutamylphenylalanine *	C14H18N2O5	294.1216
5´-Methylthioadenosine **	$C_{11}H_{15}N_5O_3S$	297.0896
Tyramine 4-O-Hex **	$C_{14}H_{21}NO_6$	299.1369
Quercetin (Q) **	$C_{15}H_{10}O_7$	302.0427
Porric acid A *	$C_{16}H_{14}O_6$	302.0790
Di-2-propenyl heptasulfide *	$C_6H_{10}S_7$	305.8827
gamma-Glutamyl-S-(1-propenyl) cysteine sulfoxide *	$C_{11}H_{18}N_2O_6S$	306.0886
g-Glu-Cys(Propyl) S-Oxide **	$C_{11}H_{20}N_2O_6S$	308.1042
g-Glu-Tyr **	$C_{14}H_{18}N_2O_6$	310.1165
N-Feruloyl-tyramine **	$C_{18}H_{19}NO_4$	313.1314
Isorhamnetin (I) **	$C_{16}H_{12}O_7$	316.0583
L-gamma-Glutamyl-S-allylthio-L-cysteine *	$C_{11}H_{18}N_2O_5S_2$	322.0657
3-Methoxytyramine 4-O-Hex **	$C_{15}H_{23}NO_7$	329.1475

5´-O-b-Glucosylpyridoxin **	$C_{14}H_{21}NO_8$	331.1267
g-Glu-Trp **	$C_{16}H_{19}N_3O_5$	333.1325
Cys(Prop-1-enyl) S-Oxide - Cys(Propen-1-yl) S-Oxide[b] **	$C_{12}H_{20}N_2O_5S_2$	336.0814
N-(1-Deoxy-b-D-fructopyranosyl) (R)C(S)S-alliin *	$C_{12}H_{21}NO_8S$	339.0988
Sucrose (DP2) **	$C_{12}H_{22}O_{11}$	342.1162
N-Feruloyl-3-methoxytyramine **	$C_{19}H_{21}NO_5$	343.1420
g-Glu-Cys (SMe)-Gly **	$C_{11}H_{19}N_3O_6S_2$	353.0715
g-Glu-Cys(SProp-1-enyl)-Gly **	$C_{13}H_{21}N_3O_6S_2$	379.0872
g-Glu-Cys(2-CE)-Gly[d] **	$C_{13}H_{21}N_3O_8S$	379.1049
g-Glu-Cys(SPropyl)-Gly **	$C_{13}H_{23}N_3O_6S_2$	381.1028
Fistulosin *	$C_{26}H_{43}NO$	385.3345
Sinapic acid O-Hex **	$C_{17}H_{22}O_{10}$	386.1213
gamma-L-Glutamyl-S-(2-carboxy-1-propyl) cysteinylglycine *	$C_{14}H_{23}N_3O_8S$	393.1206
Lunularic acid O-Hex **	$C_{21}H_{24}O_9$	420.1420
Cepagenin *	$C_{27}H_{42}O_5$	446.3032
K-4´-O-b-Glc **	$C_{21}H_{20}O_{11}$	448.1006
Porrigenin A *	$C_{27}H_{44}O_5$	448.3189
Cyanidin 4'-glucoside *	$C_{21}H_{21}O_{11}$	449.1084
3´-Methoxylunularic acid O-Hex **	$C_{22}H_{26}O_{10}$	450.1526
2,3-Secoporrigenin *	$C_{27}H_{40}O_6$	460.2825
Peonidin-3-O-b-Glc **	$C_{22}H_{23}O_{11}$	463.1240
Quercetin 4'-glucoside *	$C_{21}H_{20}O_{12}$	464.0955
Alliumoside A *	$C_{22}H_{22}O_{12}$	478.1111
I-4´-O-b-Glc **	$C_{22}H_{24}O_{12}$	480.1268
1-Kestose (DP3) *	$C_{18}H_{32}O_{16}$	504.1690
Cyanidin 3-(3''-malonyl-glucoside) *	$C_{24}H_{23}O_{14}$	535.1088
N,N'-Bis(g-glutamyl)-3,3'-(1,2-propylenedithio)dialanine *	$C_{19}H_{32}N_4O_{10}S_2$	540.1560
Pe-3-O-b-(Malonyl-Glc) **	$C_{25}H_{25}O_{14}$	549.1244
g-Glu-Cys(2-CP)-Gly Hexoside[c] **	$C_{20}H_{33}N_3O_{13}S$	555.1734
K-3,4´-di-O- b-Glc **	$C_{27}H_{30}O_{16}$	610.1534
Cyanidin 3,4'-diglucoside *	$C_{27}H_{31}O_{16}$	611.1612
Quercetin 4',7-diglucoside *	$C_{27}H_{30}O_{17}$	626.1483
Quercetin 3,4'-diglucoside *	$C_{27}H_{30}O_{17}$	626.5169
I-3,4´-O-b-Glc **	$C_{28}H_{32}O_{17}$	640.1639
Nystose (DP4) **	$C_{24}H_{42}O_{21}$	666.2219
AS 1-1 *	$C_{38}H_{71}NO_9$	685.5129

Cy-Malonyl-Hex-Hex **	$C_{30}H_{33}O_{19}$	697.1616
AS 1-2 *	$C_{39}H_{73}NO_9$	699.5285
AS 1-5 *	$C_{40}H_{77}NO_9$	715.5598
Ophiopogonin C *	$C_{39}H_{62}O_{12}$	722.4241
Alliospiroside C *	$C_{38}H_{60}O_{13}$	724.4034
Isonuatigenin 3-[rhamnosyl-(1->2)-glucoside] *	$C_{39}H_{62}O_{13}$	738.4190
25-Epiruizgenin 3-[4''-rhamnosylglucoside] *	$C_{39}H_{64}O_{13}$	740.4347
Alliosterol 1-rhamnoside 16-galactoside *	$C_{39}H_{66}O_{13}$	742.4503
Alliospiroside D *	$C_{39}H_{62}O_{14}$	754.4140
Tuberoside J *	$C_{39}H_{64}O_{14}$	756.4296
(3b,5a,25R)-3-Hydroxyspirostan-6-one 3-[2-acetylarabinosyl-(1->6)-glucoside] *	$C_{40}H_{62}O_{14}$	766.4140
Aginoside progenin *	$C_{39}H_{64}O_{15}$	772.4245
Kaempferol 3-sophoroside 7-glucuronide *	$C_{33}H_{38}O_{22}$	786.1855
Quercetin 3,7,4'-O-triglucoside *	$C_{33}H_{40}O_{22}$	788.2011
Quercetin 7-glucuronoside 3-sophoroside *	$C_{33}H_{38}O_{23}$	802.1804
Oligosaccharides (DP5) **	$C_{30}H_{52}O_{26}$	828.2747
Cyanidin 3-(3-glucosyl-6-malonylglucoside) 4'-glucoside *	$C_{38}H_{47}O_{22}$	855.2559
Deltonin *	$C_{45}H_{72}O_{17}$	884.4770
Chinenoside III *	$C_{44}H_{70}O_{18}$	886.4562
Tuberoside D *	$C_{45}H_{74}O_{17}$	886.4926
Ceposide A *	$C_{44}H_{72}O_{18}$	888.4719
Fistuloside B *	$C_{45}H_{72}O_{18}$	900.4719
Kaempferol 3-neohesperidoside-7-(2''-p-coumarylglucoside) *	$C_{42}H_{46}O_{22}$	902.2481
Chinenoside VI *	$C_{44}H_{70}O_{19}$	902.4511
Tuberoside E *	$C_{45}H_{74}O_{18}$	902.4875
Alliosterol 1-(4''-galactosylrhamnoside) 16-galactoside *	$C_{45}H_{76}O_{18}$	904.5032
3b-Pregnadienolone 3-[rhamnosyl-(1->4)-rhamnosyl-(1->4)-rhamnosyl-(1->4)-glucoside] *	$C_{45}H_{70}O_{19}$	914.4511
Fistuloside C *	$C_{45}H_{72}O_{19}$	916.4668
Neogitogenin 3-[glucosyl-(1->2)-glucosyl-(1->4)-galactoside] *	$C_{45}H_{74}O_{19}$	918.4824
Cyanidin 3-O-[4-Hydroxy-E-cinnamoyl-(->6)-b-D-glucopyranosyl-(1->2)-b-D-glucopyranoside] 5-glucoside *	$C_{42}H_{47}O_{23}$	919.2508
Kaempferol 3-neohesperidoside-7-(2''-ferulylglucoside) *	$C_{43}H_{48}O_{23}$	932.2586
Ampeloside Bs1 *	$C_{45}H_{74}O_{20}$	934.4773
Kaempferol 3-(2-feruloylglucoside) 4',7-diglucoside *	$C_{43}H_{48}O_{24}$	948.2536
Ampeloside Bf2 *	$C_{45}H_{76}O_{21}$	952.4879

Oligosaccharides (DP6) **	$C_{36}H_{62}O_{31}$	990.3275
Chinenoside II *	$C_{49}H_{78}O_{22}$	1018.4985
Diosgenin 3-[glucosyl-(1->4)-rhamnosyl-(1->4)-[rhamnosyl-(1->2)]-glucoside] *	$C_{51}H_{82}O_{21}$	1030.5349
Chinenoside I *	$C_{49}H_{80}O_{23}$	1036.5090
Chinenoside IV *	$C_{50}H_{80}O_{23}$	1048.5090
Tuberoside B (Allium tuberosum) *	$C_{51}H_{84}O_{22}$	1048.5454
b-Chlorogenin 3-[4''-(2'''-glucosyl-3'''-xylosylglucosyl) galactoside] *	$C_{50}H_{82}O_{23}$	1050.5247
Kaempferol 3-neohesperidoside-7-(2''-p-coumaryllaminaribioside) *	$C_{48}H_{56}O_{27}$	1064.3009
12-Ketoporrigenin 3-[4'-(2''-glucosyl-3''-xylosyl)-glucosyl)-galactoside] *	$C_{50}H_{80}O_{24}$	1064.5040
Tuberoside L *	$C_{51}H_{84}O_{23}$	1064.5403
(3b,5a,6b,25R)-3,6-Dihydroxyspirostane-2,12-dione 3-[4'-(2''-glucosyl-3''-xylosyl)-galactoside] *	$C_{50}H_{78}O_{25}$	1078.4832
Isoeruboside B *	$C_{51}H_{84}O_{24}$	1080.5353
Yayoisaponin C *	$C_{51}H_{84}O_{25}$	1096.5302
Ampeloside Bf1 *	$C_{51}H_{86}O_{26}$	1114.5407
Oligosaccharides (DP7) **	$C_{42}H_{72}O_{36}$	1152.3803
Ceposide D *	$C_{56}H_{90}O_{26}$	1178.5720
Diosgenin 3-[glucosyl-(1->6)-glucosyl-(1->4)-rhamnosyl-(1->4) [rhamnosyl-(1->2)]-glucoside] *	$C_{57}H_{92}O_{26}$	1192.5877
Sativoside R2 *	$C_{56}H_{92}O_{27}$	1196.5826
b-Chlorogenin 3-[4-(2-((3-glucosyl) glucosyl-3-xylosyl)-glucosyl)-galactoside] *	$C_{56}H_{92}O_{28}$	1212.5775
Yayoisaponin B *	$C_{56}H_{90}O_{29}$	1226.5568
Yayoisaponin A *	$C_{56}H_{92}O_{29}$	1229.3123
(3b,5a,6b,22a,25R)-Furostane-22-methoxy-3,6,26-triol 3-[glucosyl-(1->2)-[xylosyl-(1->3)]-glucosyl-(1->4)-galactoside] 26-glucoside *	$C_{57}H_{96}O_{29}$	1244.6037
Protoisoeruboside B *	$C_{57}H_{96}O_{30}$	1260.5986
Allium schoenoprasum Anthocyanin-flavonol *	$C_{57}H_{59}O_{35}$	1303.2837
Oligosaccharides (DP8) **	$C_{48}H_{82}O_{41}$	1314.4332
Allium schoenoprasum Anthocyanin-flavonol 3''-acetate *	$C_{59}H_{61}O_{36}$	1345.2943
Diosgenin 3-[glucosyl-(1->4)-[glucopyranosyl-(1->6)-glucopyranosyl-(1->4)-rhamnosyl-(1->4)-[rhamnosyl-(1->2)]-glucoside] *	$C_{63}H_{102}O_{31}$	1354.6405
Sativoside R1 *	$C_{62}H_{104}O_{33}$	1376.6460
Sativoside B1 *	$C_{63}H_{106}O_{35}$	1422.6515
Oligosaccharides (DP9) **	$C_{54}H_{92}O_{46}$	1476.4860
Oligosaccharides (DP10) **	$C_{60}H_{102}O_{51}$	1638.5388
Oligosaccharides (DP11) **	$C_{66}H_{112}O_{56}$	1800.5916
Oligosaccharides (DP12) **	$C_{72}H_{122}O_{61}$	1962.6444

* Yannai, S., *Dictionary of Food Compounds with CD-ROM: Additives.* Flavors, and Ingredients, 2004: p. 1784.

** Böttcher, C., et al., *Comprehensive metabolite profiling of onion bulbs (Allium cepa) using liquid chromatography coupled with electrospray ionization quadrupole time-of-flight mass spectrometry.* Metabolomics, 2017. **13**(4): p. 35.

List 4-1. Onion metabolite database generated from previous reports.

Chemical name	Chemical formula	Theoretical m/z	Measured m/z	PPM
Adenosine	$C_{10}H_{13}N_5O_4(+H^+)$	268.1046	268.1056	3.77
Adenosine	$C_{10}H_{13}N_5O_4(+NH_4^+)$	285.1312	285.1327	5.46
g-Glu-Val	$C_{10}H_{18}N_2O_5(+H^+)$	247.1294	247.1308	5.42
Trp	$C_{11}H_{12}N_2O_2(+H^+)$	205.0977	205.0984	3.14
5´-Methylthioadenosine	$C_{11}H_{15}N_5O_3S(+NH_4^+)$	315.1240	315.1222	-5.48
g-Glu-His	$C_{11}H_{16}N_4O_5(+H-H_2O^+)$	267.1094	267.1101	2.77
g-Glu-Cys(SMe)-Gly	$C_{11}H_{19}N_3O_6S_2(+Na^+)$	376.0613	376.0621	2.27
g-Glu-Cys(SMe)-Gly	$C_{11}H_{19}N_3O_6S_2(+NH_4^+)$	371.1059	371.1052	-1.94
g-Glu-Leu	$C_{11}H_{20}N_2O_5(+H^+)$	261.1450	261.1460	3.80
g-Glu-Cys(Propyl) S-Oxide	$C_{11}H_{20}N_2O_6S(+H^+)$	309.1120	309.1123	0.78
Sucrose (DP2)	$C_{12}H_{22}O_{11}(+H^+)$	343.1240	343.1263	6.49
Sucrose (DP2)	$C_{12}H_{22}O_{11}(+H-2H_2O^+)$	307.1029	307.1049	6.47
Sucrose (DP2)	$C_{12}H_{22}O_{11}(+H-H_2O^+)$	325.1135	325.1155	6.37
Sucrose (DP2)	$C_{12}H_{22}O_{11}(+K^+)$	381.0799	381.0825	6.73
Sucrose (DP2)	$C_{12}H_{22}O_{11}(+Na^+)$	365.1060	365.1071	3.13
Sucrose (DP2)	$C_{12}H_{22}O_{11}(+NH_4^+)$	360.1506	360.1524	4.95
g-Glu-Cys(2-CE)-Gly[d]	$C_{13}H_{21}N_3O_8S(+H^+)$	380.1127	380.1103	-6.26
g-Glu-Cys(2-CE)-Gly[d]	$C_{13}H_{21}N_3O_8S(+H-H_2O^+)$	362.1022	362.0991	-8.49
Tsibulin 1	$C_{13}H_{22}O_2(+H^+)$	211.1698	211.1706	3.95
Tsibulin 1	$C_{13}H_{22}O_2(+H-H_2O^+)$	193.1592	193.1603	5.49
Porric acid C	$C_{14}H_{10}O_5(+H^+)$	259.0606	259.0595	-4.27
gamma-Glutamylphenylalanine	C14H18N2O5(+H+)	295.1294	295.1312	6.23
g-Glu-Tyr	$C_{14}H_{18}N_2O_6(+H^+)$	311.1243	311.1266	7.23
gamma-L-Glutamyl-S-(2-carboxy-1-propyl) cysteinylglycine	$C_{14}H_{23}N_3O_8S(+H^+)$	394.1284	394.1307	5.78
Quercetin (Q)	$C_{15}H_{10}O_7(+H-2H_2O^+)$	267.0294	267.0289	-2.00
Porric acid B	$C_{15}H_{12}O_6(+H^+)$	289.0712	289.0707	-1.89
Lunularic acid	$C_{15}H_{14}O_4(+H^+)$	259.0970	259.0961	-3.50
Lunularic acid	$C_{15}H_{14}O_4(+H-2H_2O^+)$	223.0759	223.0743	-7.29
Lunularic acid	$C_{15}H_{14}O_4(+H-H_2O^+)$	241.0865	241.0853	-4.66
3´-Methoxylunularic acid	$C_{16}H_{16}O_5(+H-H_2O^+)$	271.0971	271.0963	-2.92
1-Kestose (DP3)	$C_{18}H_{32}O_{16}(+H-H_2O^+)$	487.1663	487.1707	9.14
1-Kestose (DP3)	$C_{18}H_{32}O_{16}(+K^+)$	543.1327	543.1360	6.00
1-Kestose (DP3)	$C_{18}H_{32}O_{16}(+Na^+)$	527.1588	527.1628	7.70

1-Kestose (DP3)	$C_{18}H_{32}O_{16}(+NH_4^+)$	522.2034	522.2058	4.57
K-4´-O-b-Glc	$C_{21}H_{20}O_{11}(+K^+)$	487.0643	487.0649	1.25
Peonidin-3-O-b-Glc	$C_{22}H_{23}O_{11}(+H-H_2O^+)$	446.1213	446.1230	4.00
3´-Methoxylunularic acid O-Hex	$C_{22}H_{26}O_{10}(+K^+)$	489.1163	489.1157	-1.17
Nystose (DP4)	$C_{24}H_{42}O_{21}(+K^+)$	705.1856	705.1895	5.48
Nystose (DP4)	$C_{24}H_{42}O_{21}(+Na^+)$	689.2117	689.2168	7.38
Nystose (DP4)	$C_{24}H_{42}O_{21}(+NH_4^+)$	684.2563	684.2618	8.08
Pe-3-O-b-(Malonyl-Glc)	$C_{25}H_{25}O_{14}(+NH_4^+)$	567.1588	567.1576	-2.02
Oligosaccharides (DP5)	$C_{30}H_{52}O_{26}(+Na^+)$	851.2645	851.2712	7.85
Oligosaccharides (DP6)	$C_{36}H_{62}O_{31}(+K^+)$	1029.2912	1029.2974	6.05
Oligosaccharides (DP6)	$C_{36}H_{62}O_{31}(+Na^+)$	1013.3173	1013.3269	9.47
Kaempferol 3-neohesperidoside-7-(2"-p-coumarylglucoside)	$C_{42}H_{46}O_{22}(+H-H_2O^+)$	885.2453	885.2539	9.72
Malic acid	$C_4H_6O_5(+Na^+)$	157.0113	157.0122	5.64
Methyl 2-propenyl trisulfide	$C_4H_8S_3(+H^+)$	152.9866	152.9871	2.74
(S)C(S)S-S-Methylcysteine sulfoxide (Methiin)	$C_4H_9NO_3S(+H^+)$	152.0381	152.0390	5.34
(Z)-Methyl 3-(methylsulfinyl)-1-propenyl disulfide	$C_5H_{10}OS_3(+H^+)$	182.9972	182.9979	3.69
Methyl 1-(methylsulfinyl)propyl disulfide	$C_5H_{12}OS_3(+H^+)$	185.0129	185.0136	4.10
pyro-Glu	$C_5H_7NO_3(+Na^+)$	152.0324	152.0329	3.71
Cycloalliin	$C_6H_{11}NO_3S(+H^+)$	178.0538	178.0543	3.08
Cycloalliin	$C_6H_{11}NO_3S(+H-H_2O^+)$	160.0432	160.0442	5.92
Cycloalliin	$C_6H_{11}NO_3S(+K^+)$	216.0097	216.0105	3.87
Cycloalliin	$C_6H_{11}NO_3S(+Na^+)$	200.0357	200.0369	5.95
Glucose (DP1)	$C_6H_{12}O_6(+H-H_2O^+)$	163.0607	163.0615	5.00
Glucose (DP1)	$C_6H_{12}O_6(+K^+)$	219.0271	219.0281	4.74
Glucose (DP1)	$C_6H_{12}O_6(+Na^+)$	203.0532	203.0540	3.89
Glucose (DP1)	$C_6H_{12}O_6(+NH_4^+)$	198.0978	198.0986	3.96
R-Propyl 1-propenesulfinothioate	$C_6H_{12}OS_2(+H^+)$	165.0408	165.0411	1.96
1-Propenyl propyl sulfide	$C_6H_{12}S(+K^+)$	155.0297	155.0293	-2.19
Citrullin	$C_6H_{13}N_3O_3(+H^+)$	176.1035	176.1045	5.30
(R)C(R)S-S-Propylcysteine sulfoxide (propiin)	$C_6H_{13}NO_3S(+H^+)$	180.0694	180.0704	5.20
Arg	$C_6H_{14}N_4O_2(+H^+)$	175.1195	175.1202	3.79
Citric acid	$C_6H_8O_7(+K^+)$	230.9907	230.9919	5.21

2-Vinyl-4H-1,3-dithiine	$C_6H_8S_2(+NH_4^+)$	162.0411	162.0400	-7.05
His	$C_6H_9N_3O_2(+H^+)$	156.0773	156.0782	5.35
(2R,2'S)-Isobuteine	$C_7H_{13}NO_4S(+NH_4^+)$	225.0909	225.0917	3.43
Pro Betaine (N,N-Dimethyl-Pro)	$C_7H_{14}NO_2(+Na^+)$	167.0923	167.0912	-6.44
Methyl 1-(1-propenylthio) propyl disulfide	$C_7H_{14}S_3(+H\text{-}H_2O^+)$	177.0230	177.0245	8.17
N^w-Methyl-Arg	$C_7H_{16}N_4O_2(+K^+)$	227.0910	227.0907	-1.24
g-Glu-Ala	$C_8H_{14}N_2O_5(+K^+)$	257.0540	257.0526	-5.38
Butyl 1-(methylthio)propyl disulfide	$C_8H_{18}S_3(+H\text{-}H_2O^+)$	193.0543	193.0552	4.77
Glycerophosphorylcholine	$C_8H_{21}NO_6P(+H\text{-}H_2O^+)$	241.1079	241.1062	-7.05
Methyl 2,4,6-trihydroxybenzoate	$C_8H_8O_5(+Na^+)$	207.0269	207.0259	-5.11
Phe	$C_9H_{11}NO_2(+H^+)$	166.0868	166.0875	4.08
Tyr	$C_9H_{11}NO_3(+H^+)$	182.0817	182.0825	4.11
3-Methoxytyramine	$C_9H_{13}NO_2(+K^+)$	206.0583	206.0568	-7.10
gamma-Glutamyl-S-methylcysteine sulfoxide	$C_9H_{16}N_2O_6S(+H\text{-}2H_2O^+)$	245.0596	245.0619	9.24

*DP=Degree of polymerization, [a]VL = Verification level according to Sumner et al. Metabolomics 2007, 3(3), 211-221; [b]dipeptide of isoalliin; [c]2-CP = 2-carboxypropyl; [d]2-CE = 2-carboxyethyl

List 4-2. Putative metabolite identification in single onion cell analysis.

Chemical name	Chemical formula	Theoretical m/z	Measured m/z	PPM
pyro-Glu	$C_5H_7NO_3(+Na^+)$	152.0324	152.0329	3.71
Methyl 2-propenyl trisulfide	$C_4H_8S_3(+H^+)$	152.9866	152.9871	2.74
1-Propenyl propyl sulfide	$C_6H_{12}S(+K^+)$	155.0297	155.0293	-2.19
His	$C_6H_9N_3O_2(+H^+)$	156.0773	156.0782	5.35
Malic acid	$C_4H_6O_5(+Na^+)$	157.0113	157.0122	5.64
Cycloalliin	$C_6H_{11}NO_3S(+H-H_2O^+)$	160.0432	160.0442	5.92
Glucose (DP1)	$C_6H_{12}O_6(+H-H_2O^+)$	163.0607	163.0615	5.00
R-Propyl 1-propenesulfinothioate	$C_6H_{12}OS_2(+H^+)$	165.0408	165.0411	1.96
Arg	$C_6H_{14}N_4O_2(+H^+)$	175.1195	175.1202	3.79
Citrullin	$C_6H_{13}N_3O_3(+H^+)$	176.1035	176.1045	5.30
Methyl 1-(1-propenylthio) propyl disulfide	$C_7H_{14}S_3(+H-H_2O^+)$	177.0230	177.0245	8.17
Cycloalliin	$C_6H_{11}NO_3S(+H^+)$	178.0538	178.0543	3.08
(R)C(R)S-S-Propylcysteine sulfoxide (propiin)	$C_6H_{13}NO_3S(+H^+)$	180.0694	180.0704	5.20
Tyr	$C_9H_{11}NO_3(+H^+)$	182.0817	182.0825	4.11
(Z)-Methyl 3-(methylsulfinyl)-1-propenyl disulfide	$C_5H_{10}OS_3(+H^+)$	182.9972	182.9979	3.69
Glucose (DP1)	$C_6H_{12}O_6(+NH_4^+)$	198.0978	198.0986	3.96
Cycloalliin	$C_6H_{11}NO_3S(+Na^+)$	200.0357	200.0369	5.95
Glucose (DP1)	$C_6H_{12}O_6(+Na^+)$	203.0532	203.0540	3.89
Trp	$C_{11}H_{12}N_2O_2(+H^+)$	205.0977	205.0984	3.14
3-Methoxytyramine	$C_9H_{13}NO_2(+K^+)$	206.0583	206.0568	-7.10
Cycloalliin	$C_6H_{11}NO_3S(+K^+)$	216.0097	216.0105	3.87
Methyl 1-(1-propenylthio) propyl disulfide	$C_7H_{14}S_3(+Na^+)$	217.0155	217.0144	-5.04
Glucose (DP1)	$C_6H_{12}O_6(+K^+)$	219.0271	219.0281	4.74
Lunularic acid	$C_{15}H_{14}O_4(+H-2H_2O^+)$	223.0759	223.0743	-7.29
Glycerophosphorylcholine	$C_8H_{21}NO_6P(+H-2H_2O^+)$	223.0973	223.0972	-0.67
(2R,2'S)-Isobuteine	$C_7H_{13}NO_4S(+NH_4^+)$	225.0909	225.0917	3.43
Lunularic acid	$C_{15}H_{14}O_4(+H-H_2O^+)$	241.0865	241.0853	-4.66
gamma-Glutamyl-S-methylcysteine sulfoxide	$C_9H_{16}N_2O_6S(+H-2H_2O^+)$	245.0596	245.0619	9.24
Porric acid C	$C_{14}H_{10}O_5(+H^+)$	259.0606	259.0595	-4.27

3´-Methoxylunularic acid	$C_{16}H_{16}O_5(+H\text{-}H_2O^+)$	271.0971	271.0963	-2.92
Porric acid B	$C_{15}H_{12}O_6(+H^+)$	289.0712	289.0707	-1.89
gamma-Glutamylphenylalanine	$C_{14}H_{18}N_2O_5(+H^+)$	295.1294	295.1312	6.23
Sucrose (DP2)	$C_{12}H_{22}O_{11}(+H\text{-}2H_2O^+)$	307.1029	307.1049	6.47
g-Glu-Cys(Propyl) S-Oxide	$C_{11}H_{20}N_2O_6S(+H^+)$	309.1120	309.1123	0.78
g-Glu-Tyr	$C_{14}H_{18}N_2O_6(+H^+)$	311.1243	311.1266	7.23
Sucrose (DP2)	$C_{12}H_{22}O_{11}(+H\text{-}H_2O^+)$	325.1135	325.1155	6.37
Sucrose (DP2)	$C_{12}H_{22}O_{11}(+H^+)$	343.1240	343.1263	6.49
gamma-Glutamyl-S-(1-propenyl) cysteine sulfoxide	$C_{11}H_{18}N_2O_6S(+K^+)$	345.0523	345.0529	1.92
Sucrose (DP2)	$C_{12}H_{22}O_{11}(+NH_4^+)$	360.1506	360.1524	4.95
g-Glu-Cys(2-CE)-Gly[d]	$C_{13}H_{21}N_3O_8S(+H\text{-}H_2O^+)$	362.1022	362.0991	-8.49
Sucrose (DP2)	$C_{12}H_{22}O_{11}(+Na^+)$	365.1060	365.1071	3.13
g-Glu-Cys(SMe)-Gly	$C_{11}H_{19}N_3O_6S_2(+NH_4^+)$	371.1059	371.1052	-1.94
g-Glu-Cys(2-CE)-Gly[d]	$C_{13}H_{21}N_3O_8S(+H^+)$	380.1127	380.1103	-6.26
Sucrose (DP2)	$C_{12}H_{22}O_{11}(+K^+)$	381.0799	381.0825	6.73
gamma-L-Glutamyl-S-(2-carboxy-1-propyl) cysteinylglycine	$C_{14}H_{23}N_3O_8S(+H^+)$	394.1284	394.1307	5.78
K-4´-O-b-Glc	$C_{21}H_{20}O_{11}(+Na^+)$	471.0904	471.0866	-8.05
K-4´-O-b-Glc	$C_{21}H_{20}O_{11}(+K^+)$	487.0643	487.0649	1.25
1-Kestose (DP3)	$C_{18}H_{32}O_{16}(+H\text{-}H_2O^+)$	487.1663	487.1707	9.14
3´-Methoxylunularic acid O-Hex	$C_{22}H_{26}O_{10}(+K^+)$	489.1163	489.1157	-1.17
Pe-3-O-b-(Malonyl-Glc)	$C_{25}H_{25}O_{14}(+H\text{-}2H_2O^+)$	514.1111	514.1113	0.36
1-Kestose (DP3)	$C_{18}H_{32}O_{16}(+NH_4^+)$	522.2034	522.2058	4.57
1-Kestose (DP3)	$C_{18}H_{32}O_{16}(+Na^+)$	527.1588	527.1628	7.70
1-Kestose (DP3)	$C_{18}H_{32}O_{16}(+K^+)$	543.1327	543.1360	6.00
Pe-3-O-b-(Malonyl-Glc)	$C_{25}H_{25}O_{14}(+NH_4^+)$	567.1588	567.1576	-2.02
Nystose (DP4)	$C_{24}H_{42}O_{21}(+NH_4^+)$	684.2563	684.2618	8.08
Nystose (DP4)	$C_{24}H_{42}O_{21}(+Na^+)$	689.2117	689.2168	7.38
Nystose (DP4)	$C_{24}H_{42}O_{21}(+K^+)$	705.1856	705.1895	5.48
Oligosaccharides (DP5)	$C_{30}H_{52}O_{26}(+Na^+)$	851.2645	851.2712	7.85
Oligosaccharides (DP5)	$C_{30}H_{52}O_{26}(+K^+)$	867.2384	867.2470	9.91
Kaempferol 3-neohesperidoside-7-(2"-p-coumarylglucoside)	$C_{42}H_{46}O_{22}(+H\text{-}H_2O^+)$	885.2453	885.2539	9.72

Oligosaccharides (DP6)	$C_{36}H_{62}O_{31}(+K^+)$	1029.2912	1029.2974	6.05

List 4-3. Putative metabolite identification of the upregulated mass features between the 10 s and 2 s injection time runs.

Chemical name	Chemical formula	Theoretical m/z	Measured m/z	PPM
pyro-Glu	$C_5H_7NO_3(+Na^+)$	152.0324	152.0329	3.71
Methyl 2-propenyl trisulfide	$C_4H_8S_3(+H^+)$	152.9866	152.9871	2.74
1-Propenyl propyl sulfide	$C_6H_{12}S(+K^+)$	155.0297	155.0293	-2.19
His	$C_6H_9N_3O_2(+H^+)$	156.0773	156.0782	5.35
Malic acid	$C_4H_6O_5(+Na^+)$	157.0113	157.0122	5.64
Cycloalliin	$C_6H_{11}NO_3S(+H-H_2O^+)$	160.0432	160.0442	5.92
Glucose (DP1)	$C_6H_{12}O_6(+H-H_2O^+)$	163.0607	163.0615	5.00
R-Propyl 1-propenesulfinothioate	$C_6H_{12}OS_2(+H^+)$	165.0408	165.0411	1.96
Arg	$C_6H_{14}N_4O_2(+H^+)$	175.1195	175.1202	3.79
Citrullin	$C_6H_{13}N_3O_3(+H^+)$	176.1035	176.1045	5.30
Methyl 1-(1-propenylthio) propyl disulfide	$C_7H_{14}S_3(+H-H_2O^+)$	177.0230	177.0245	8.17
Cycloalliin	$C_6H_{11}NO_3S(+H^+)$	178.0538	178.0543	3.08
(R)C(R)S-S-Propylcysteine sulfoxide (propiin)	$C_6H_{13}NO_3S(+H^+)$	180.0694	180.0704	5.20
Tyr	$C_9H_{11}NO_3(+H^+)$	182.0817	182.0825	4.11
(Z)-Methyl 3-(methylsulfinyl)-1-propenyl disulfide	$C_5H_{10}OS_3(+H^+)$	182.9972	182.9979	3.69
Glucose (DP1)	$C_6H_{12}O_6(+NH_4^+)$	198.0978	198.0986	3.96
Cycloalliin	$C_6H_{11}NO_3S(+Na^+)$	200.0357	200.0369	5.95
Glucose (DP1)	$C_6H_{12}O_6(+Na^+)$	203.0532	203.0540	3.89
Trp	$C_{11}H_{12}N_2O_2(+H^+)$	205.0977	205.0984	3.14
3-Methoxytyramine	$C_9H_{13}NO_2(+K^+)$	206.0583	206.0568	-7.10
Cycloalliin	$C_6H_{11}NO_3S(+K^+)$	216.0097	216.0105	3.87
Methyl 1-(1-propenylthio) propyl disulfide	$C_7H_{14}S_3(+Na^+)$	217.0155	217.0144	-5.04
Glucose (DP1)	$C_6H_{12}O_6(+K^+)$	219.0271	219.0281	4.74
Lunularic acid	$C_{15}H_{14}O_4(+H-2H_2O^+)$	223.0759	223.0743	-7.29
Glycerophosphorylcholine	$C_8H_{21}NO_6P(+H-2H_2O^+)$	223.0973	223.0972	-0.67
(2R,2'S)-Isobuteine	$C_7H_{13}NO_4S(+NH_4^+)$	225.0909	225.0917	3.43
Lunularic acid	$C_{15}H_{14}O_4(+H-H_2O^+)$	241.0865	241.0853	-4.66
gamma-Glutamyl-S-methylcysteine sulfoxide	$C_9H_{16}N_2O_6S(+H-2H_2O^+)$	245.0596	245.0619	9.24
Porric acid C	$C_{14}H_{10}O_5(+H^+)$	259.0606	259.0595	-4.27
3´-Methoxylunularic acid	$C_{16}H_{16}O_5(+H-H_2O^+)$	271.0971	271.0963	-2.92
Porric acid B	$C_{15}H_{12}O_6(+H^+)$	289.0712	289.0707	-1.89

gamma-Glutamylphenylalanine	$C_{14}H_{18}N_2O_5(+H^+)$	295.1294	295.1312	6.23
Sucrose (DP2)	$C_{12}H_{22}O_{11}(+H-2H_2O^+)$	307.1029	307.1049	6.47
g-Glu-Cys(Propyl) S-Oxide	$C_{11}H_{20}N_2O_6S(+H^+)$	309.1120	309.1123	0.78
g-Glu-Tyr	$C_{14}H_{18}N_2O_6(+H^+)$	311.1243	311.1266	7.23
Sucrose (DP2)	$C_{12}H_{22}O_{11}(+H-H_2O^+)$	325.1135	325.1155	6.37
Sucrose (DP2)	$C_{12}H_{22}O_{11}(+H^+)$	343.1240	343.1263	6.49
gamma-Glutamyl-S-(1-propenyl) cysteine sulfoxide	$C_{11}H_{18}N_2O_6S(+K^+)$	345.0523	345.0529	1.92
Sucrose (DP2)	$C_{12}H_{22}O_{11}(+NH_4^+)$	360.1506	360.1524	4.95
g-Glu-Cys(2-CE)-Gly[d]	$C_{13}H_{21}N_3O_8S(+H-H_2O^+)$	362.1022	362.0991	-8.49
Sucrose (DP2)	$C_{12}H_{22}O_{11}(+Na^+)$	365.1060	365.1071	3.13
g-Glu-Cys(SMe)-Gly	$C_{11}H_{19}N_3O_6S_2(+NH_4^+)$	371.1059	371.1052	-1.94
g-Glu-Cys(2-CE)-Gly[d]	$C_{13}H_{21}N_3O_8S(+H^+)$	380.1127	380.1103	-6.26
Sucrose (DP2)	$C_{12}H_{22}O_{11}(+K^+)$	381.0799	381.0825	6.73
gamma-L-Glutamyl-S-(2-carboxy-1-propyl) cysteinylglycine	$C_{14}H_{23}N_3O_8S(+H^+)$	394.1284	394.1307	5.78
K-4´-O-b-Glc	$C_{21}H_{20}O_{11}(+Na^+)$	471.0904	471.0866	-8.05
K-4´-O-b-Glc	$C_{21}H_{20}O_{11}(+K^+)$	487.0643	487.0649	1.25
1-Kestose (DP3)	$C_{18}H_{32}O_{16}(+H-H_2O^+)$	487.1663	487.1707	9.14
3´-Methoxylunularic acid O-Hex	$C_{22}H_{26}O_{10}(+K^+)$	489.1163	489.1157	-1.17
Pe-3-O-b-(Malonyl-Glc)	$C_{25}H_{25}O_{14}(+H-2H_2O^+)$	514.1111	514.1113	0.36
1-Kestose (DP3)	$C_{18}H_{32}O_{16}(+NH_4^+)$	522.2034	522.2058	4.57
1-Kestose (DP3)	$C_{18}H_{32}O_{16}(+Na^+)$	527.1588	527.1628	7.70
1-Kestose (DP3)	$C_{18}H_{32}O_{16}(+K^+)$	543.1327	543.1360	6.00
Pe-3-O-b-(Malonyl-Glc)	$C_{25}H_{25}O_{14}(+NH_4^+)$	567.1588	567.1576	-2.02
Nystose (DP4)	$C_{24}H_{42}O_{21}(+NH_4^+)$	684.2563	684.2618	8.08
Nystose (DP4)	$C_{24}H_{42}O_{21}(+Na^+)$	689.2117	689.2168	7.38
Nystose (DP4)	$C_{24}H_{42}O_{21}(+K^+)$	705.1856	705.1895	5.48
Oligosaccharides (DP5)	$C_{30}H_{52}O_{26}(+Na^+)$	851.2645	851.2712	7.85
Oligosaccharides (DP5)	$C_{30}H_{52}O_{26}(+K^+)$	867.2384	867.2470	9.91
Kaempferol 3-neohesperidoside-7-(2''-p-coumarylglucoside)	$C_{42}H_{46}O_{22}(+H-H_2O^+)$	885.2453	885.2539	9.72
Oligosaccharides (DP6)	$C_{36}H_{62}O_{31}(+K^+)$	1029.2912	1029.2974	6.05

List 4-4. Putative metabolite identification of the detected mass features in single-cell CZE-MS analysis.

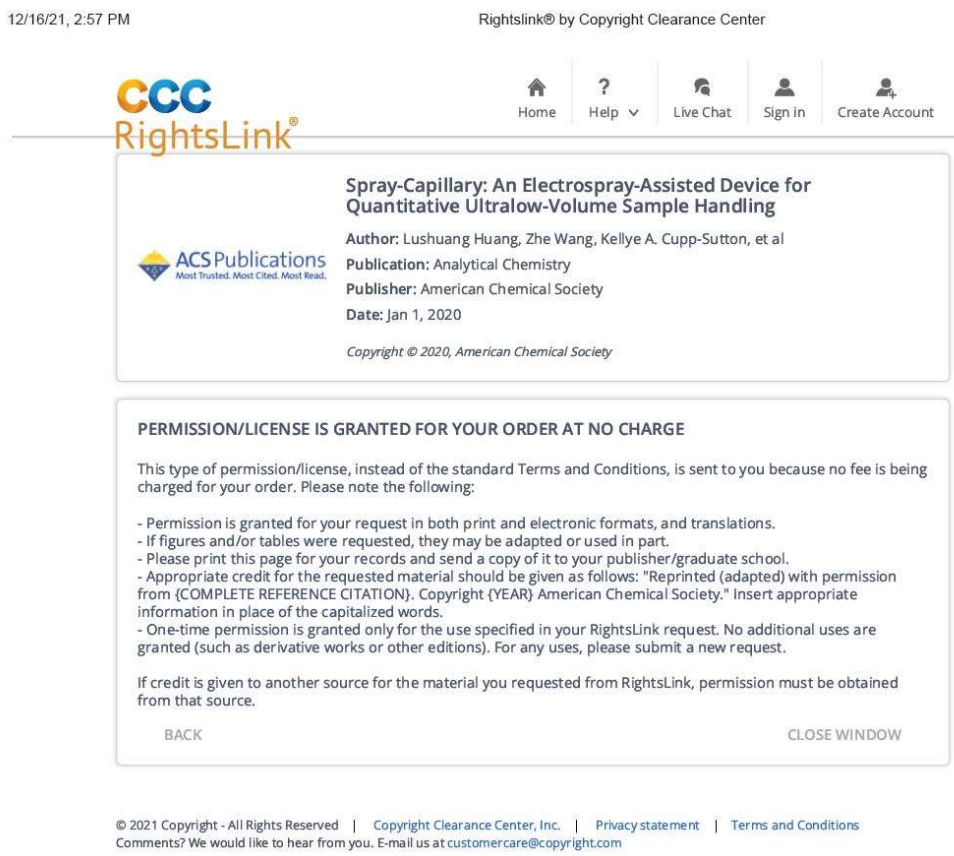

Copyright permission for chapter 2

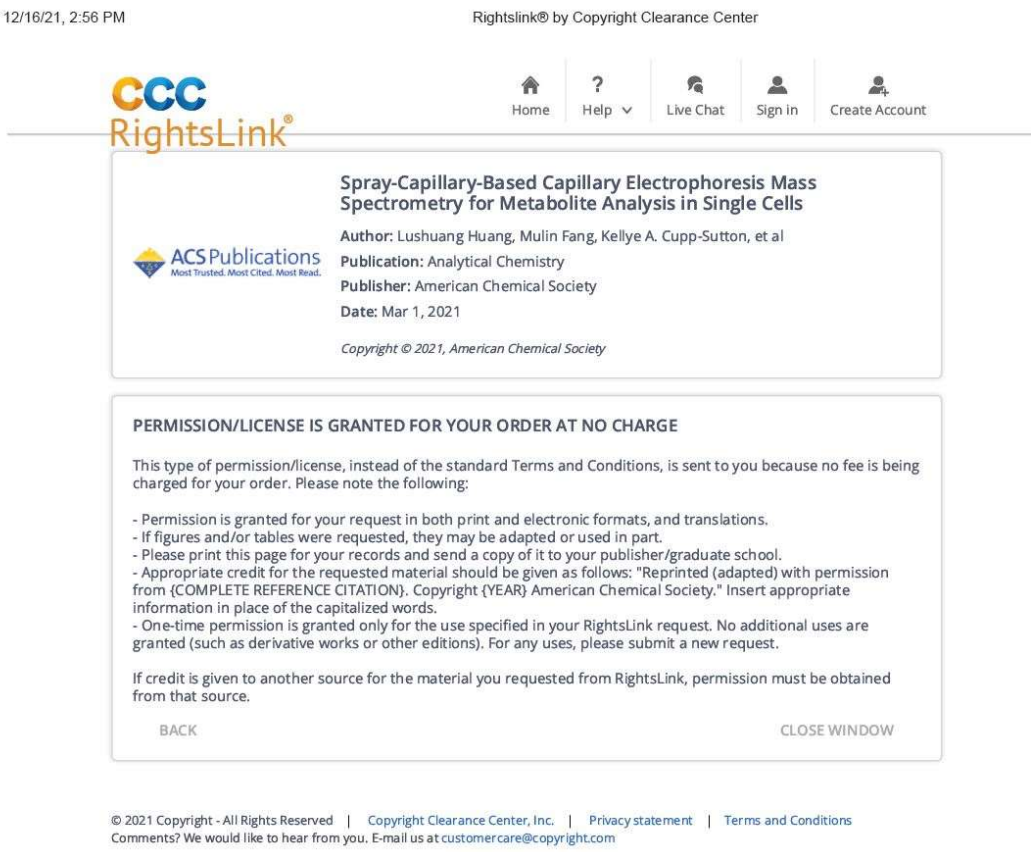

Copyright permission for chapter 4

Reference

1. Yi, L., et al., *Advances in microscale separations towards nanoproteomics applications.* Journal of Chromatography A, 2017. **1523**: p. 40-48.
2. Yang, L., et al., *Single-Cell, Multiplexed Protein Detection of Rare Tumor Cells Based on a Beads-on-Barcode Antibody Microarray.* Anal Chem, 2016. **88**(22): p. 11077-11083.
3. Sinkala, E., et al., *Profiling protein expression in circulating tumour cells using microfluidic western blotting.* Nature communications, 2017. **8**(1): p. 1-12.
4. Bendall, S.C., et al., *A deep profiler's guide to cytometry.* Trends in immunology, 2012. **33**(7): p. 323-332.
5. Bandura, D.R., et al., *Mass cytometry: technique for real time single cell multitarget immunoassay based on inductively coupled plasma time-of-flight mass spectrometry.* Anal Chem, 2009. **81**(16): p. 6813-22.
6. Perfetto, S.P., P.K. Chattopadhyay, and M. Roederer, *Seventeen-colour flow cytometry: unravelling the immune system.* Nat Rev Immunol, 2004. **4**(8): p. 648-55.
7. Holscher, D. and B. Schneider, *Laser microdissection and cryogenic nuclear magnetic resonance spectroscopy: an alliance for cell type-specific metabolite profiling.* Planta, 2007. **225**(3): p. 763-70.
8. Svatos, A., *Single-cell metabolomics comes of age: new developments in mass spectrometry profiling and imaging.* Anal Chem, 2011. **83**(13): p. 5037-44.
9. Zhang, Z., et al., *High-throughput proteomics.* Annu Rev Anal Chem (Palo Alto Calif), 2014. **7**: p. 427-54.
10. Rose, R.J., et al., *High-sensitivity Orbitrap mass analysis of intact macromolecular assemblies.* Nat Methods, 2012. **9**(11): p. 1084-6.
11. Swearingen, K.E. and R.L. Moritz, *High-field asymmetric waveform ion mobility spectrometry for mass spectrometry-based proteomics.* Expert Rev Proteomics, 2012. **9**(5): p. 505-17.
12. Meier, F., M.A. Park, and M. Mann, *Trapped Ion Mobility Spectrometry and Parallel Accumulation–Serial Fragmentation in Proteomics.* Molecular & Cellular Proteomics, 2021. **20**.
13. Yang, Z. and L. Sun, *Recent technical progress in sample preparation and liquid-phase separation-mass spectrometry for proteomic analysis of mass-limited samples.* Anal Methods, 2021. **13**(10): p. 1214-1225.
14. Ramautar, R., et al., *Human metabolomics: strategies to understand biology.* Curr Opin Chem Biol, 2013. **17**(5): p. 841-6.
15. Finka, A. and P. Goloubinoff, *Proteomic data from human cell cultures refine mechanisms of chaperone-mediated protein homeostasis.* Cell Stress Chaperones, 2013. **18**(5): p. 591-605.
16. Altelaar, A.F. and A.J. Heck, *Trends in ultrasensitive proteomics.* Curr Opin Chem Biol, 2012. **16**(1-2): p. 206-13.
17. Zhou, B., et al., *LC-MS-based metabolomics.* Mol Biosyst, 2012. **8**(2): p. 470-81.
18. Duncan, K.D., J. Fyrestam, and I. Lanekoff, *Advances in mass spectrometry based single-cell metabolomics.* Analyst, 2019. **144**(3): p. 782-793.
19. Laskin, J., et al., *Tissue imaging using nanospray desorption electrospray ionization mass spectrometry.* Analytical chemistry, 2012. **84**(1): p. 141-148.

20. Lee, J.K., et al., *High-resolution live-cell imaging and analysis by laser desorption/ionization droplet delivery mass spectrometry.* Analytical chemistry, 2016. **88**(10): p. 5453-5461.
21. Pan, N., et al., *The single-probe: a miniaturized multifunctional device for single cell mass spectrometry analysis.* Analytical chemistry, 2014. **86**(19): p. 9376-9380.
22. Shrestha, B. and A. Vertes, *In situ metabolic profiling of single cells by laser ablation electrospray ionization mass spectrometry.* Analytical chemistry, 2009. **81**(20): p. 8265-8271.
23. Eikel, D. and J. Henion, *Liquid extraction surface analysis (LESA) of food surfaces employing chip‐based nano‐electrospray mass spectrometry.* Rapid Communications in Mass Spectrometry, 2011. **25**(16): p. 2345-2354.
24. Yoshimura, K., et al., *Physical properties of the probe electrospray ionization (PESI) needle applied to the biological samples.* Journal of mass spectrometry, 2009. **44**(6): p. 978-985.
25. Smith, L.M. and N.L. Kelleher, *Proteoform: a single term describing protein complexity.* Nature methods, 2013. **10**(3): p. 186-187.
26. Mellors, J.S. and J.W. Jorgenson, *Use of 1.5-microm porous ethyl-bridged hybrid particles as a stationary-phase support for reversed-phase ultrahigh-pressure liquid chromatography.* Anal Chem, 2004. **76**(18): p. 5441-50.
27. Cong, Y., et al., *Improved single-cell proteome coverage using narrow-bore packed NanoLC columns and ultrasensitive mass spectrometry.* Analytical chemistry, 2020. **92**(3): p. 2665-2671.
28. Shen, Y., et al., *Ultrasensitive proteomics using high-efficiency on-line micro-SPE-nanoLC-nanoESI MS and MS/MS.* Anal Chem, 2004. **76**(1): p. 144-54.
29. Xiang, P., et al., *Picoflow Liquid Chromatography–Mass Spectrometry for Ultrasensitive Bottom-Up Proteomics Using 2-µm-id Open Tubular Columns.* Analytical chemistry, 2020. **92**(7): p. 4711-4715.
30. Harstad, R.K., et al., *Capillary electrophoresis.* Analytical chemistry, 2016. **88**(1): p. 299-319.
31. Gomes, F.P. and J.R. Yates III, *Recent trends of capillary electrophoresis‐mass spectrometry in proteomics research.* Mass spectrometry reviews, 2019. **38**(6): p. 445-460.
32. Maxwell, E.J. and D.D. Chen, *Twenty years of interface development for capillary electrophoresis-electrospray ionization-mass spectrometry.* Anal Chim Acta, 2008. **627**(1): p. 25-33.
33. Smith, R.D., C.J. Barinaga, and H.R. Udseth, *Improved electrospray ionization interface for capillary zone electrophoresis-mass spectrometry.* Analytical chemistry, 1988. **60**(18): p. 1948-1952.
34. Sun, L., et al., *Third-generation electrokinetically pumped sheath-flow nanospray interface with improved stability and sensitivity for automated capillary zone electrophoresis-mass spectrometry analysis of complex proteome digests.* J Proteome Res, 2015. **14**(5): p. 2312-21.
35. Moini, M., *Simplifying CE− MS operation. 2. Interfacing low-flow separation techniques to mass spectrometry using a porous tip.* Analytical chemistry, 2007. **79**(11): p. 4241-4246.

36. Busnel, J.-M., et al., *High capacity capillary electrophoresis-electrospray ionization mass spectrometry: coupling a porous sheathless interface with transient-isotachophoresis.* Analytical chemistry, 2010. **82**(22): p. 9476-9483.
37. Shintani, H., *Handbook of capillary electrophoresis applications*. 2012: Springer Science & Business Media.
38. Zhu, G., L. Sun, and N.J. Dovichi, *Thermally-initiated free radical polymerization for reproducible production of stable linear polyacrylamide coated capillaries, and their application to proteomic analysis using capillary zone electrophoresis–mass spectrometry.* Talanta, 2016. **146**: p. 839-843.
39. Santos, M., et al., *A covalent, cationic polymer coating method for the CESI-MS analysis of intact proteins and polypeptides.* SCIEX Separations application note, 2015.
40. Chien, R.L., *Mathematical modeling of field-amplified sample injection in high-performance capillary electrophoresis.* Analytical chemistry, 1991. **63**(24): p. 2866-2869.
41. Simpson Jr, S.L., J.P. Quirino, and S. Terabe, *On-line sample preconcentration in capillary electrophoresis: Fundamentals and applications.* Journal of Chromatography A, 2008. **1184**(1-2): p. 504-541.
42. Britz-McKibbin, P. and D.D. Chen, *Selective focusing of catecholamines and weakly acidic compounds by capillary electrophoresis using a dynamic pH junction.* Anal Chem, 2000. **72**(6): p. 1242-52.
43. Chen, D., X. Shen, and L. Sun, *Capillary zone electrophoresis–mass spectrometry with microliter-scale loading capacity, 140 min separation window and high peak capacity for bottom-up proteomics.* Analyst, 2017. **142**(12): p. 2118-2127.
44. Lubeckyj, R.A., et al., *Large-Scale Qualitative and Quantitative Top-Down Proteomics Using Capillary Zone Electrophoresis-Electrospray Ionization-Tandem Mass Spectrometry with Nanograms of Proteome Samples.* J Am Soc Mass Spectrom, 2019. **30**(8): p. 1435-1445.
45. Onjiko, R.M., et al., *In situ microprobe single-cell capillary electrophoresis mass spectrometry: metabolic reorganization in single differentiating cells in the live vertebrate (Xenopus laevis) embryo.* Analytical chemistry, 2017. **89**(13): p. 7069-7076.
46. Doerr, A., *DIA mass spectrometry.* Nature Methods, 2015. **12**(1): p. 35-35.
47. Xiao, J.F., B. Zhou, and H.W. Ressom, *Metabolite identification and quantitation in LC-MS/MS-based metabolomics.* TrAC Trends in Analytical Chemistry, 2012. **32**: p. 1-14.
48. Liu, X., et al., *Protein identification using top-down spectra.* Molecular & cellular proteomics, 2012. **11**(6).
49. Jones, A.W. and H.J. Cooper, *Dissociation techniques in mass spectrometry-based proteomics.* Analyst, 2011. **136**(17): p. 3419-3429.
50. Schrimpe-Rutledge, A.C., et al., *Untargeted Metabolomics Strategies-Challenges and Emerging Directions.* J Am Soc Mass Spectrom, 2016. **27**(12): p. 1897-1905.
51. Kelly, R.T., *Single-cell Proteomics: Progress and Prospects.* Mol Cell Proteomics, 2020. **19**(11): p. 1739-1748.
52. Lapainis, T., S.S. Rubakhin, and J.V. Sweedler, *Capillary electrophoresis with electrospray ionization mass spectrometric detection for single-cell metabolomics.* Analytical chemistry, 2009. **81**(14): p. 5858-5864.

53. Liang, Y., et al., *Spatially resolved proteome profiling of< 200 cells from tomato fruit pericarp by integrating laser-capture microdissection with nanodroplet sample preparation.* Analytical chemistry, 2018. **90**(18): p. 11106-11114.
54. Brunner, A.-D., et al., *Ultra-high sensitivity mass spectrometry quantifies single-cell proteome changes upon perturbation.* BioRxiv, 2021: p. 2020.12. 22.423933.
55. Onjiko, R.M., S.A. Moody, and P. Nemes, *Single-cell mass spectrometry reveals small molecules that affect cell fates in the 16-cell embryo.* Proceedings of the National Academy of Sciences, 2015. **112**(21): p. 6545-6550.
56. Kitagawa, F. and K. Otsuka, *Recent applications of on-line sample preconcentration techniques in capillary electrophoresis.* Journal of chromatography A, 2014. **1335**: p. 43-60.
57. Nakatani, K., et al., *An Analytical System for Single-Cell Metabolomics of Typical Mammalian Cells Based on Highly Sensitive Nano-Liquid Chromatography Tandem Mass Spectrometry.* Mass Spectrom (Tokyo), 2020. **9**(1): p. A0080.
58. Huang, L., et al., *Spray-capillary-based capillary electrophoresis mass spectrometry for metabolite analysis in single cells.* Analytical Chemistry, 2021. **93**(10): p. 4479-4487.
59. Kawai, T., et al., *Ultrasensitive Single Cell Metabolomics by Capillary Electrophoresis-Mass Spectrometry with a Thin-Walled Tapered Emitter and Large-Volume Dual Sample Preconcentration.* Anal Chem, 2019. **91**(16): p. 10564-10572.
60. Nemes, P., et al., *Qualitative and quantitative metabolomic investigation of single neurons by capillary electrophoresis electrospray ionization mass spectrometry.* Nature protocols, 2013. **8**(4): p. 783-799.
61. Sun, L., et al., *Single cell proteomics using frog (Xenopus laevis) blastomeres isolated from early stage embryos, which form a geometric progression in protein content.* Analytical chemistry, 2016. **88**(13): p. 6653-6657.
62. Duncan, K.D. and I. Lanekoff, *Spatially defined surface sampling capillary electrophoresis mass spectrometry.* Analytical chemistry, 2019. **91**(12): p. 7819-7827.
63. Tian, R., et al., *Rare cell proteomic reactor applied to stable isotope labeling by amino acids in cell culture (SILAC)-based quantitative proteomics study of human embryonic stem cell differentiation.* Mol Cell Proteomics, 2011. **10**(2): p. M110 000679.
64. Chen, Q., et al., *Ultrasensitive proteome profiling for 100 living cells by direct cell injection, online digestion and nano-LC-MS/MS analysis.* Analytical chemistry, 2015. **87**(13): p. 6674-6680.
65. Huang, E.L., et al., *SNaPP: Simplified Nanoproteomics Platform for Reproducible Global Proteomic Analysis of Nanogram Protein Quantities.* Endocrinology, 2016. **157**(3): p. 1307-14.
66. Safdar, M., J. Sproß, and J. Jänis, *Microscale immobilized enzyme reactors in proteomics: latest developments.* Journal of Chromatography A, 2014. **1324**: p. 1-10.
67. Yang, Z., et al., *Toward a universal sample preparation method for denaturing top-down proteomics of complex proteomes.* Journal of Proteome Research, 2020. **19**(8): p. 3315-3325.

68. Ouni, E., et al., *Divide-and-Conquer Matrisome Protein (DC-MaP) Strategy: An MS-Friendly Approach to Proteomic Matrisome Characterization.* International journal of molecular sciences, 2020. **21**(23): p. 9141.
69. Waanders, L.F., et al., *Quantitative proteomic analysis of single pancreatic islets.* Proc Natl Acad Sci U S A, 2009. **106**(45): p. 18902-7.
70. Moggridge, S., et al., *Extending the compatibility of the SP3 paramagnetic bead processing approach for proteomics.* Journal of proteome research, 2018. **17**(4): p. 1730-1740.
71. Yang, Z., et al., *Nanoparticle-Aided Nanoreactor for Nanoproteomics.* Analytical Chemistry, 2021. **93**(30): p. 10568-10576.
72. Zhu, Y., et al., *Nanodroplet processing platform for deep and quantitative proteome profiling of 10-100 mammalian cells.* Nat Commun, 2018. **9**(1): p. 882.
73. Liang, Y., et al., *Fully automated sample processing and analysis workflow for low-input proteome profiling.* Analytical chemistry, 2020. **93**(3): p. 1658-1666.
74. Li, Z.-Y., et al., *Nanoliter-scale oil-air-droplet chip-based single cell proteomic analysis.* Analytical chemistry, 2018. **90**(8): p. 5430-5438.
75. Altelaar, A.M. and A.J. Heck, *Trends in ultrasensitive proteomics.* Current opinion in chemical biology, 2012. **16**(1-2): p. 206-213.
76. Shen, Y., et al., *High-efficiency nanoscale liquid chromatography coupled on-line with mass spectrometry using nanoelectrospray ionization for proteomics.* Anal Chem, 2002. **74**(16): p. 4235-49.
77. Sun, L., et al., *Ultrasensitive and fast bottom-up analysis of femtogram amounts of complex proteome digests.* Angew Chem Int Ed Engl, 2013. **52**(51): p. 13661-4.
78. Wojcik, R., et al., *Simplified capillary electrophoresis nanospray sheath-flow interface for high efficiency and sensitive peptide analysis.* Rapid Commun Mass Spectrom, 2010. **24**(17): p. 2554-60.
79. Wilm, M. and M. Mann, *Analytical properties of the nanoelectrospray ion source.* Anal Chem, 1996. **68**(1): p. 1-8.
80. Choi, S.B., et al., *Tapered-Tip Capillary Electrophoresis Nano-Electrospray Ionization Mass Spectrometry for Ultrasensitive Proteomics: the Mouse Cortex.* J Am Soc Mass Spectrom, 2017. **28**(4): p. 597-607.
81. Yang, Y., et al., *Single-cell analysis by ambient mass spectrometry.* TrAC Trends in Analytical Chemistry, 2017. **90**: p. 14-26.
82. Kelly, R.T., et al., *The ion funnel: theory, implementations, and applications.* Mass Spectrom Rev, 2010. **29**(2): p. 294-312.
83. Saha-Shah, A., et al., *Nanopipettes: probes for local sample analysis.* Chem Sci, 2015. **6**(6): p. 3334-3341.
84. Morris, C.A., A.K. Friedman, and L.A. Baker, *Applications of nanopipettes in the analytical sciences.* Analyst, 2010. **135**(9): p. 2190-2202.
85. Laforge, F.O., et al., *Electrochemical attosyringe.* Proc Natl Acad Sci U S A, 2007. **104**(29): p. 11895-900.
86. Actis, P., et al., *Compartmental genomics in living cells revealed by single-cell nanobiopsy.* ACS Nano, 2014. **8**(1): p. 546-53.
87. Shi, W., et al., *Nanopipette delivery: influence of surface charge.* Analyst, 2015. **140**(14): p. 4835-42.
88. Masujima, T., *Live single-cell mass spectrometry.* Analytical Sciences, 2009. **25**(8): p. 953-960.

89. Gholipour, Y., et al., *Living cell manipulation, manageable sampling, and shotgun picoliter electrospray mass spectrometry for profiling metabolites.* Anal Biochem, 2013. **433**(1): p. 70-8.
90. Liu, J.-X., et al., *Analysis of endogenous nucleotides by single cell capillary electrophoresis-mass spectrometry.* Analyst, 2014. **139**(22): p. 5835-5842.
91. Chen, A., et al., *Tunable Electroosmosis-Based Femto-Liter Pipette: A Promising Tool toward Living-Cell Surgery.* Anal Chem, 2017. **89**(20): p. 10806-10812.
92. Zhang, L. and A. Vertes, *Energy Charge, Redox State, and Metabolite Turnover in Single Human Hepatocytes Revealed by Capillary Microsampling Mass Spectrometry.* Anal Chem, 2015. **87**(20): p. 10397-405.
93. Aerts, J.T., et al., *Patch clamp electrophysiology and capillary electrophoresis-mass spectrometry metabolomics for single cell characterization.* Anal Chem, 2014. **86**(6): p. 3203-8.
94. Saha-Shah, A., J.A. Karty, and L.A. Baker, *Local collection, reaction and analysis with theta pipette emitters.* Analyst, 2017. **142**(9): p. 1512-1518.
95. Lombard-Banek, C., et al., *Microsampling capillary electrophoresis mass spectrometry enables single-cell proteomics in complex tissues: developing cell clones in live Xenopus laevis and zebrafish embryos.* Analytical chemistry, 2019. **91**(7): p. 4797-4805.
96. Yin, R., V. Prabhakaran, and J. Laskin, *Quantitative extraction and mass spectrometry analysis at a single-cell level.* Analytical chemistry, 2018. **90**(13): p. 7937-7945.
97. Huang, X., W.F. Coleman, and R.N. Zare, *Analysis of factors causing peak broadening in capillary zone electrophoresis.* Journal of Chromatography A, 1989. **480**: p. 95-110.
98. Rose, D.J. and J.W. Jorgenson, *Characterization and automation of sample introduction methods for capillary zone electrophoresis.* Analytical Chemistry, 1988. **60**(7): p. 642-648.
99. Honda, S., S. Iwase, and S. Fujiwara, *Evaluation of an automtic siphonic sampler for capillary zone electrophoresis.* Journal of Chromatography A, 1987. **404**: p. 313-320.
100. Krylov, S.N., et al., *Instrumentation for chemical cytometry.* Analytical chemistry, 2000. **72**(4): p. 872-877.
101. Zhang, L., et al., *Subcellular Peptide Localization in Single Identified Neurons by Capillary Microsampling Mass Spectrometry.* Sci Rep, 2018. **8**(1): p. 12227.
102. Guillaume-Gentil, O., et al., *Single-Cell Mass Spectrometry of Metabolites Extracted from Live Cells by Fluidic Force Microscopy.* Anal Chem, 2017. **89**(9): p. 5017-5023.
103. Prager, D.J., R.L. Bowman, and G.G. Vurek, *Constant volume, self-filling nanoliter pipette: Construction and calibration.* Science, 1965. **147**(3658): p. 606-608.
104. Zhou, M., C. Huang, and V.H. Wysocki, *Surface-induced dissociation of ion mobility-separated noncovalent complexes in a quadrupole/time-of-flight mass spectrometer.* Anal Chem, 2012. **84**(14): p. 6016-23.
105. Wohlfarth, C., et al., *Viscosity of Pure Organic Liquids and Binary Liquid Mixtures*. 2001: Springer.
106. Giddings, J.C., *Unified separation science*. 1991: Wiley.
107. Faserl, K., et al., *Optimization and evaluation of a sheathless capillary electrophoresis-electrospray ionization mass spectrometry platform for peptide*

analysis: comparison to liquid chromatography-electrospray ionization mass spectrometry. Anal Chem, 2011. **83**(19): p. 7297-305.
108. Zhu, Y., et al., *Nanoproteomics comes of age.* Expert review of proteomics, 2018. **15**(11): p. 865-871.
109. Kolakowski, B.M. and Z. Mester, *Review of applications of high-field asymmetric waveform ion mobility spectrometry (FAIMS) and differential mobility spectrometry (DMS).* Analyst, 2007. **132**(9): p. 842-64.
110. Shen, Y., et al., *High-resolution ultrahigh-pressure long column reversed-phase liquid chromatography for top-down proteomics.* J Chromatogr A, 2017. **1498**: p. 99-110.
111. Huang, E.L., et al., *SNaPP: simplified nanoproteomics platform for reproducible global proteomic analysis of nanogram protein quantities.* Endocrinology, 2016. **157**(3): p. 1307-1314.
112. Murthy, T.V., D. Kroncke, and P.D. Bonin, *Adding precise nanoliter volume capabilities to liquid-handling automation for compound screening experimentation.* J Lab Autom, 2011. **16**(3): p. 221-8.
113. Petelski, A.A., et al., *Multiplexed single-cell proteomics using SCoPE2.* bioRxiv, 2021.
114. Kharaji, Z.G., M. Bayareh, and V. Kalantar, *A review on acoustic field-driven micromixers.* International Journal of Chemical Reactor Engineering, 2021. **19**(6): p. 553-569.
115. Haber, C., M. Boillat, and B. van der Schoot, *Precise nanoliter fluid handling system with integrated high-speed flow sensor.* Assay Drug Dev Technol, 2005. **3**(2): p. 203-12.
116. Councill, E.E.A., et al., *Adapting a Low-Cost and Open-Source Commercial Pipetting Robot for Nanoliter Liquid Handling.* SLAS TECHNOLOGY: Translating Life Sciences Innovation, 2021. **26**(3): p. 311-319.
117. Williams, S.M., et al., *Automated coupling of nanodroplet sample preparation with liquid chromatography–mass spectrometry for high-throughput single-cell proteomics.* Analytical Chemistry, 2020. **92**(15): p. 10588-10596.
118. Yan, L., et al., *In-tip nanoreactors for cancer cells proteome profiling.* Anal Chim Acta, 2017. **949**: p. 43-52.
119. Huang, L., et al., *Spray-Capillary: An Electrospray-Assisted Device for Quantitative Ultralow-Volume Sample Handling.* Analytical chemistry, 2019. **92**(1): p. 640-646.
120. Sarg, B., et al., *Comparing and combining capillary electrophoresis electrospray ionization mass spectrometry and nano–liquid chromatography electrospray ionization mass spectrometry for the characterization of post-translationally modified histones.* Molecular & cellular proteomics, 2013. **12**(9): p. 2640-2656.
121. Lubeckyj, R.A., et al., *Single-shot top-down proteomics with capillary zone electrophoresis-electrospray ionization-tandem mass spectrometry for identification of nearly 600 Escherichia coli proteoforms.* Analytical chemistry, 2017. **89**(22): p. 12059-12067.
122. DeLaney, K., et al., *Recent advances and new perspectives in capillary electrophoresis-mass spectrometry for single cell "omics".* Molecules, 2019. **24**(1): p. 42.
123. Yin, L., et al., *Recent advances in single-cell analysis by mass spectrometry.* Analyst, 2019. **144**(3): p. 824-845.

124. Evers, T.M., et al., *Deciphering metabolic heterogeneity by single-cell analysis*. 2019, ACS Publications.
125. Nemes, P., et al., *Single-cell metabolomics: changes in the metabolome of freshly isolated and cultured neurons.* ACS chemical neuroscience, 2012. **3**(10): p. 782-792.
126. Gahoual, R., et al., *Revealing the potential of capillary electrophoresis/mass spectrometry: the tipping point.* Rapid Communications in Mass Spectrometry, 2019. **33**: p. 11-19.
127. Sun, L., et al., *Third-generation electrokinetically pumped sheath-flow nanospray interface with improved stability and sensitivity for automated capillary zone electrophoresis–mass spectrometry analysis of complex proteome digests.* Journal of proteome research, 2015. **14**(5): p. 2312-2321.
128. Faserl, K., et al., *Optimization and evaluation of a sheathless capillary electrophoresis–electrospray ionization mass spectrometry platform for peptide analysis: comparison to liquid chromatography–electrospray ionization mass spectrometry.* Analytical chemistry, 2011. **83**(19): p. 7297-7305.
129. Cecala, C. and J.V. Sweedler, *Sampling techniques for single-cell electrophoresis.* Analyst, 2012. **137**(13): p. 2922-2929.
130. Liao, H.-W., et al., *Enhanced single-cell metabolomics by capillary electrophoresis electrospray ionization-mass spectrometry with field amplified sample injection.* Analytica Chimica Acta, 2020. **1118**: p. 36-43.
131. Sánchez-López, E., et al., *Sheathless CE-MS based metabolic profiling of kidney tissue section samples from a mouse model of Polycystic Kidney Disease.* Scientific reports, 2019. **9**(1): p. 1-9.
132. Liu, R., et al., *Integrating a generalized data analysis workflow with the Single-probe mass spectrometry experiment for single cell metabolomics.* Analytica chimica acta, 2019. **1064**: p. 71-79.
133. Fujii, T., et al., *Direct metabolomics for plant cells by live single-cell mass spectrometry.* Nature protocols, 2015. **10**(9): p. 1445-1456.
134. Nakashima, T., et al., *Single-cell metabolite profiling of stalk and glandular cells of intact trichomes with internal electrode capillary pressure probe electrospray ionization mass spectrometry.* Analytical Chemistry, 2016. **88**(6): p. 3049-3057.
135. Zhang, X.-C., et al., *Integrated droplet-based microextraction with ESI-MS for removal of matrix interference in single-cell analysis.* Scientific reports, 2016. **6**(1): p. 1-9.
136. Zhang, X.-C., et al., *Combination of droplet extraction and pico-ESI-MS allows the identification of metabolites from single cancer cells.* Analytical chemistry, 2018. **90**(16): p. 9897-9903.
137. Esaki, T. and T. Masujima, *Fluorescence probing live single-cell mass spectrometry for direct analysis of organelle metabolism.* Analytical Sciences, 2015. **31**(12): p. 1211-1213.
138. Saha-Shah, A., et al., *Segmented flow sampling with push–pull theta pipettes.* Analyst, 2016. **141**(6): p. 1958-1965.
139. Xu, M., et al., *Molecular profiling of single axons and dendrites in living neurons using electrosyringe-assisted electrospray mass spectrometry.* Analyst, 2019. **144**(3): p. 954-960.

140. Choi, S.B., et al., *Tapered-tip capillary electrophoresis nano-electrospray ionization mass spectrometry for ultrasensitive proteomics: the mouse cortex.* Journal of the American Society for Mass Spectrometry, 2016. **28**(4): p. 597-607.
141. Onjiko, R.M., et al., *Single-cell mass spectrometry with multi-solvent extraction identifies metabolic differences between left and right blastomeres in the 8-cell frog (Xenopus) embryo.* Analyst, 2016. **141**(12): p. 3648-3656.
142. Kawai, T., et al., *Ultrasensitive Single Cell Metabolomics by Capillary Electrophoresis–Mass Spectrometry with a Thin-Walled Tapered Emitter and Large-Volume Dual Sample Preconcentration.* Analytical chemistry, 2019. **91**(16): p. 10564-10572.
143. Aerts, J.T., et al., *Patch clamp electrophysiology and capillary electrophoresis–mass spectrometry metabolomics for single cell characterization.* Analytical chemistry, 2014. **86**(6): p. 3203-3208.
144. Li, X., et al., *A microchip electrophoresis-mass spectrometric platform with double cell lysis nano-electrodes for automated single cell analysis.* Journal of Chromatography A, 2016. **1451**: p. 156-163.
145. Klepárník, K., *Recent advances in the combination of capillary electrophoresis with mass spectrometry: From element to single‐cell analysis.* Electrophoresis, 2013. **34**(1): p. 70-85.
146. Comi, T.J., et al., *MALDI MS guided liquid microjunction extraction for capillary electrophoresis–electrospray ionization MS analysis of single pancreatic islet cells.* Analytical chemistry, 2017. **89**(14): p. 7765-7772.
147. Shrestha, B., J.M. Patt, and A. Vertes, *In situ cell-by-cell imaging and analysis of small cell populations by mass spectrometry.* Anal Chem, 2011. **83**(8): p. 2947-55.
148. Misra, B.B., S.M. Assmann, and S. Chen, *Plant single-cell and single-cell-type metabolomics.* Trends in plant science, 2014. **19**(10): p. 637-646.
149. Gong, X., et al., *Single cell analysis with probe ESI-mass spectrometry: detection of metabolites at cellular and subcellular levels.* Analytical chemistry, 2014. **86**(8): p. 3809-3816.
150. Kessner, D., et al., *ProteoWizard: open source software for rapid proteomics tools development.* Bioinformatics, 2008. **24**(21): p. 2534-2536.
151. Smith, C.A., et al., *METLIN: a metabolite mass spectral database.* Therapeutic drug monitoring, 2005. **27**(6): p. 747-751.
152. Böttcher, C., et al., *Comprehensive metabolite profiling of onion bulbs (Allium cepa) using liquid chromatography coupled with electrospray ionization quadrupole time-of-flight mass spectrometry.* Metabolomics, 2017. **13**(4): p. 35.
153. Wishart, D.S., et al., *HMDB 4.0: the human metabolome database for 2018.* Nucleic acids research, 2018. **46**(D1): p. D608-D617.
154. Yannai, S., *Dictionary of Food Compounds with CD-ROM: Additives.* Flavors, and Ingredients, 2004: p. 1784.
155. Kafle, K., et al., *Cellulose microfibril orientation in onion (Allium cepa L.) epidermis studied by atomic force microscopy (AFM) and vibrational sum frequency generation (SFG) spectroscopy.* Cellulose, 2014. **21**(2): p. 1075-1086.
156. Suslov, D., J.-P. Verbelen, and K. Vissenberg, *Onion epidermis as a new model to study the control of growth anisotropy in higher plants.* Journal of experimental botany, 2009. **60**(14): p. 4175-4187.
157. Breu, W., *Allium cepa L.(onion) Part 1: Chemistry and analysis.* Phytomedicine, 1996. **3**(3): p. 293-306.

158. Han, X., et al., *In-line separation by capillary electrophoresis prior to analysis by top-down mass spectrometry enables sensitive characterization of protein complexes.* Journal of proteome research, 2014. **13**(12): p. 6078-6086.